Cosmic Ray Atmospheric Transport and Dosimetry

Christopher J. Mertens

NASA Langley Research Center, Hampton, Virginia USA

European Research Course on Atmospheres

Grenoble, France

January 27, 2010

Discovery of Cosmic Rays

- **Around 1900: X-rays and radioactive emanations ionize gases, enabling them to conduct electricity**
- **Puzzle: Open-air ionization and electric charge leakage no matter how well electroscope was insulated and without an obvious source of ionizing radiation**
- **C. T. R. Wilson connected this "continuous atmospheric radiation" with radioactive emanations seeping from the ground (~ 20 ions per cm^3 per second)**

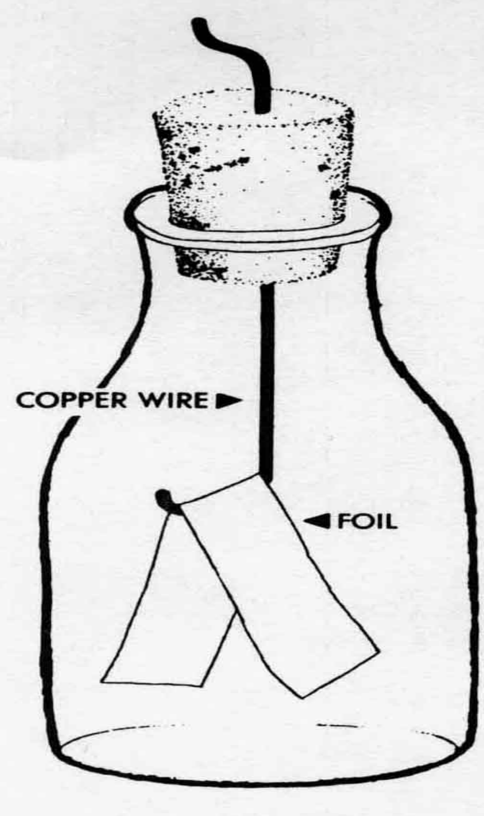

FIGURE 1. A homemade electroscope.

Discovery of Cosmic Rays

- **Wilson's hypothesis should result in a decrease in air ionizing with height**
- **1910: Father Thomas Wulf conducted sensitive electroscope charge leakage measurements from the Eiffel Tower (330 m)**
  - **64% drop in leakage rate**
  - **Expected a much greater reduction**
  - **Deduced an additional source of ionizing radiation from the upper atmosphere**

Discovery of Cosmic Rays

- **1911-1913: High altitude balloon electroscope measurements made by Victor Hess**
  - **Ionization rate first decreased with altitude**
  - **Ionization rate was same as ground level rate by 5000 ft.**
  - **Ionization rate several times ground level rate at 17,500 ft.**
  - **Hess hypothesized extra-terrestrial source of atmospheric ionizing radiation**
- **1925: *Cosmic rays* coined by Millikan**

Sources of Cosmic Rays

- **Galactic Cosmic Rays (GCR)**
  - Originate from outside the solar system
  - Best explanation: supernova remnants + interstellar shock acceleration
- **Solar Cosmic Rays, or Solar Energetic Particles (SEP)**
  - Originate from solar flares and shock-associated coronal mass ejections (CMEs)
  - Interplanetary shock acceleration

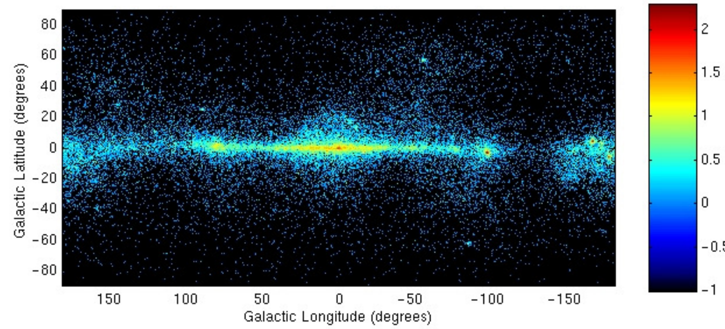

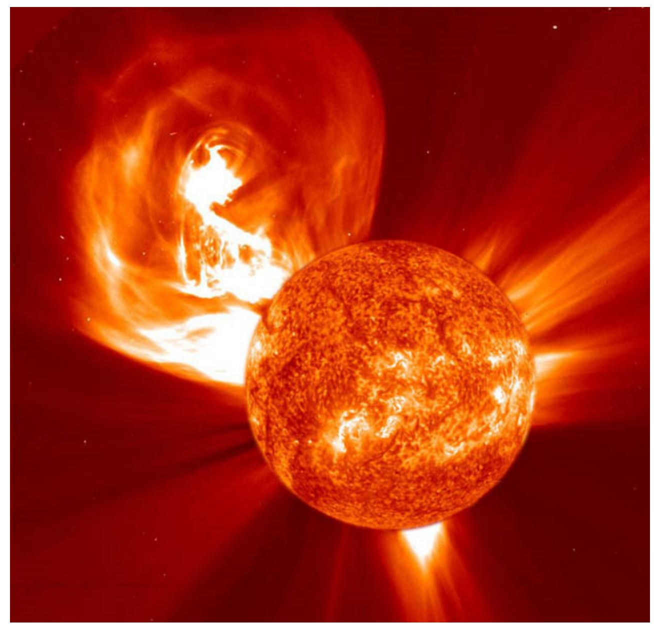

GCR Energy Spectrum

- **Power-law energy spectrum (10^{10} – 10^{20} eV)**

$$dJ / dE \sim E^{-2.7} \ (\mathrm{m}^2 \ \mathrm{sr\ s\ GeV})^{-1}$$

- **Irregularities in energy spectrum**
  - ***Knee* at 10^{16} eV (not totally understood)**
  - ***Angle* at 10^{18} eV (not totally understood)**
  - ***Toe* at 10^{20} eV (cause unknown)**

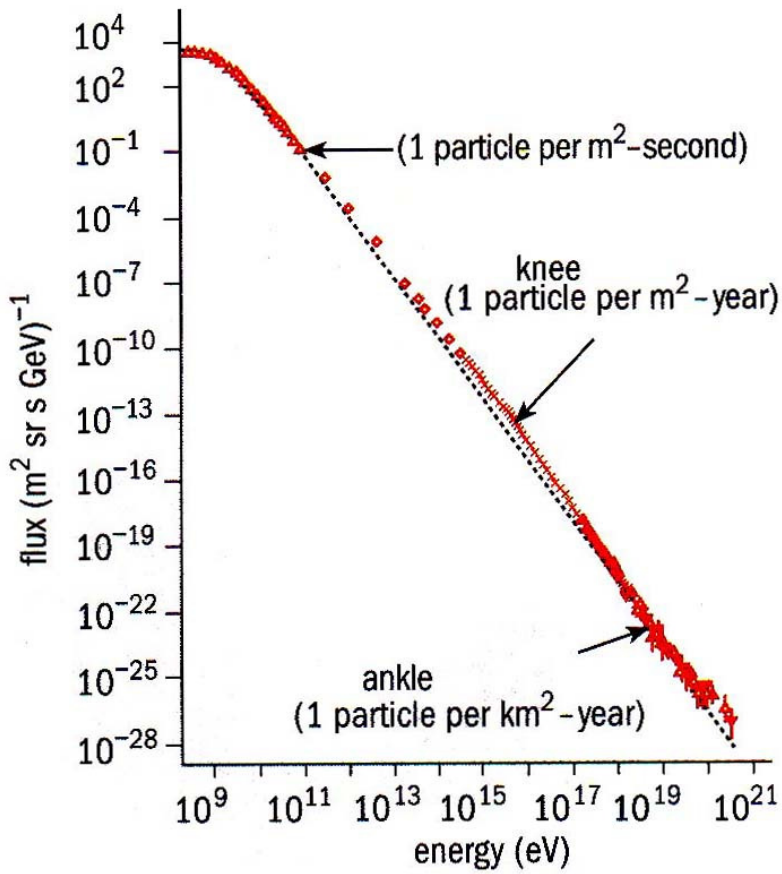

SEP Energy Spectrum

- **Power-law energy spectrum ($E < 10^{10}$ eV)**

  $$dJ/dE \sim E^{-\gamma}\ (\mathrm{cm}^2\ \mathrm{sr\ s\ MeV/n})^{-1}$$

- **Properties**
  - **Power index varies throughout a SEP event and from one event to the next**
  - **Originate from seed populations from corona (solar wind) and flares**
  - **Power law arises from acceleration in turbulent magnetic field**
  - **Power index is a function of the shock compression ratio**

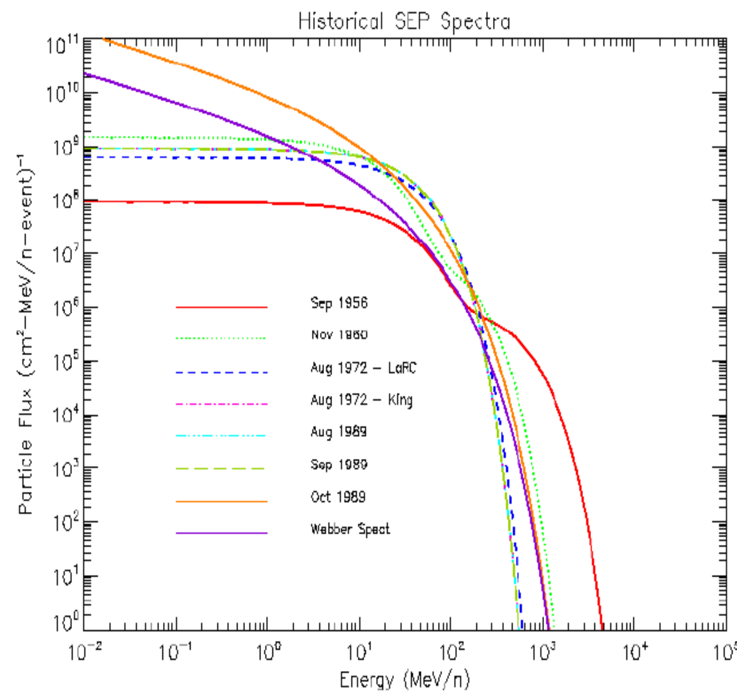

Cosmic Ray Composition

- **GCR**
  - 98% nuclei, 2% e^-/e^+
  - Nuclear component
    - 87% Hydrogen (protons)
    - 12% Helium (alpha)
    - 1% heavy nuclei
- **SEP**
  - Protons, alphas, and electrons

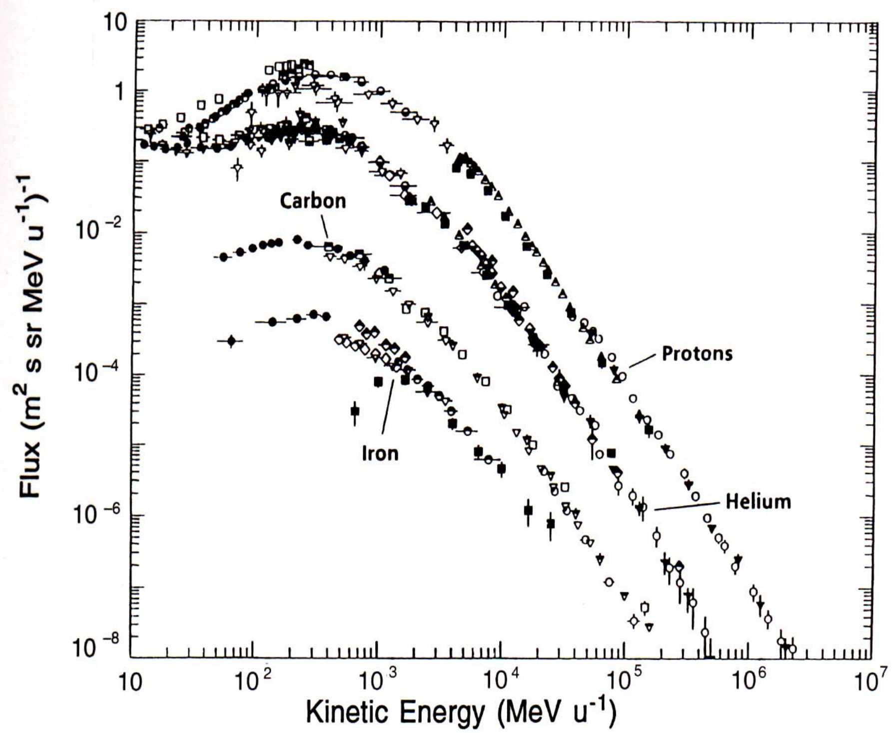

Fig. 2. Energy spectra of major GCR ions as a function of kinetic energy (Simpson, 1983).

GCR Composition

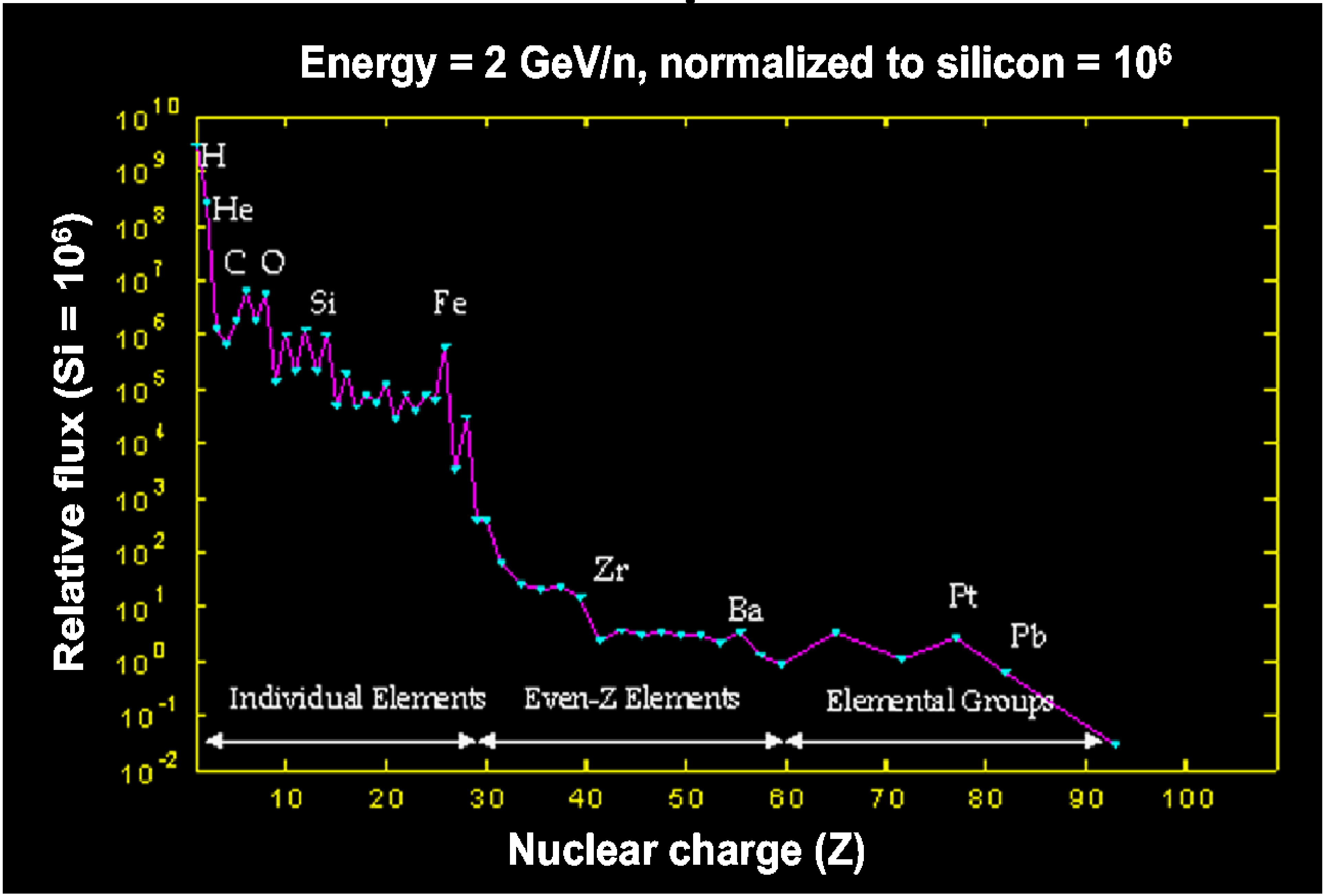

Cosmic Ray Interactions

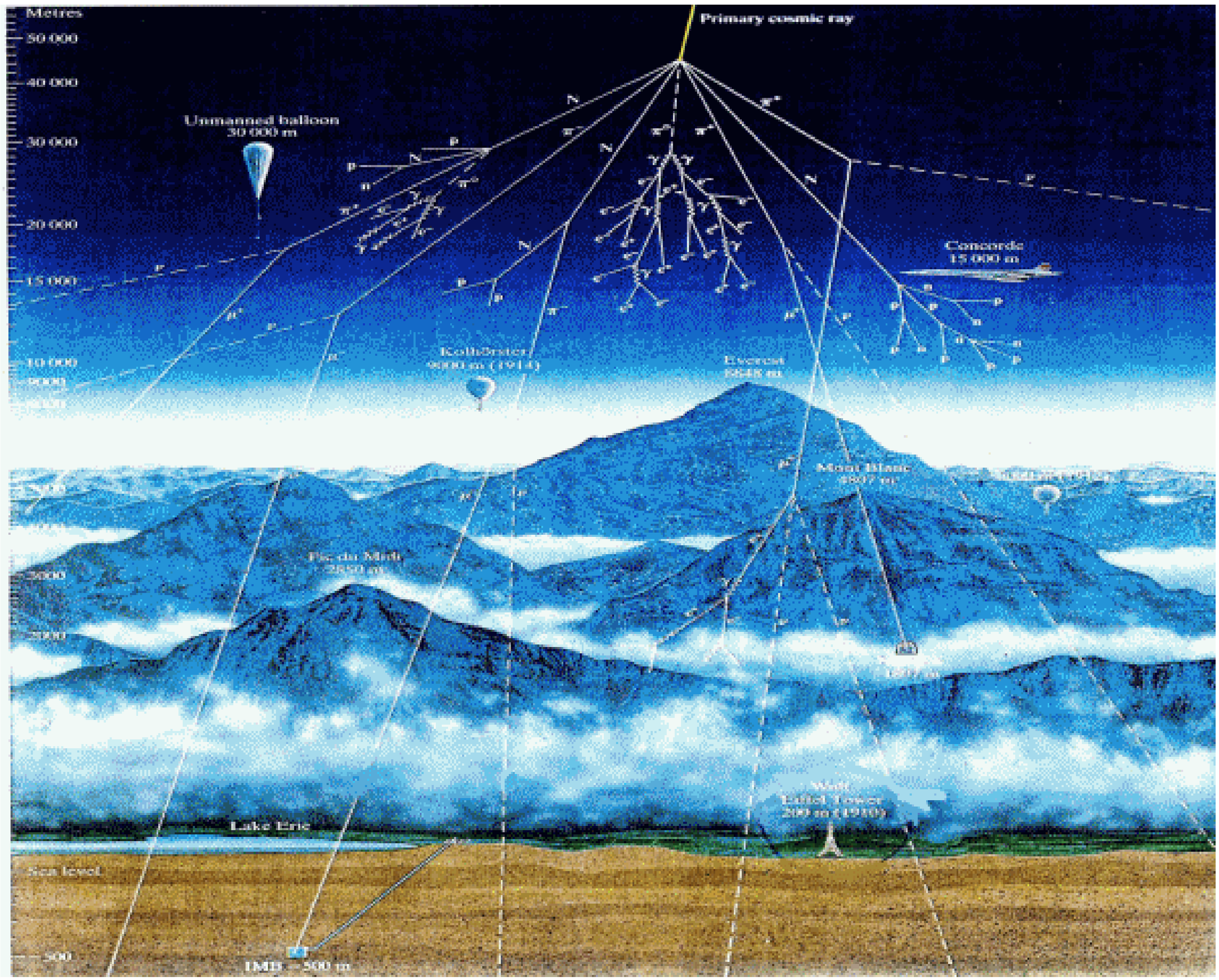

Cosmic Ray Research

- High-Energy Particle Physics
  - Provided radiation source for early research in high-energy particle physics
  - Study of fundamental matter-field interactions: atomic (excitation and ionization) and nuclear (absorption, fragmentation, radioactive decay)
  - Led to discovery of positron, charged mesons, and source of atmospheric neutrons
- Cosmology and Astrophysics
  - What is origin of GCRs?
  - How are GCRs accelerated to such high energies?
  - What role do GCRs play in the dynamics of the Galaxy and the Universe?
  - Why are there large differences between GCR composition and chemical composition of our solar system? What does this tell us about matter outside our solar system?
- Dosimetry (the focus of this talk)
  - Study of heavy-ion tracks in nuclear emulsion detectors on high-altitude balloon experiments led to (Frier et al., 1948):
  - Possibility of human radiation exposure in high-altitude aircraft and future space travel (Armstrong et al., 1949; Schaefer, 1950)

Ways to damage DNA

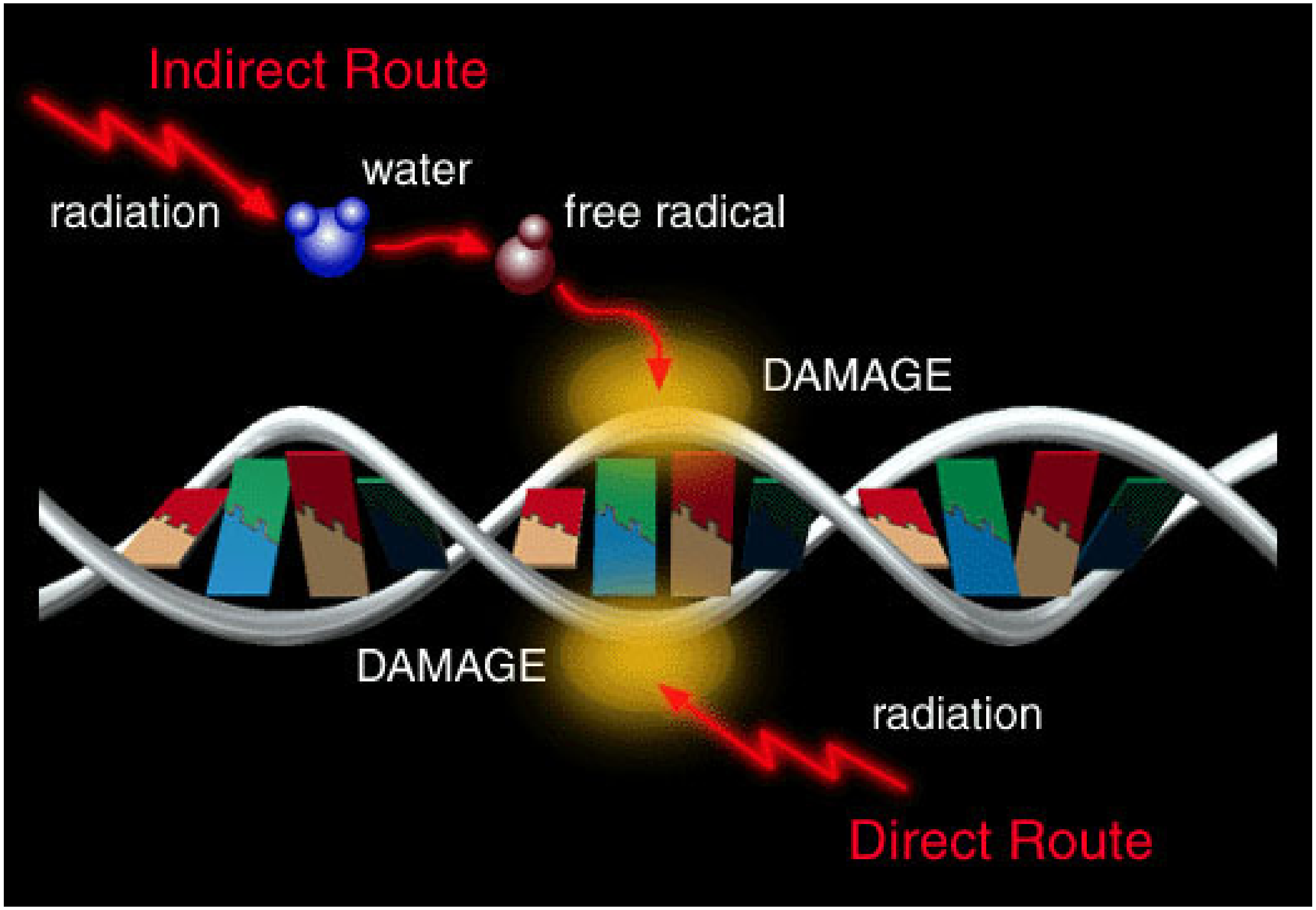

Types of DNA Damage

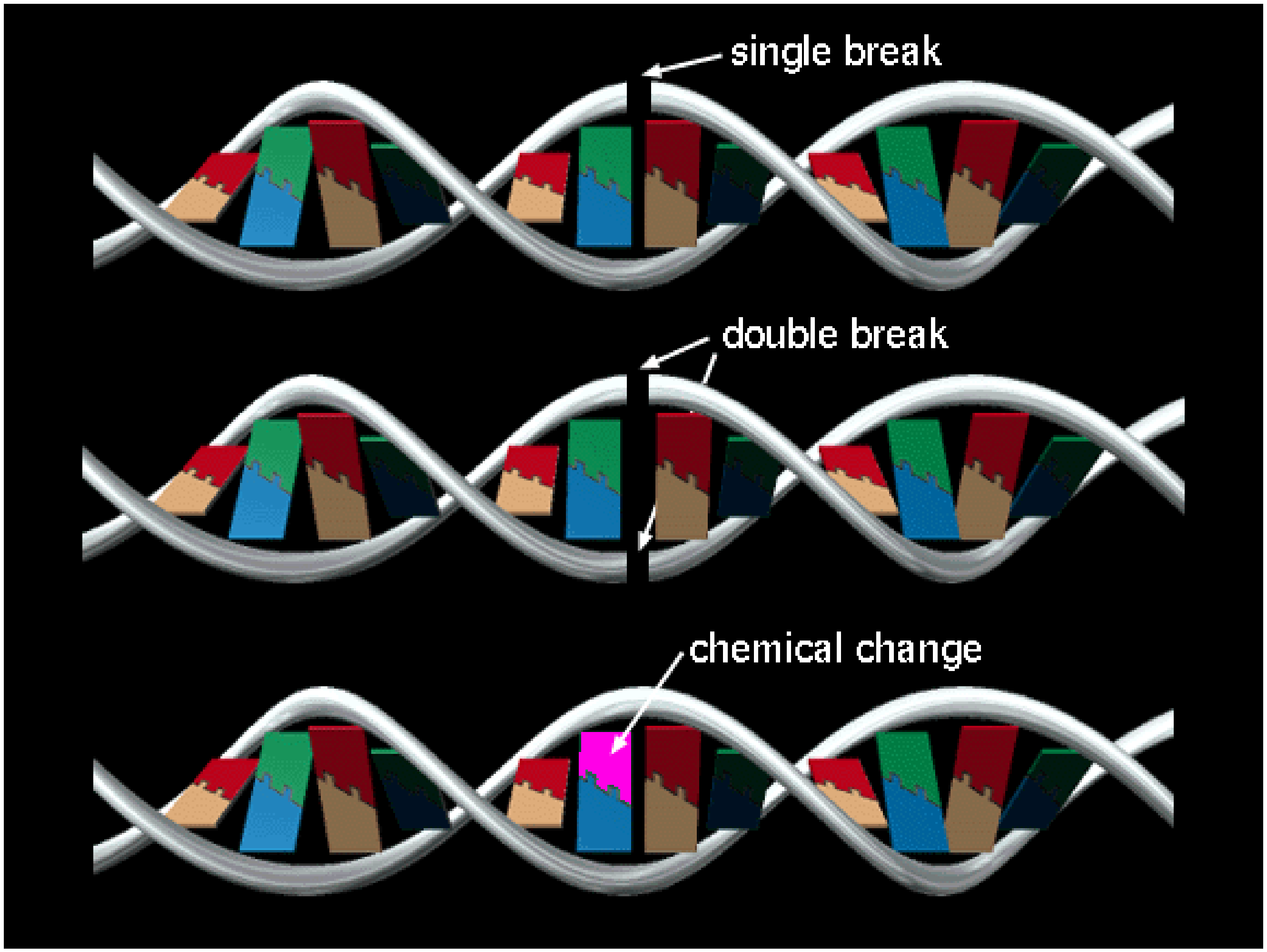

Units Overview

- Unit of absorbed dose:
  - 1 Gray == 1 J/kg
- Radiation weighting factor: w_R
  - Sievert = Gray x w_R
- ICRP estimate:
  - 1 in 20,000 risk of fatal cancer per 1mSv dose (lifetime).

Radiation Weighting Factors (ICRP publl. 60)

Radiation		w_R
x- & γ-rays, all energies		1
electrons, muons, all energies		1
Neutrons	< 10 keV	5
	10-100 keV	10
	100keV to 2MeV	20
	2 - 20 MeV	10
	> 20 MeV	5
Protons	> 2MeV	5
α, fission fragments, heavy ions		20-40

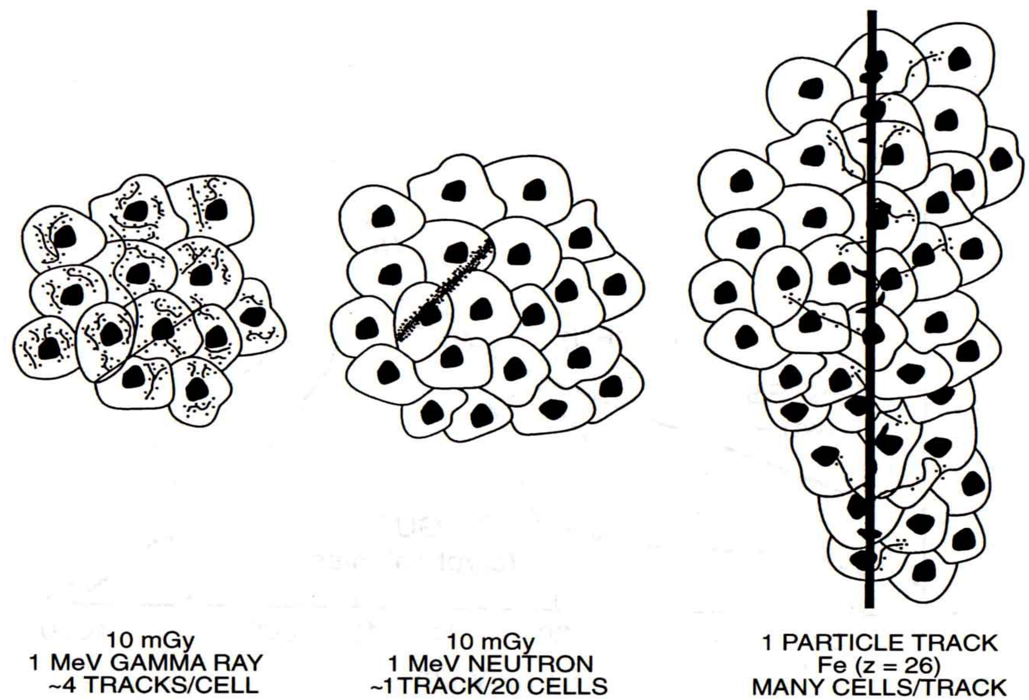

Radiation Doses

- Chest x-ray ~ .1 mSv

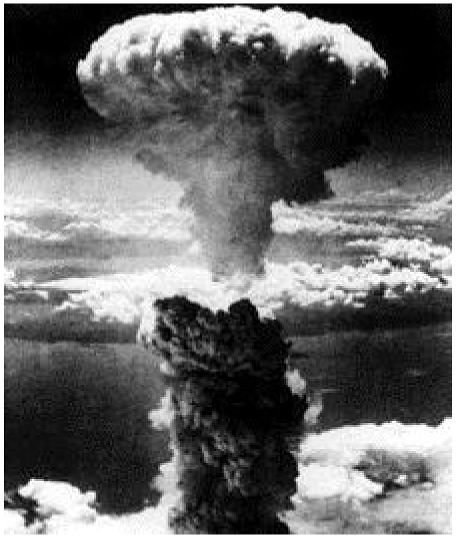

- USA background ~ 4 mSv/yr
- No observed effects(Abomb)
- <200mSv (instantaneous)
- Death > 3 Sv (instantaneous)

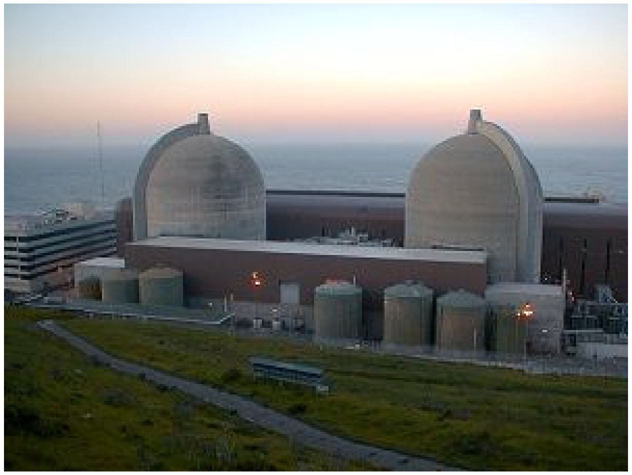

- Public annual limit < ***1 mSv/yr***
- Radiation worker limit < ***20mSv/yr***

Atmospheric Radiation Transport and Dosimetry

Brief NASA LaRC History

- Foelsche began detailed study of atmospheric ionizing radiation with possible development of HSCT (NASATN D-7715, 1974).
  - Over 300 airplane flights and 25 balloon experiments from 1965-1971
  - Theoretical program developed to extend neutron measurement to lower and higher energies
  - Neutrons found to be a major source of radiation exposure at aircraft altitudes

NASA LaRC Parametric Atmospheric Ionizing Radiation (AIR) Version 0 Model

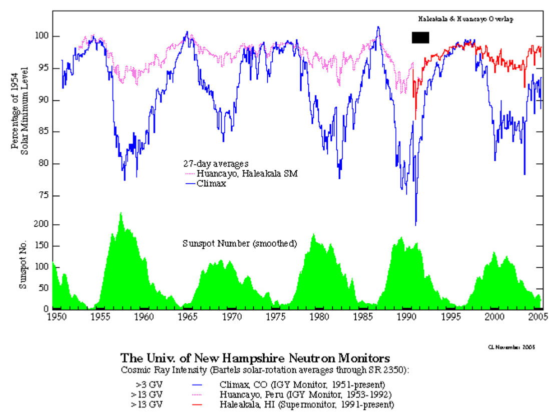

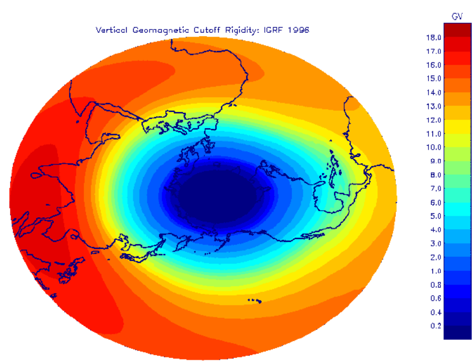

- **Development**
  - More than 300 high-altitude aircraft and 25 balloon flights over most of solar cycle 20 (1965-1971)
  - Air ionization chamber, neutron spectrometer, tissue equivalent ion chamber, nuclear emulsion
  - Monte Carlo simulations to extend neutron spectra measurements to higher and lower energies
- **Parameterization**
  - Solar Cycle → Neutron monitor measurements
  - Atmospheric Shielding → Column abundance
  - Momentum Shielding → Geomagnetic cutoff rigidities (GV)

Atmospheric Radiation Transport and Dosimetry
Brief NASA LaRC History

- **Conclusions from Foelsche Study:**
  - Exposure at supersonic altitudes is a problem
  - Exposure at subsonic altitudes is within limits for the general populations

Atmospheric Radiation Transport and Dosimetry

Renewed Interest and Concern. Why?

- **The highly ionizing components of atmospheric radiations are found to be more biologically damaging than previously assumed.**
- **The associated relative biological effectiveness for fatal cancer has been increased [*ICRU* 1986; *ICRP* 1991].**
- **Recent studies on developmental injury in mice embryos indicate large relative biological effectiveness for protection in prenatal exposures [*Jiang et al.,* 1994].**
- **Flight crews are logging greatly increased hours [*Bramlitt,* 1985; *Wilson and Townsend,* 1988; *Friedberg et al.,* 1989; *Barish,* 1990].**
- **Airline crew members are now classified as radiation workers [*McMeekin*, 1990; *ICRP* 1991].**

Global distribution of dose equivalent rate (mSv/1000 hr) predicted by the parametric AIR model at 12 km for <u>solar maximum</u> conditions (year 2000) of cycle 23.

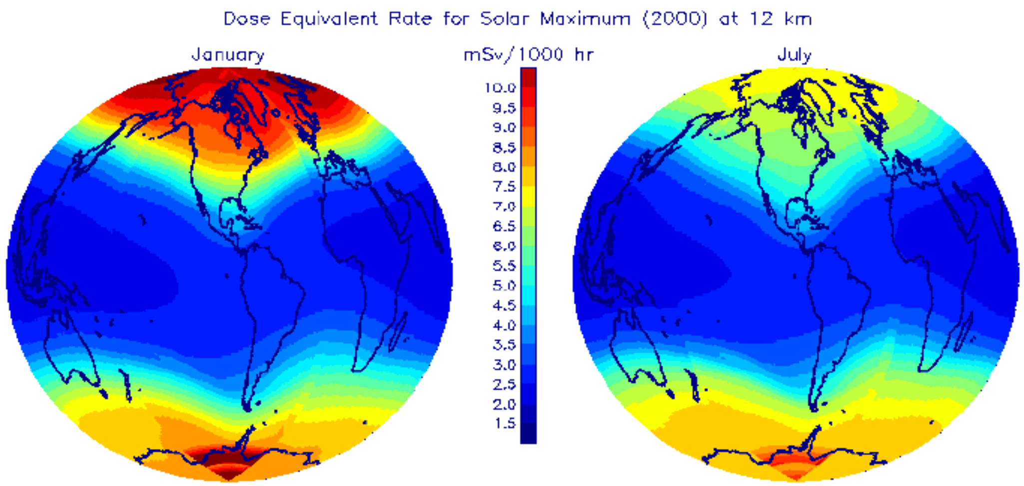

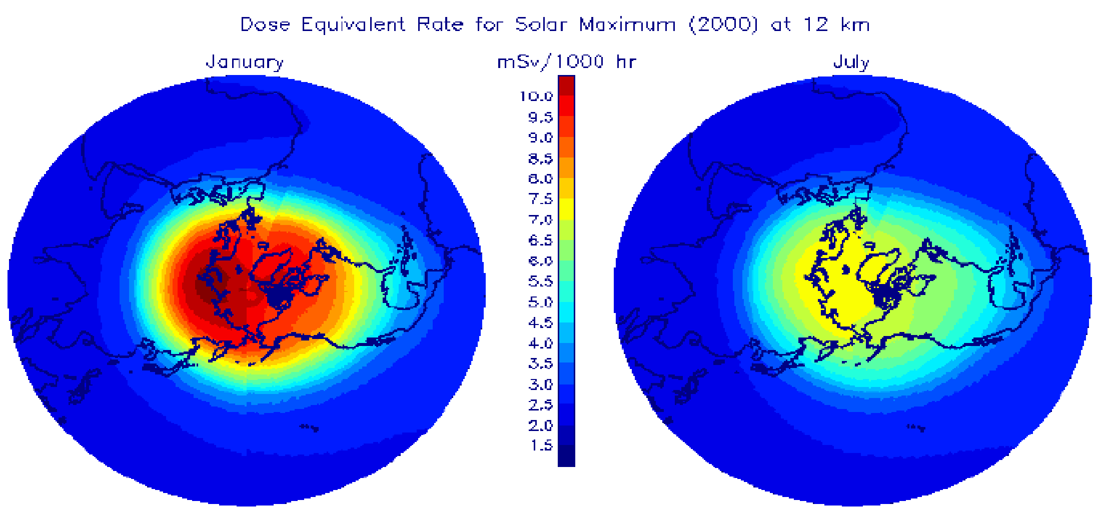

Aircrew logging 1000-hours on high-latitude flights can reach ~ 70% of recommended NCRP annual dose limit

Global distribution of dose equivalent rate (mSv/1000 hr) predicted by the parametric AIR model at 12 km for solar minimum conditions (year 1996) of cycle 23.

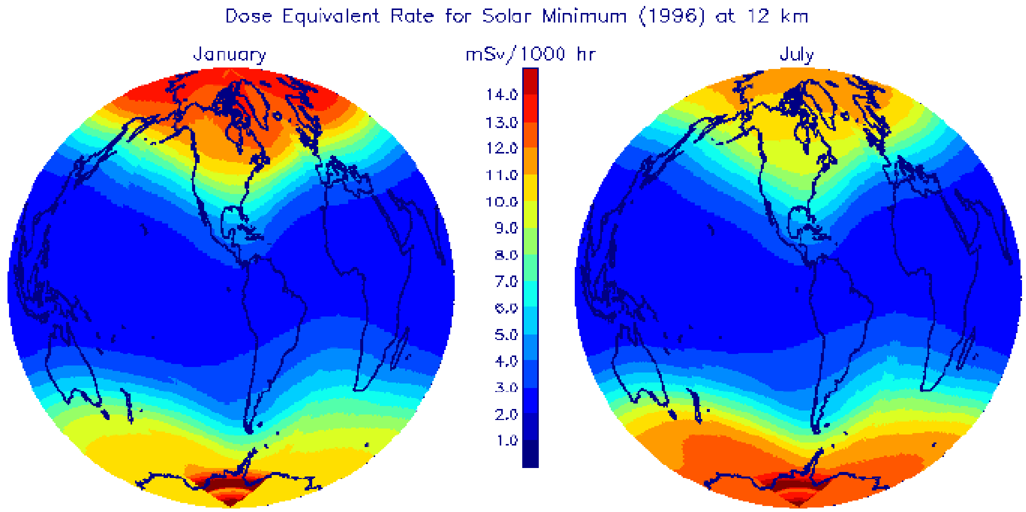

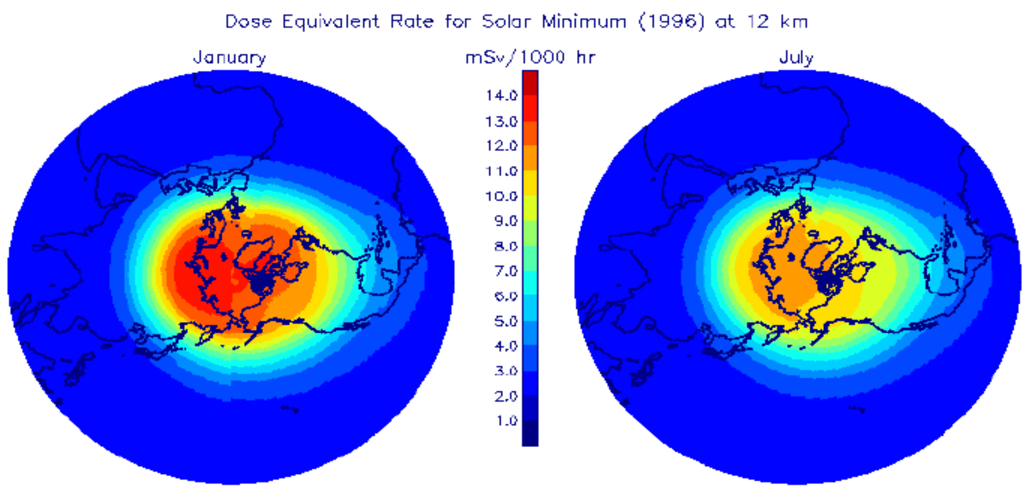

Aircrew logging 1000-hours on high-latitude flights can exceed recommended NCRP annual dose limit

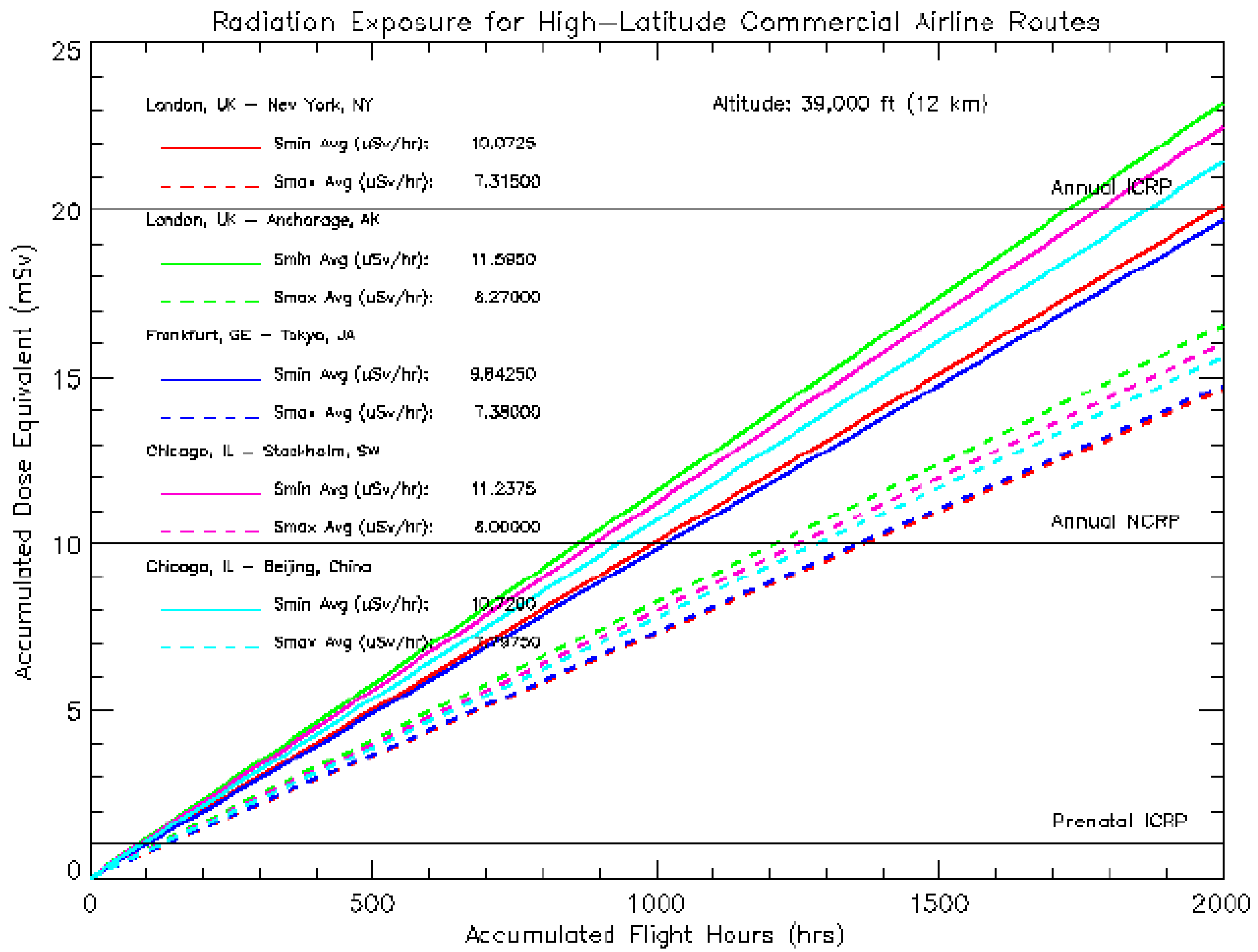

Radiation Exposure for High–Latitude Commercial Airline Routes
London, UK – Nev York, NY
Smin Avg (uSv/hr): 10.0725
Smax Avg (uSv/hr): 7.31500
London, UK – Anchorage, AK
Smin Avg (uSv/hr): 11.5850
Smax Avg (uSv/hr): 8.27000
Frankfurt, GE – Tokyo, JA
Smin Avg (uSv/hr): 9.84250
Smax Avg (uSv/hr): 7.38000
Chicago, IL – Stockholm, Sw
Smin Avg (uSv/hr): 11.2375
Smax Avg (uSv/hr): 8.00000
Chicago, IL – Beijing, China
Smin Avg (uSv/hr): 10.7200
Smax Avg (uSv/hr):
Altitude: 39,000 ft (12 km)
Annual ICRP
Annual NCRP
Prenatal ICRP
Accumulated Dose Equivalent (mSv)
Accumulated Flight Hours (hrs)
0
5
10
15
20
25
500
1000
1500
2000

Nowcast of Atmospheric Ionizing Radiation for Aviation Safety (NAIRAS)

Earth System Models

Radiation Dose Rates:

AIR (parametric)

HZETRN (physics-based)

Near-Earth Space Environment

•Badhwar/O'Neill GCR Model

•Empirical Cutoff Rigidity

(IGRF+T05)

•Physics-based Cutoff Rigidity

(LFM/CMIT+SEP-trajectory)

Earth Observations

Near-Earth Space Environment

NASA/ACE

NASA/HEAO-3

NOAA/GOES

Assimilated Atmospheric

Atmospheric Depth (NCEP/GFS)

Ground-Based

Neutron Count Monitors

Predictions/Forecasts

Ionizing Radiation Nowcast

3-D Effective Dose

3-D Differential Flux

NAIRAS Distributed Network System

High-Performance Computer Systems

Server Interface

Operational and Archival

Databases

Differential Particle Flux

HZE Particles (A=5-56)

Light-Ions (A=1-4)

Neutrons

Pions and Muons

Electromagnetic Cascasde Particles

Observations, Parameters & Products

Decision Support Systems, Assessments, Management Actions

NAIRAS decision support tool for NOAA/SEC space weather forecasts, warnings, and advisories

NAIRAS available at NOAA/ADD experimental aviation-related weather forecasts, observations, and analysis

Specific analyses to support the decision making

Predict real-time radiation exposure at commercial airline altitudes (includes background GCR and SEP events)

Provide accumulated radiation exposures for representative set of domestic, international, and polar routes

Specific Decisions / Actions

Limit aircrew flight hours to within recommended annual and career limits

Alter route and/or altitude during SEP events

Value & Benefits to Society

Improvements in the decision-making, decisions, and actions

First-ever, data-driven, real-time prediction of biologically harmful radiation exposure levels at commercial airline altitudes

Quantitative and qualitative benefits from the improved decisions

Comprehensive database of radiation dose rates to formulate recommended annual and career limits to ionizing radiation exposure

Comprehensive database of radiation dose rates for airlines to assess cost/risk of polar routes

Real-time prediction of radiation exposure levels to enable optimal balance between airline cost and air traveler health risk during solar storm (SEP) events

Improve understanding of biological effects of atmospheric ionizing radiation on aircrew and passengers through collaboration of epidemiological studies by NIOSH

Nowcast of Atmospheric Ionizing Radiation for Aviation Safety (NAIRAS) Model

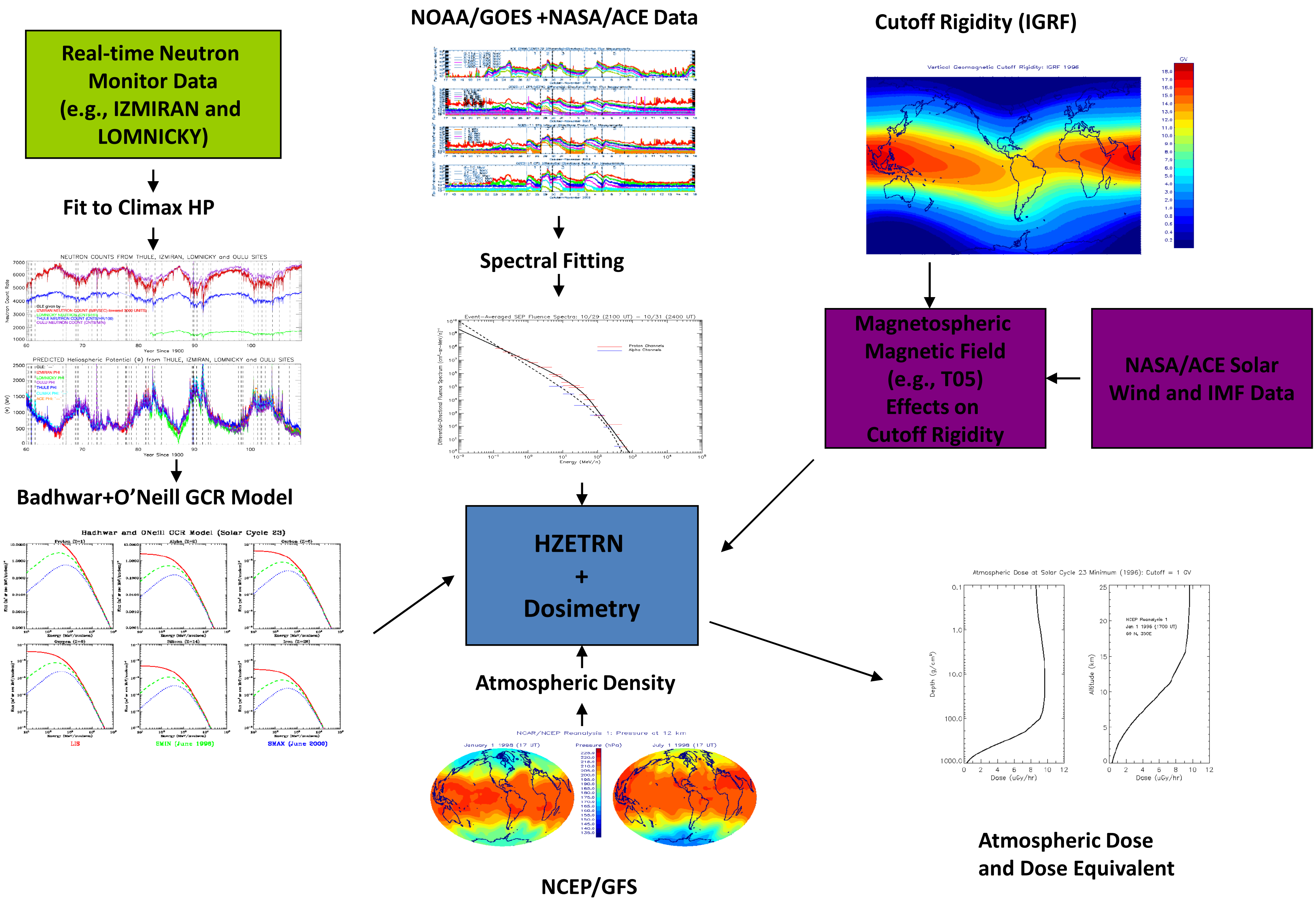

Solving for the Fluence Spectra in HZETRN

HZE Transport: Linear Boltzmann Equation

$$\boldsymbol{\Omega} \bullet \nabla \Phi_j(\mathbf{x}, \boldsymbol{\Omega}, E) = \sum_k \int \sigma_{jk}(\boldsymbol{\Omega}, \boldsymbol{\Omega}', \mathrm{E}, \mathrm{E}')\Phi_k(\mathbf{x}, \boldsymbol{\Omega}', E')d\boldsymbol{\Omega}' dE' - \sigma_j(E)\Phi_j(\mathbf{x}, \boldsymbol{\Omega}, E),$$

Total Cross Section

$$\sigma_j(E) = \sigma_{j,at}(E) + \sigma_{j,el}(E) + \sigma_{j,r}(E)$$

$\sigma_{j,at}(E) \sim 10^{-16}\ \mathrm{cm}^{-2};\ \Delta E_{at} \sim 10^{2}\ \mathrm{eV}$ **Atomic: Ion-Electron Scattering**

$\sigma_{j,el}(E) \sim 10^{-19}\ \mathrm{cm}^{-2};\ \Delta \mathrm{E}_{el} \sim 10^{6}\ \mathrm{eV}$ **Elastic Nucleon Scattering**

$\sigma_{j,r}(E) \sim 10^{-24}\ \mathrm{cm}^{-2};\ \Delta \mathrm{E}_{r} \sim 10^{8}\ \mathrm{eV}$ **Nuclear Reactions**

Methods for Solving for the Fluence Spectra $\phi_j(x,\Omega,E)$

Boltzmann Transport: Operator Form

$$\mathbf{D}\bullet\mathbf{\Phi}=\left(\mathbf{I}_{at}+\mathbf{I}_{el}+\mathbf{I}_{r}\right)\bullet\mathbf{\Phi}$$

$$\mathbf{\Phi}=[\Phi_j(\mathbf{x},\mathbf{\Omega},E)]$$ **(Vector of Particle Fields)**

$$\mathbf{D}=[\mathbf{\Omega}\bullet\nabla]$$ **(Diagonal Drift Operator)**

$$\mathbf{I}=\left[\sum_k\int\sigma_{jk}(\mathbf{\Omega},\mathbf{\Omega}',E,E')d\mathbf{\Omega}'dE'-\sigma_j(E)\right]$$

(Non-Diagonal Interaction Operator)

Perturbation Expansion

$$\sigma_{j,at}:\sigma_{j,el}:\sigma_{j,r}\Rightarrow 10^6:10^3:1$$

First Physical Perturbation: Atomic Interactions

Boltzmann Transport

$$\left[\mathbf{D} - \mathbf{I}_{at}\right] \bullet \mathbf{\Phi} = 0$$

$$\left\langle E_j(z) \right\rangle = \int E\Phi_j(z, E)dE$$

$$\left\langle E_j^2(z) \right\rangle = \int E^2\Phi_j(z, E)dE$$

Energy-Moments

$$s_j^2(z) = \left\langle E_j^2(z) \right\rangle - \left\langle E_j(z) \right\rangle^2$$

Energy Straggling

Solution Approach

Energy-Moment Expansion of Boltzmann Equation to Second-Order

First Physical Perturbation: Atomic Interactions

Solution for Mono-Energetic Ion Beam

$$\Phi_j(z,E) = \frac{1}{\sqrt{2\pi}s_j(z)} \exp\left[\frac{-\left(E-\left\langle E_j(z)\right\rangle\right)^2}{2s_j^2(z)}\right]$$

$$S_j(E) = -\frac{d\left\langle E(z)\right\rangle}{dz} = \sum_n \sigma_{jn}^{at}(E)\varepsilon_n$$ ← **Stopping Power**

$$= \frac{4\pi Z_p^2 Z_T e^4}{mv^2} N\left\{B_0 - \frac{C(\beta)}{Z_T} + Z_P L_1(\beta) + Z_P^2 L_2(\beta) + \frac{1}{2}\left[G(M_P,\beta) - \delta(\beta)\right]\right\}$$

$$B_0 = \ln\left(\frac{2mc^2\beta^2\gamma^2}{I}\right) - \beta^2$$

First Physical Perturbation: Atomic Interactions

Solution for Mono-Energetic Ion Beam

$$\Phi_j(z,E) = \frac{1}{\sqrt{2\pi}s_j(z)} \exp\left[\frac{-\left(E - \left\langle E_j(z) \right\rangle\right)^2}{2s_j^2(z)} \right]$$

$$R_j(E) = \int_0^E \frac{A_j dE'}{S_j(E')}$$ ← **Range-Energy Relation**

$$\left\langle E(z) \right\rangle = R^{-1}\left[R(E_0) - z \right]$$

$s_j(z)$ ← **Second-Order Green Function Solution**

The first physical perturbation (atomic)

Ion range/energy relation

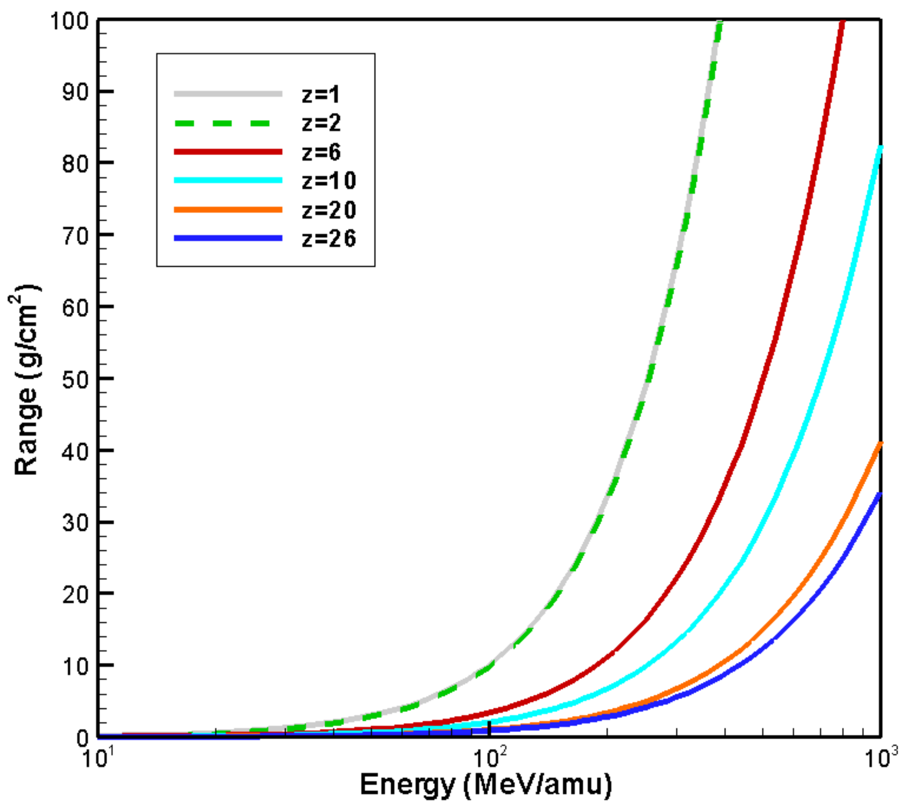

Straggling parameter for protons

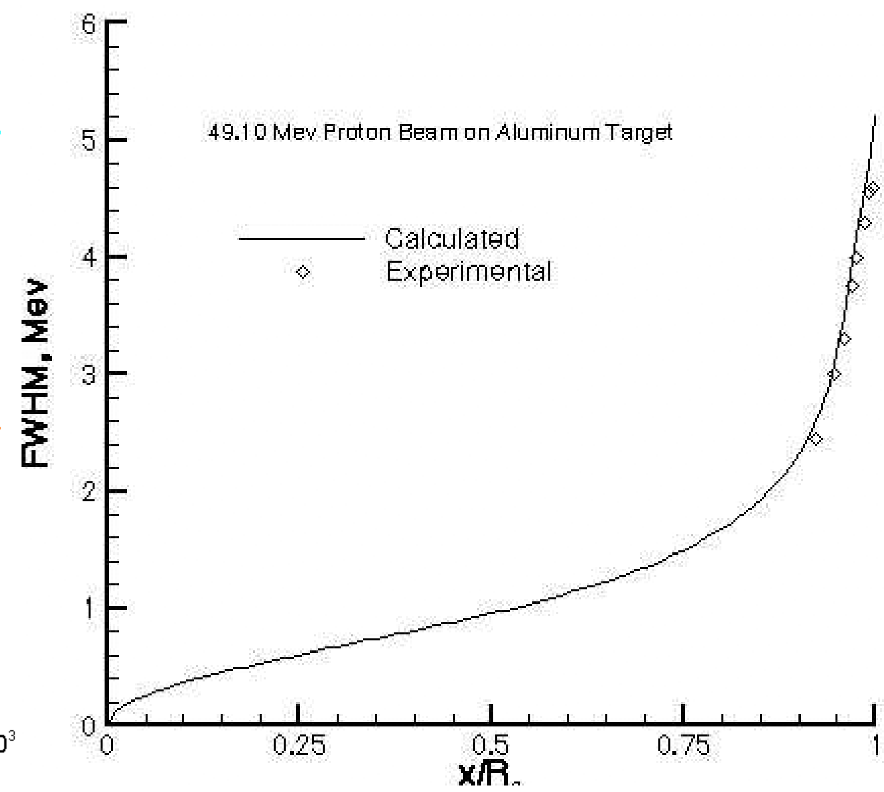

Third Physical Perturbation: Nuclear Reactions

Boltzmann Transport

$$\left[\mathbf{D} - \mathbf{I}_{at} - \mathbf{I}_{el} + \boldsymbol{\sigma}_r\right] \bullet \boldsymbol{\Phi} = \boldsymbol{\Xi}_r \bullet \boldsymbol{\Phi}$$

$$\boldsymbol{\Xi}_r = \left[\sum_k \int \sigma_{jk,r}(\boldsymbol{\Omega}, \boldsymbol{\Omega}', E, E')\, d\boldsymbol{\Omega}'\, dE'\right]$$

Integral Equation

$$\Phi_j(x, \boldsymbol{\Omega}, E) = \frac{S_j(E_\gamma)P_j(E_\gamma)}{S_j(E)P_j(E)} \Phi_j(\boldsymbol{\Gamma}_{\mathbf{x},\boldsymbol{\Omega}}, \boldsymbol{\Omega}, E_\gamma)$$

$$+ \sum_k \int_E^{E_\gamma} dE' \frac{A_j P_j(E')}{S_j(E)P_j(E)} \int_{E'}^{\infty} dE'' \int_{4\pi} d\boldsymbol{\Omega}' \sigma_{jk,r}(\boldsymbol{\Omega}, \boldsymbol{\Omega}', E', E'')$$

$$\text{x}\ \Phi_j(\mathbf{x} + (R_j(E) - R_j(E')\boldsymbol{\Omega}, \boldsymbol{\Omega}', E'')$$

Third Physical Perturbation: Nuclear Reactions

Integral Equation

$$\Phi_j(x,\mathbf{\Omega},E)=\frac{S_j(E_\gamma)P_j(E_\gamma)}{S_j(E)P_j(E)}\Phi_j(\mathbf{\Gamma}_{\mathbf{x},\mathbf{\Omega}},\mathbf{\Omega},E_\gamma)$$

$$+\sum_k\int_E^{E_\gamma}dE'\,\frac{A_jP_j(E')}{S_j(E)P_j(E)}\int_{E'}^{\infty}dE''\int_{4\pi}d\mathbf{\Omega}'\sigma_{jk,r}(\mathbf{\Omega},\mathbf{\Omega}',E',E'')$$

$$\text{x}\ \Phi_j(\mathbf{x}+(R_j(E)-R_j(E')\mathbf{\Omega},\mathbf{\Omega}',E'')$$

$$P_j(E)=\exp\left(-A_j\int_0^E\frac{\sigma_{j,r}(E')dE'}{S_j(E')}\right)$$ ← **Nuclear Survival Probability**

$$E_\gamma=R_j^{-1}\left[R_j(E)-\mathbf{\Omega}\bullet\mathbf{\Gamma}_{\mathbf{x},\mathbf{\Omega}}+\mathbf{x}\bullet\mathbf{\Omega}\right]$$

Third Physical Perturbation: Nuclear Reactions

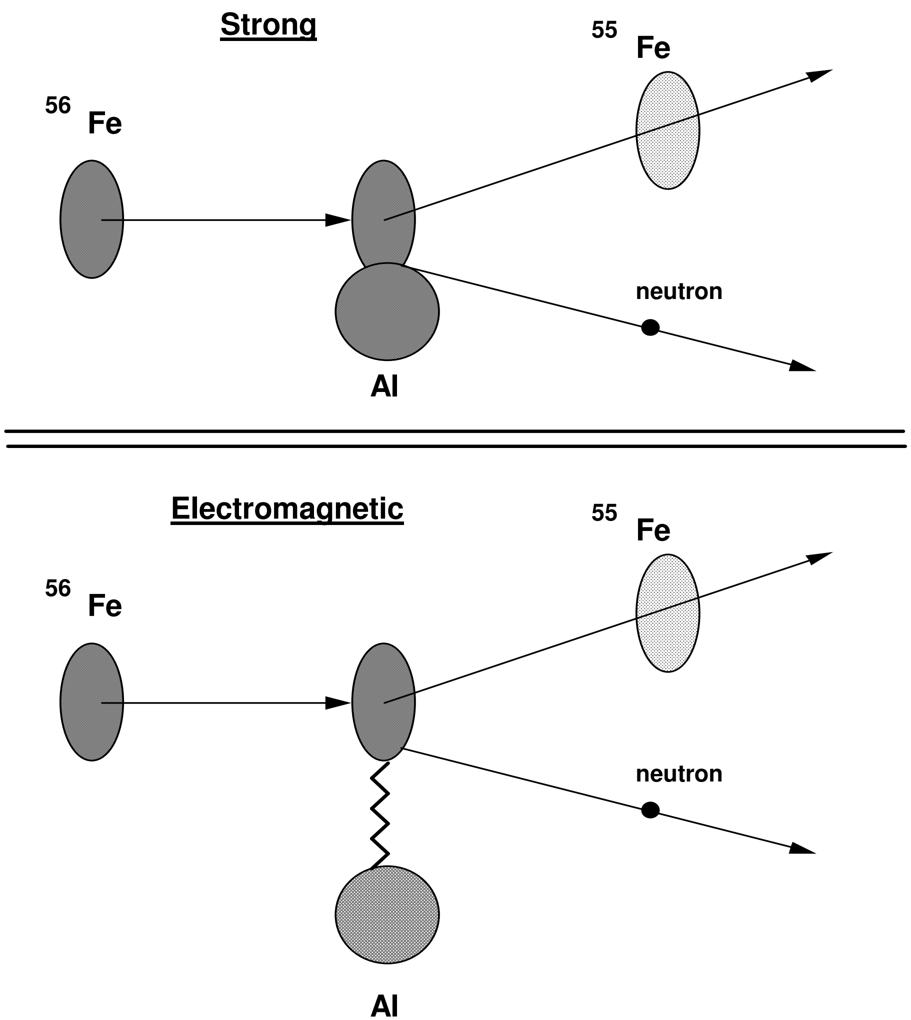

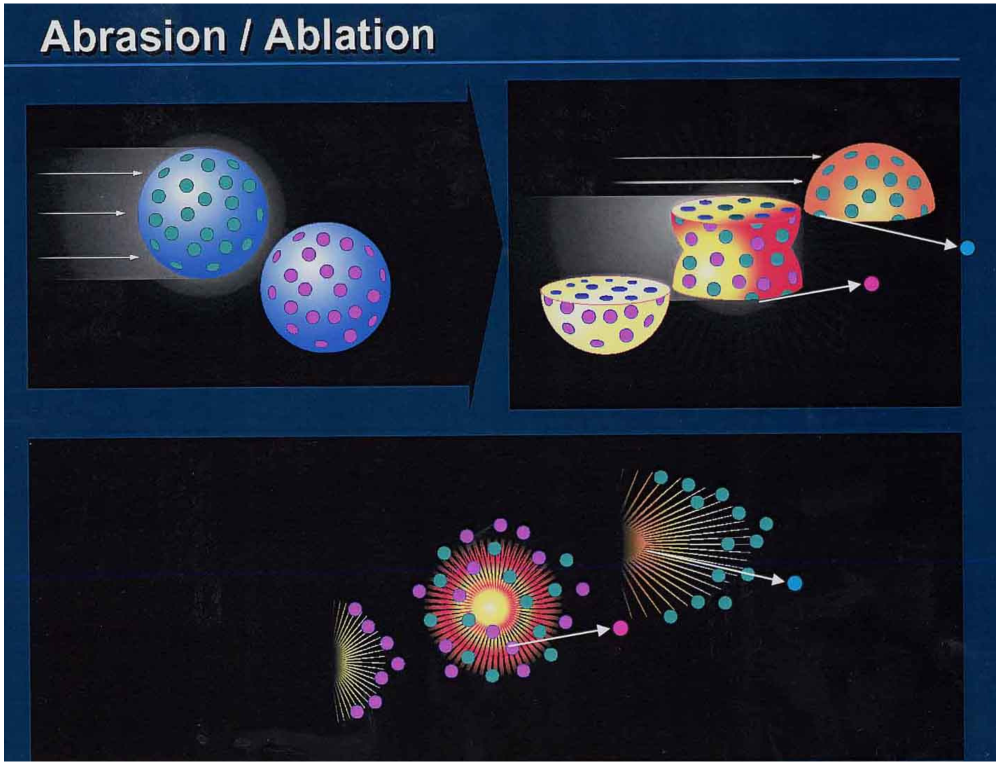

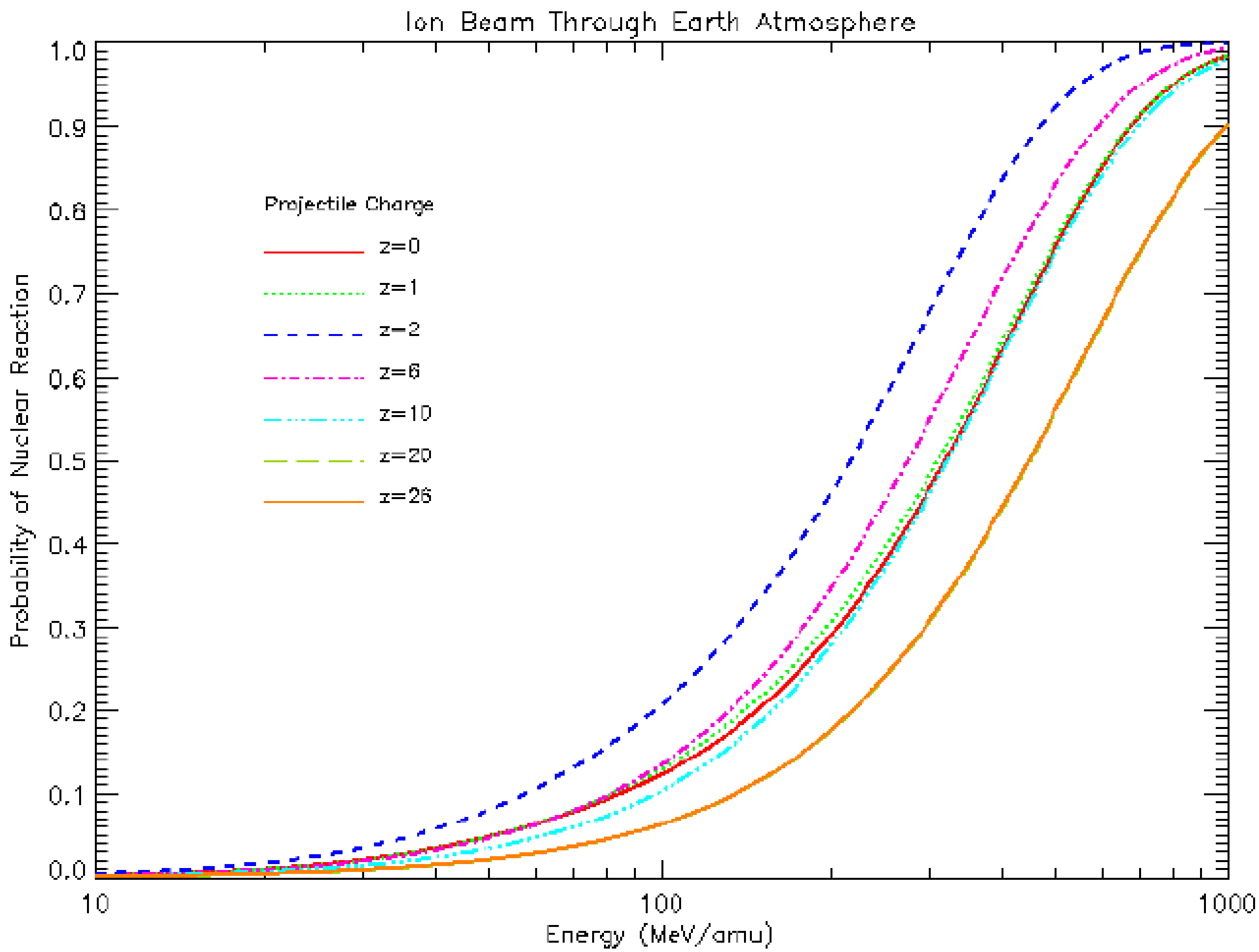
Ion Beam Through Earth Atmosphere
Probability of Nuclear Reaction
Energy (MeV/amu)
Projectile Charge
z=0
z=1
z=2
z=6
z=10
z=20
z=26
1.0
0.9
0.8
0.7
0.6
0.5
0.4
0.3
0.2
0.1
0.0
10
100
1000

Third Physical Perturbation: Nuclear Reactions

Nuclear Fragmentation in Heavy-Ion Collisions

1. Abrasion
   - Projectile and target volumes overlap
   - Nucleons sheared away in overlap region
2. Ablation
   - Projectile and target remnants form pre-fragments outside interactions zone and receive excitation energy
   - Decay by particle emission

Calculation of Fragmentation Cross Sections

1. Probability of removing a given amount of mass and charge
2. Distribution of pre-fragment excitation energies
3. Statistical decay of pre-fragments into final fragment distribution
4. Momentum distribution of light-ion fragments (p, n, d, t, h, and alpha) in the interaction zone and in the pre-fragments decay

Third Physical Perturbation: Nuclear Reactions

Heavy-Ion Beam Experiments Suggest

$$\sigma_{jk,r}(\mathbf{\Omega},\mathbf{\Omega}',E,E')=\sigma_k(E')\left[\nu_{jk}^T f_{jk}^T(\mathbf{\Omega},\mathbf{\Omega}',E,E')+\nu_{jk}^P f_{jk}^P(\mathbf{\Omega},\mathbf{\Omega}',E,E')\right]$$

$\nu_{jk}^T : \nu_{jk}^P$ **Target: Projectile Multiplicities**

Energy-Angle Probability Distribution

$$f_{jk}^P(\mathbf{\Omega},\mathbf{\Omega}',E,E')\approx\left[\frac{m}{2\pi(\Delta p_{jk}^P)^2}\right]^{3/2}\sqrt{2E}\exp\left[-\frac{\left(\sqrt{2mE}\mathbf{\Omega}-\sqrt{2mE'}\mathbf{\Omega}'\right)^2}{2(\Delta p_{jk}^P)^2}\right]$$

$$f_{jk}^T(\mathbf{\Omega},\mathbf{\Omega}',E,E')\approx\left[\frac{m}{2\pi(\Delta p_{jk}^T)^2}\right]^{3/2}\sqrt{2E}\exp\left[-\frac{mE'}{(\Delta p_{jk}^T)^2}\right]$$

Schematic of Particle Transport

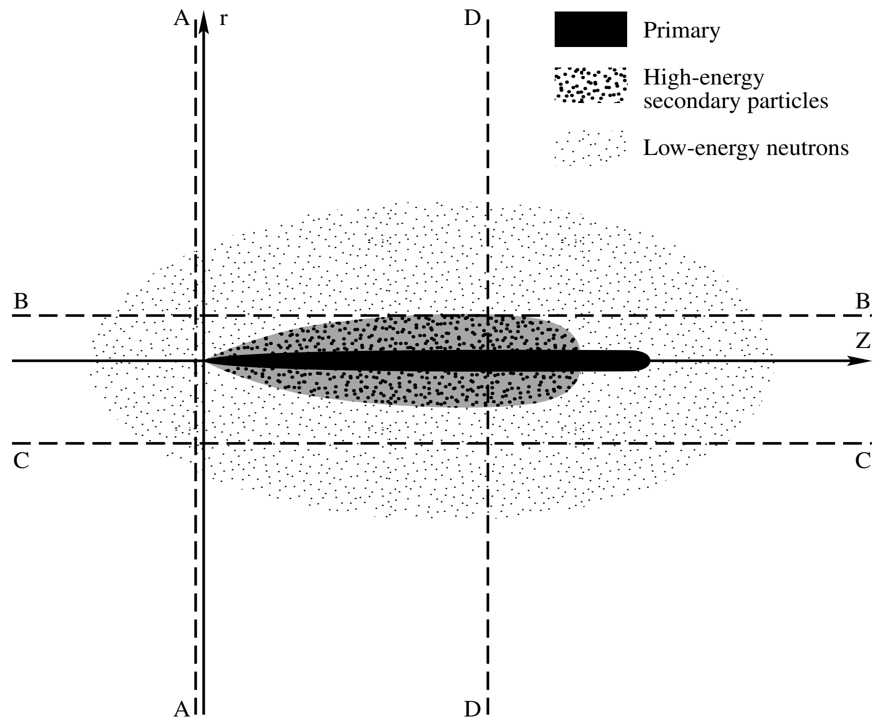

Angular distributions

The nuclear cross sections represented as

$$\sigma_{jk,r}(\Omega,\Omega',E,E') = \sigma_{jk,iso}(E,E')/4\pi + \sigma_{jk,for}(\Omega,\Omega',E,E')$$

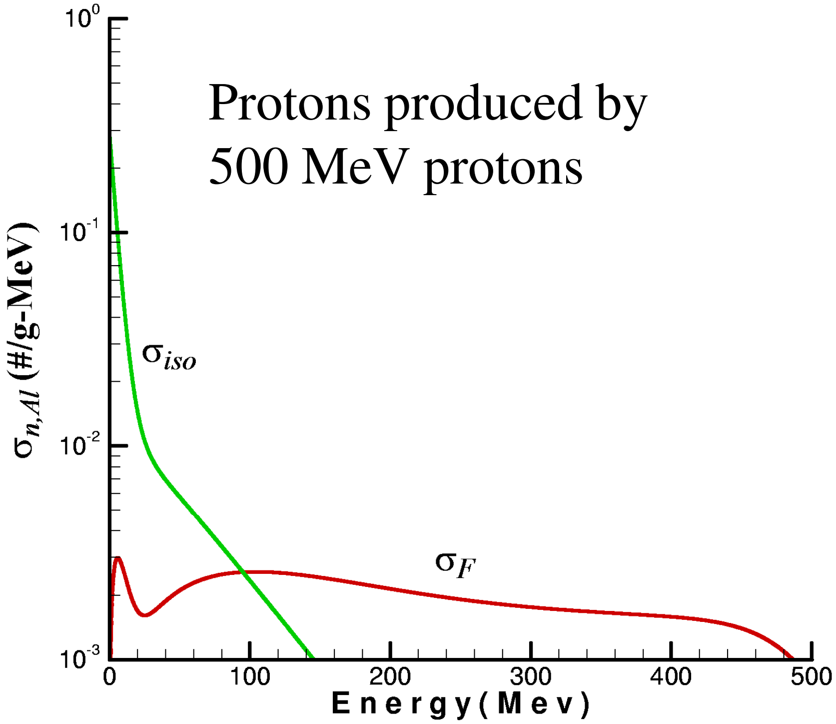

Transverse fragment spread from $A_P = 40$

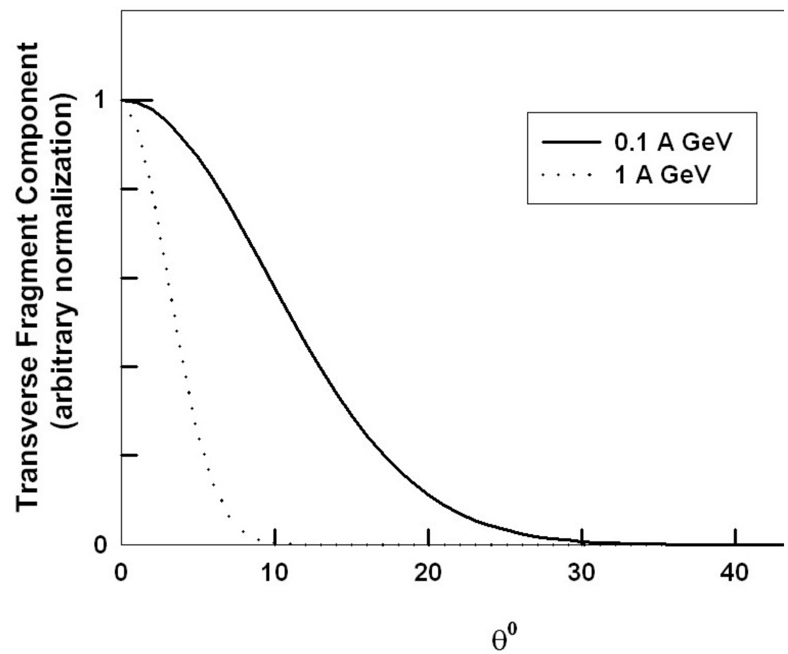

Notes: Angular spread from multiple scattering ≈ 0.06 degree and is small

Diffuse ion components are of low energy and limited range

Third Physical Perturbation: Nuclear Reactions

Secondary-Particle Transport Approximations

1. **Production of Projectile Fragments Dominate**

    Production of target fragments much smaller than production of projectile fragments

$$E \gg (\Delta p_{jk}^{T})^2 / m$$

2. **Straight-Ahead Approximation**

$$f_{jk}^{P}(\mathbf{\Omega},\mathbf{\Omega}',E,E') = f_{jk}^{P}(E,E')\,\delta\left(\mathbf{\Omega}\bullet\mathbf{\Omega}'-1\right)$$

$$\frac{2mE}{\left(\Delta p_{jk}^{P}\right)^2} \gg \frac{\left[\mathbf{\Omega}\bullet\dfrac{\partial}{\partial\mathbf{\Omega}}\Phi_k(x,\mathbf{\Omega},E)\right]}{\Phi(x,\mathbf{\Omega},E)}$$

Third Physical Perturbation: Nuclear Reactions

Decoupling of Target Fragments

1. **High-Energy Heavy-Ion Fragments**

$$\left[\mathbf{D} - \mathbf{I}_{at} - \mathbf{I}_{el} + \boldsymbol{\sigma}_{r}\right] \bullet \boldsymbol{\Phi}_{for} = \boldsymbol{\Xi}_{r,for} \bullet \boldsymbol{\Phi}_{for}$$

$$\boldsymbol{\Xi}_{r,for} = \left[\sum_{k} \int \sigma_{jk,r}^{for}(\boldsymbol{\Omega}, \boldsymbol{\Omega}', E, E')\, d\boldsymbol{\Omega}' dE'\right]$$

2. **Low-Energy Light-Ion Fragments**

$$\left[\mathbf{D} - \mathbf{I}_{at} - \mathbf{I}_{el} + \boldsymbol{\sigma}_{r}\right] \bullet \boldsymbol{\Phi}_{iso} = \boldsymbol{\Xi}_{r} \bullet \boldsymbol{\Phi}_{iso} + \boldsymbol{\Xi}_{r,iso} \bullet \boldsymbol{\Phi}_{for}$$

$$\boldsymbol{\Xi}_{r,iso} = \left[\sum_{k} \int \sigma_{jk,r}^{iso}(\boldsymbol{\Omega}, \boldsymbol{\Omega}', E, E')\, d\boldsymbol{\Omega}' dE'\right]$$

Third Physical Perturbation: Nuclear Reactions

High-Energy Heavy-Ion Transport

$$\Phi_j^{for}(x,\mathbf{\Omega},E) = \frac{S_j(E_\gamma)P_j(E_\gamma)}{S_j(E)P_j(E)}\Phi_j^{for}(\mathbf{\Gamma}_{\mathbf{x},\mathbf{\Omega}},\mathbf{\Omega},E_\gamma)$$

$$+\sum_k \int_E^{E_\gamma} dE' \frac{A_j P_j(E')}{S_j(E)P_j(E)} \int_{E'}^{\infty} dE'' \sigma_{jk,r}^{for}(E',E'')$$

$$\text{x}\ \Phi_j^{for}(\mathbf{x}+(R_j(E)-R_j(E')\mathbf{\Omega},E'')$$

Rapidly Convergent Neumann Series

$$\mathbf{\Phi}_{for} = \left[\mathbf{G}+\mathbf{G}\bullet\mathbf{\Xi}_{r,for}\bullet\mathbf{G}+\mathbf{G}\bullet\mathbf{\Xi}_{r,for}\bullet\mathbf{G}\bullet\mathbf{\Xi}_{r,for}\bullet\mathbf{G}+\cdots\right]\bullet\mathbf{\Phi}_B$$

$$\mathbf{G} = \left[\mathbf{D}-\mathbf{I}_{at}-\mathbf{I}_{el}+\boldsymbol{\sigma}_r\right]^{-1}$$

Solving for the Fluence Spectra $\phi_j(x,\Omega,E)$ *cont'*

More facts relative to solving the Boltzmann equation

Range/energy relations

Probability of nuclear reaction

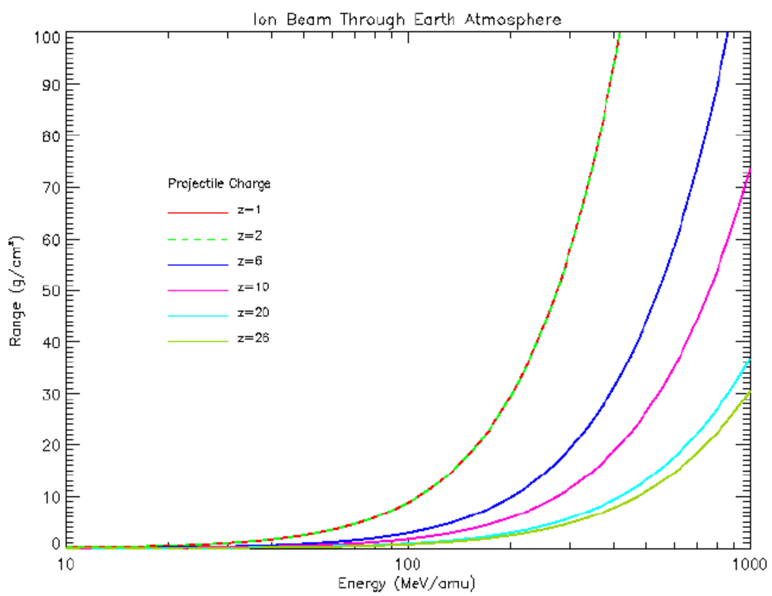

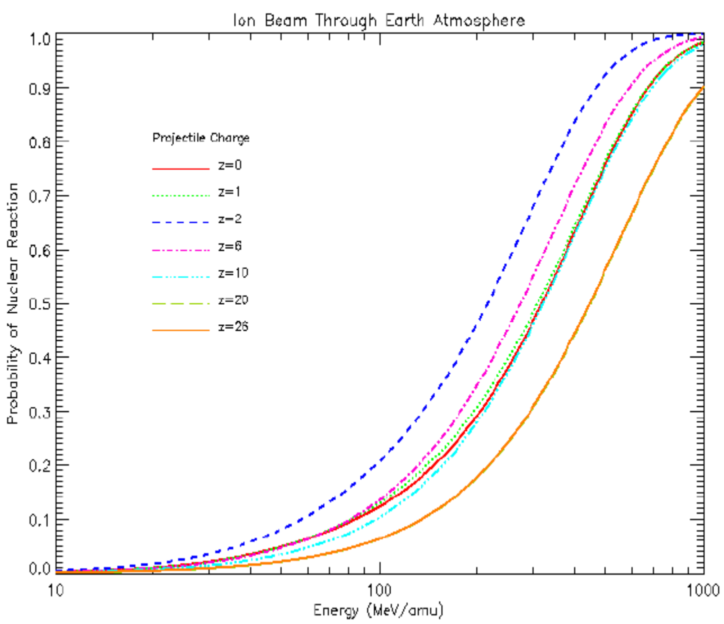

Low energy ions have limited range of penetration giving rise to rapid convergence of the Neumann series solution

Low energy ions have few nuclear reactions so the Neumann series converges rapidly

Light-Ion and Neutron Transport Code Development

- High-energy neutrons obtained from the solution of the "*for*" component
  - Converges more slowly since not range-limited by atomic interactions
- Light-Ions obtained from the solution of the "*iso*" component without nuclear reaction
- Low-energy neutrons obtained from the solution of the "*iso*" component with nuclear reactions included

Third Physical Perturbation: Nuclear Reactions

Low-Energy Light-Ion Fragments

$$\boldsymbol{\Xi}_r \bullet \boldsymbol{\Phi}_{iso} \ll \boldsymbol{\Xi}_{r,iso} \bullet \boldsymbol{\Phi}_{for}$$

$$\left[\mathbf{D} - \mathbf{I}_{at} - \mathbf{I}_{el} + \boldsymbol{\sigma}_r\right] \bullet \boldsymbol{\Phi}_{iso} \approx \boldsymbol{\Xi}_{r,iso} \bullet \boldsymbol{\Phi}_{for}$$

$$\Phi_j^{iso}(x, \boldsymbol{\Omega}, E) = \sum_k \int_E^{E_\gamma} dE' \frac{A_j P_j(E')}{S_j(E) P_j(E)} \int_{E'}^{\infty} dE'' \sigma_{jk,r}^{iso}(E', E'')$$

$$\text{x } \Phi_j^{for}(\mathbf{x} + (R_j(E) - R_j(E')\boldsymbol{\Omega}, E'')$$

Third Physical Perturbation: Nuclear Reactions

Low-Energy Neutron Transport

$$[\mathbf{D} + \boldsymbol{\sigma}_r] \bullet \boldsymbol{\Phi}_{n,iso} = \boldsymbol{\Xi}_{n,r} \bullet \boldsymbol{\Phi}_{n,iso} + \boldsymbol{\Xi}_{r,iso} \bullet \boldsymbol{\Phi}_{for}$$

$$\boldsymbol{\Phi}_{n,iso} = \boldsymbol{\Phi}^0_{n,iso} + \boldsymbol{\Phi}^1_{n,iso}$$

Coupled Neutron Transport Equations

$$[\mathbf{D} + \boldsymbol{\sigma}_r] \bullet \boldsymbol{\Phi}^0_{n,iso} = \boldsymbol{\Xi}_{r,iso} \bullet \boldsymbol{\Phi}_{for}$$

$$[\mathbf{D} + \boldsymbol{\sigma}_r] \bullet \boldsymbol{\Phi}^1_{n,iso} = \boldsymbol{\Xi}_{n,r} \bullet (\boldsymbol{\Phi}^1_{n,iso} + \boldsymbol{\Phi}^0_{n,iso})$$

Third Physical Perturbation: Nuclear Reactions

Low-Energy Neutron Transport

$$\Phi^{0}_{n,iso}(\mathbf{x},\mathbf{\Omega},E)=\sum_{k}\int_{0}^{d_\gamma}dx'\exp[-\sigma_n(E)x']\int_{E'}^{\infty}dE''\int_{4\pi}\sigma^{iso}_{nk,r}(\mathbf{\Omega},\mathbf{\Omega}',E',E'')$$

$$\text{x }\Phi^{for}_{j}(\mathbf{x}-x'\mathbf{\Omega},\mathbf{\Omega}'E'')$$

$$d_\gamma=\mathbf{x}\bullet\mathbf{\Omega}-\mathbf{\Gamma}_{\mathbf{x},\mathbf{\Omega}}\bullet\mathbf{\Omega}$$

$$[\mathbf{\Omega}\bullet\nabla+\sigma_n(E)]\Phi^{1}_{n,iso}(\mathbf{x},\mathbf{\Omega},E)=\int\sigma_n(\mathbf{\Omega},\mathbf{\Omega}',E,E')\Phi^{1}_{n,iso}(\mathbf{x},\mathbf{\Omega}',E')d\mathbf{\Omega}'dE'$$

$$+\int\sigma_n(\mathbf{\Omega},\mathbf{\Omega}',E,E')\Phi^{0}_{n,iso}(\mathbf{x},\mathbf{\Omega}',E')d\mathbf{\Omega}'dE'$$

Nowcast of Atmospheric Ionizing Radiation for Aviation Safety (NAIRAS) Model

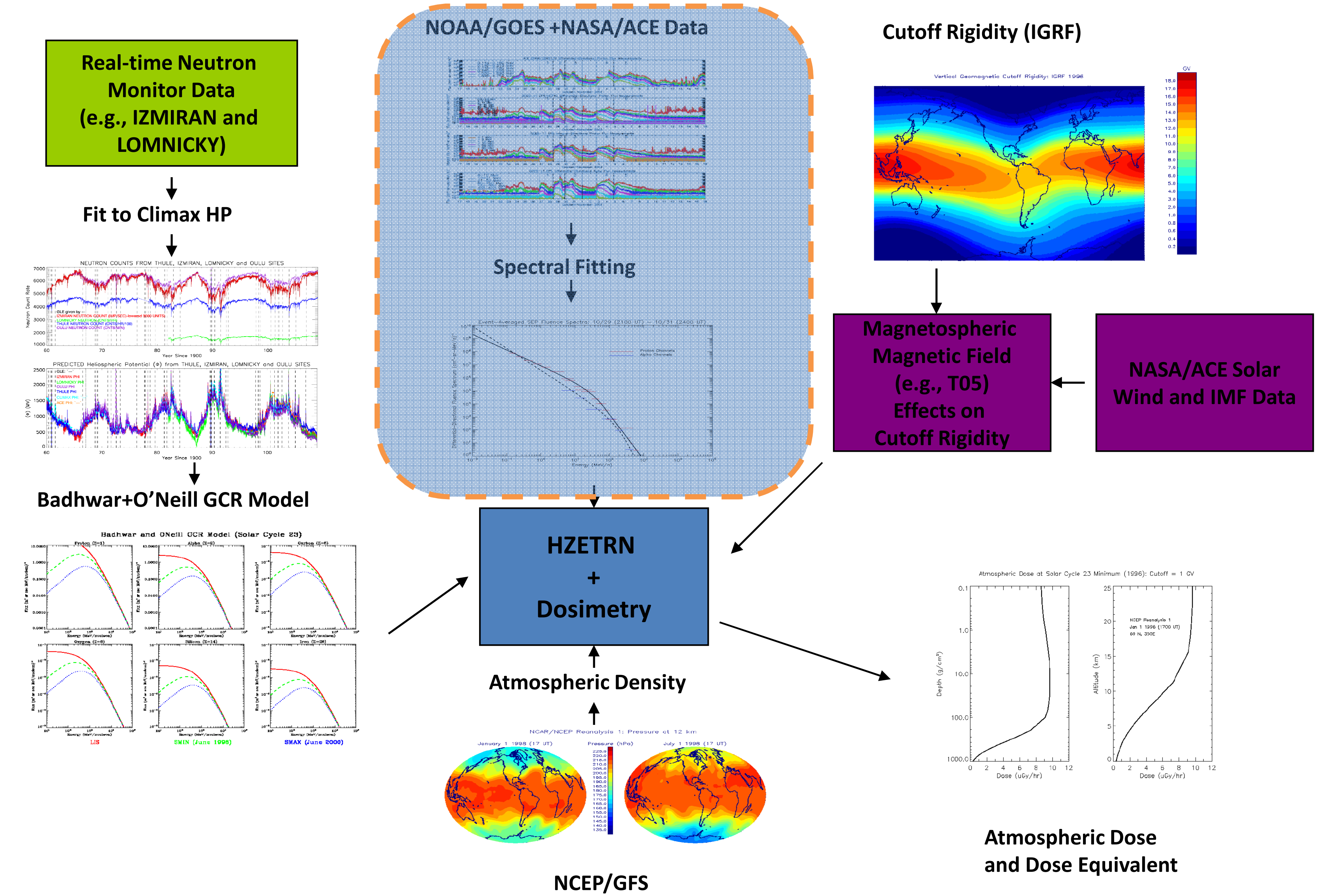

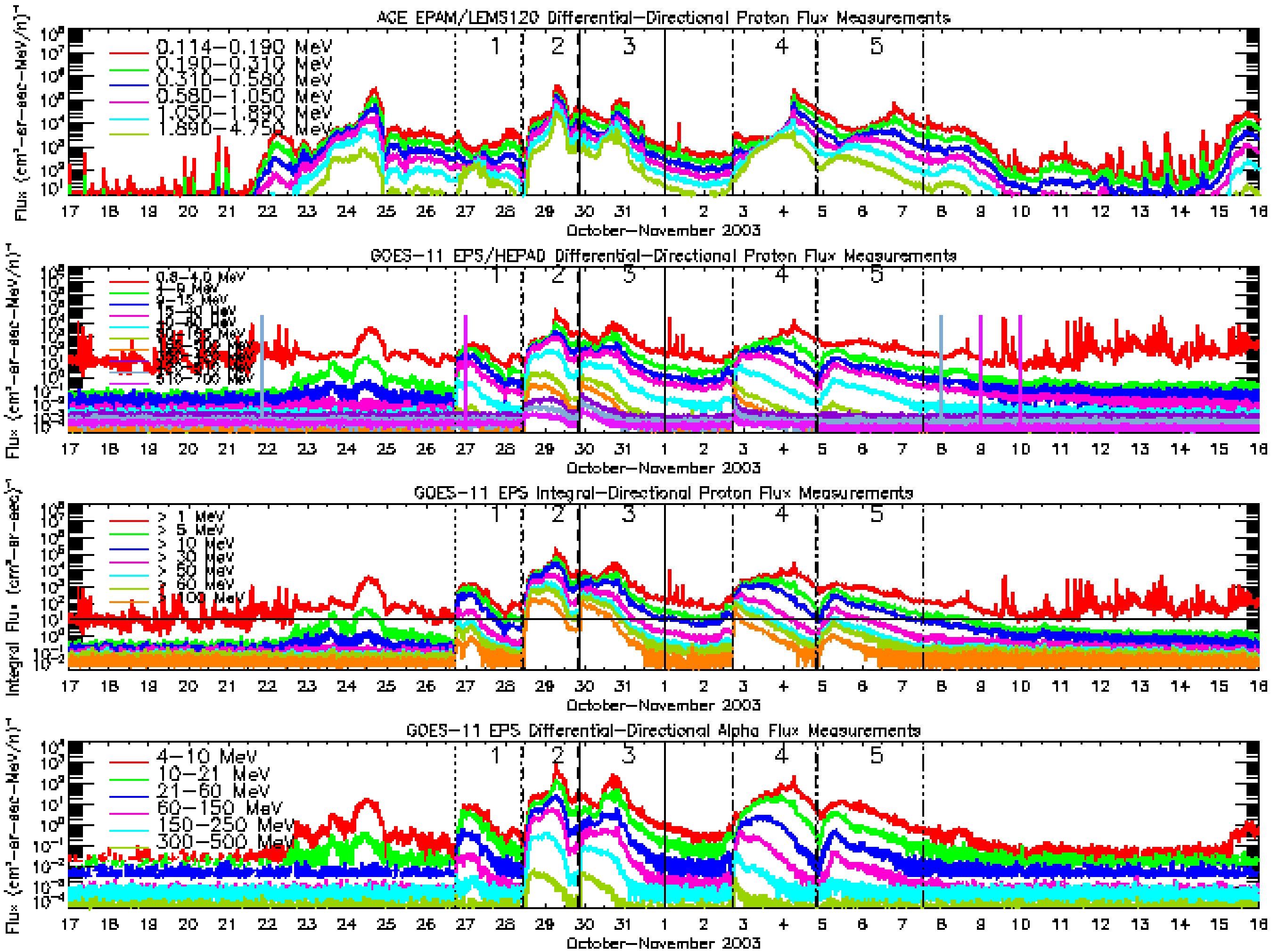
ACE EPAM/LEMS120 Differential-Directional Proton Flux Measurements
0.114–0.190 MeV
0.190–0.310 MeV
0.310–0.580 MeV
0.580–1.050 MeV
1.050–1.890 MeV
1.890–4.750 MeV
Flux (cm²-sr-sec-MeV/n)⁻¹
1
2
3
4
5
October–November 2003
GOES-11 EPS/HEPAD Differential-Directional Proton Flux Measurements
0.8–4.0 MeV
4–9 MeV
9–15 MeV
510–700 MeV
Flux (cm²-sr-sec-MeV/n)⁻¹
October–November 2003
GOES-11 EPS Integral-Directional Proton Flux Measurements
> 1 MeV
> 5 MeV
> 10 MeV
> 30 MeV
> 50 MeV
> 60 MeV
> 100 MeV
Integral Flux (cm²-sr-sec)⁻¹
October–November 2003
GOES-11 EPS Differential-Directional Alpha Flux Measurements
4–10 MeV
10–21 MeV
21–60 MeV
60–150 MeV
150–250 MeV
300–500 MeV
Flux (cm²-sr-sec-MeV/n)⁻¹
October–November 2003

SEP Fluence Spectra

- **Stochastic acceleration mechanism for particles in a turbulent magnetic field associated with an interplanetary shock**
- **Ellison and Ramaty ansatz [1985] (see Tylka [2005])**

$$dJ/dE = CE^{-\gamma}\exp(-E/E_0)$$

C : **Abundance of suprathermal seed population: corona (solar wind) + flare**

γ : Power law: acceleration in turbulent magnetic field
Power index: function of shock compression ratio

$$E_0 = E_{00}[Q/A][\sec\theta_{Bn}]^{2/(2\gamma-1)}$$ **Spatial diffusion: escape from shock**

θ_{Bn} : **Angle between shock normal and upstream B-field**

$$\theta_{Bn}(\text{limit}) = 0^o$$ **Corona seed**

$$\theta_{Bn}(\text{limit}) = 90^o$$ **Flare seed**

SEP Fluence Spectra

- Ellison & Ramaty single power-law did not fit Halloween 2003 high-energy SEP fluence spectra
- Propose double power-law spectrum [Mewaldt, 2003]
  - Two independent sources of seed population (Tylka [2005])

$$dJ/dE = CE^{-\gamma_a} \exp(-E/E_0)$$ e.g., corona seed

$$dJ/dE = DE^{-\gamma_b}$$ e.g., flare seed

Require power-law functions and first derivatives continuous at merge energy

$$dJ/dE = CE^{-\gamma_a} \exp(-E/E_0) \text{ for } E \le (\gamma_b - \gamma_a)E_0$$

$$dJ/dE = CE^{-\gamma_b} \left\{ \left[(\gamma_b - \gamma_a)E_0 \right]^{(\gamma_b - \gamma_a)} \exp(\gamma_a - \gamma_b) \right\} \text{ for } E > (\gamma_b - \gamma_a)E_0,$$

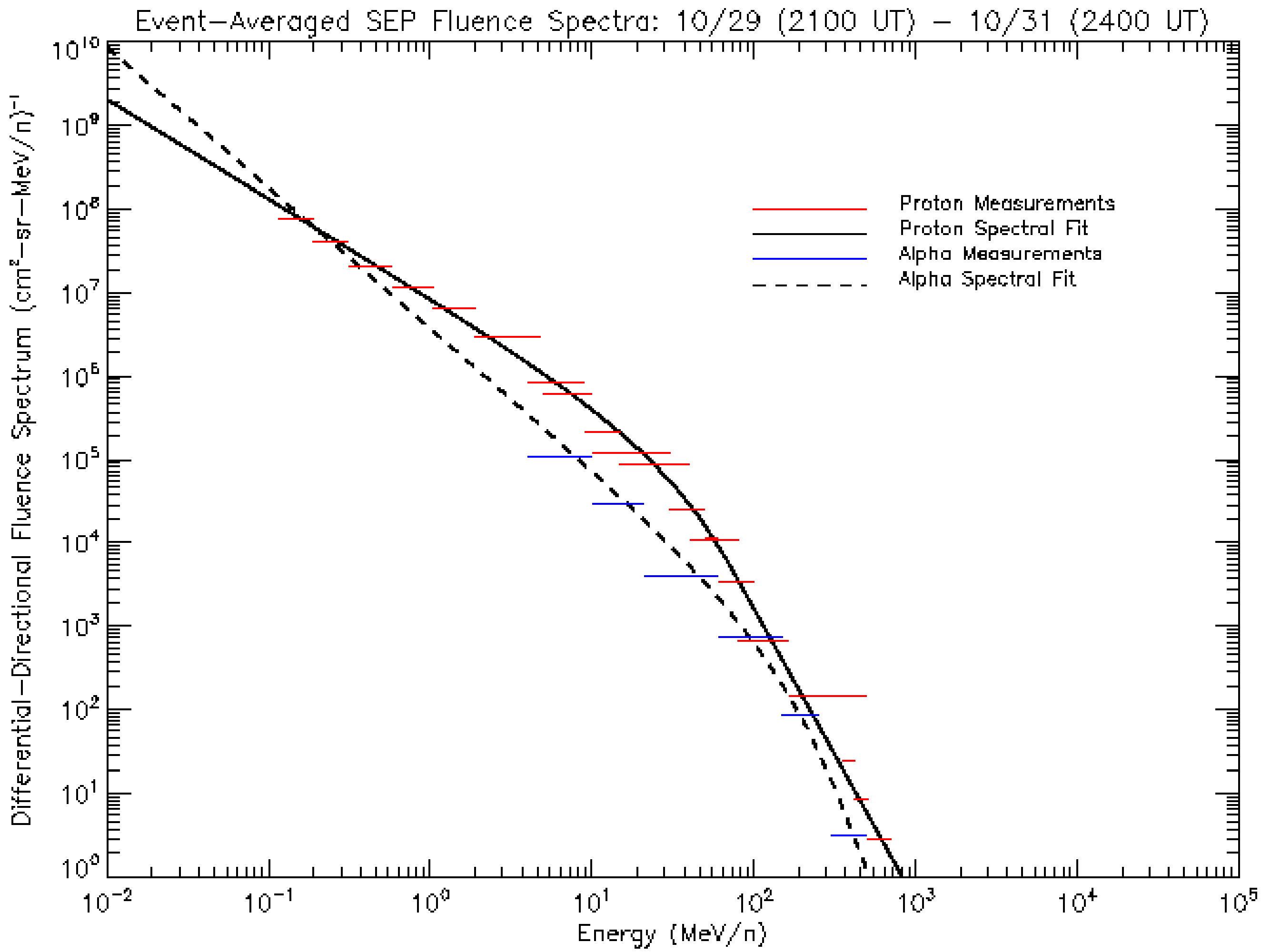

Event-Averaged SEP Fluence Spectra: 10/29 (2100 UT) – 10/31 (2400 UT)
Differential-Directional Fluence Spectrum (cm²-sr-MeV/n)⁻¹
Energy (MeV/n)
Proton Measurements
Proton Spectral Fit
Alpha Measurements
Alpha Spectral Fit

Zero Cutoff

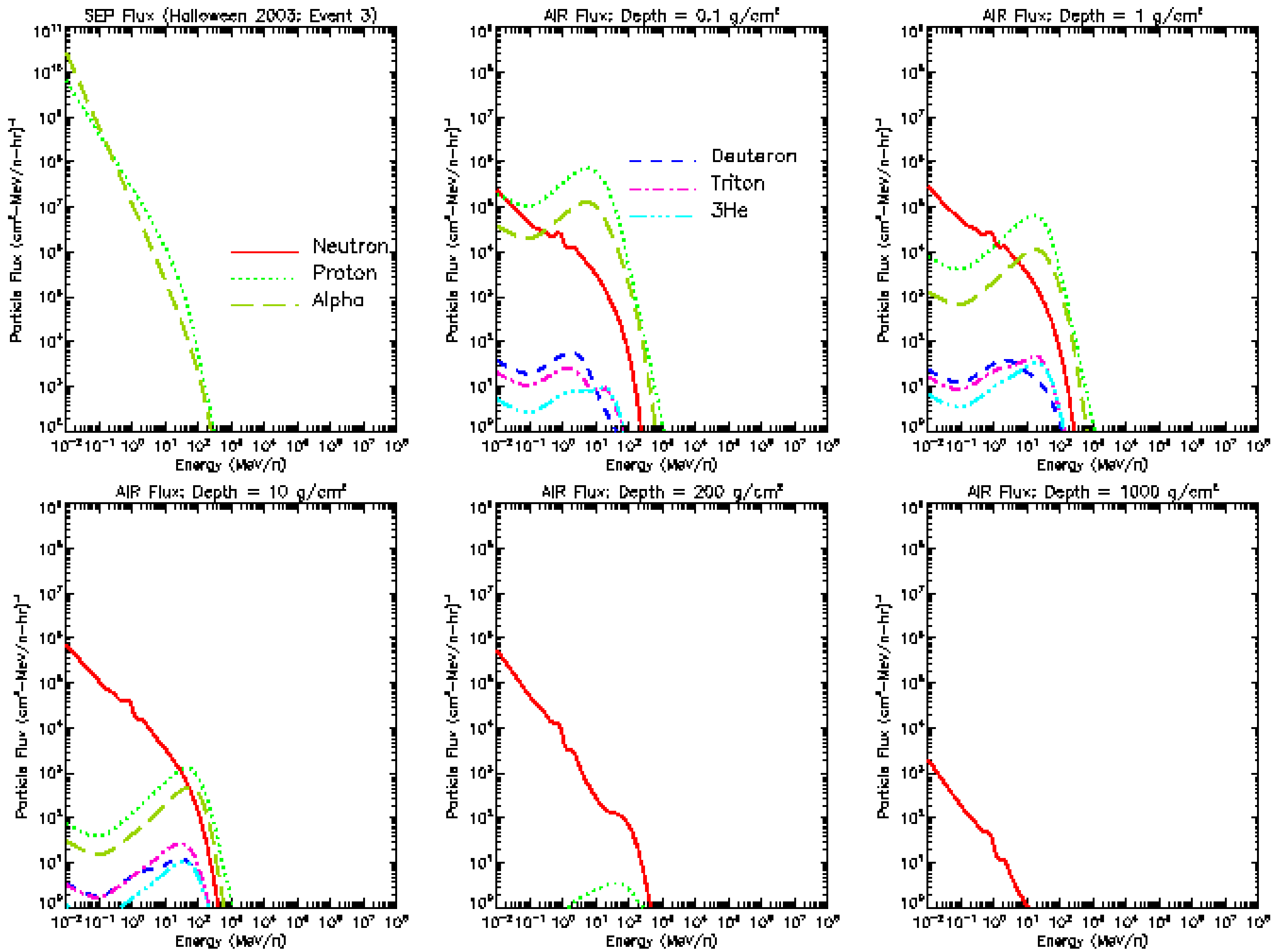
SEP Flux (Halloween 2003; Event 3)
AIR Flux; Depth = 0.1 g/cm²
AIR Flux; Depth = 1 g/cm²
AIR Flux; Depth = 10 g/cm²
AIR Flux; Depth = 200 g/cm²
AIR Flux; Depth = 1000 g/cm²
Particle Flux (cm²-MeV/n-hr)⁻¹
Energy (MeV/n)
Neutron
Proton
Alpha
Deuteron
Triton
3He

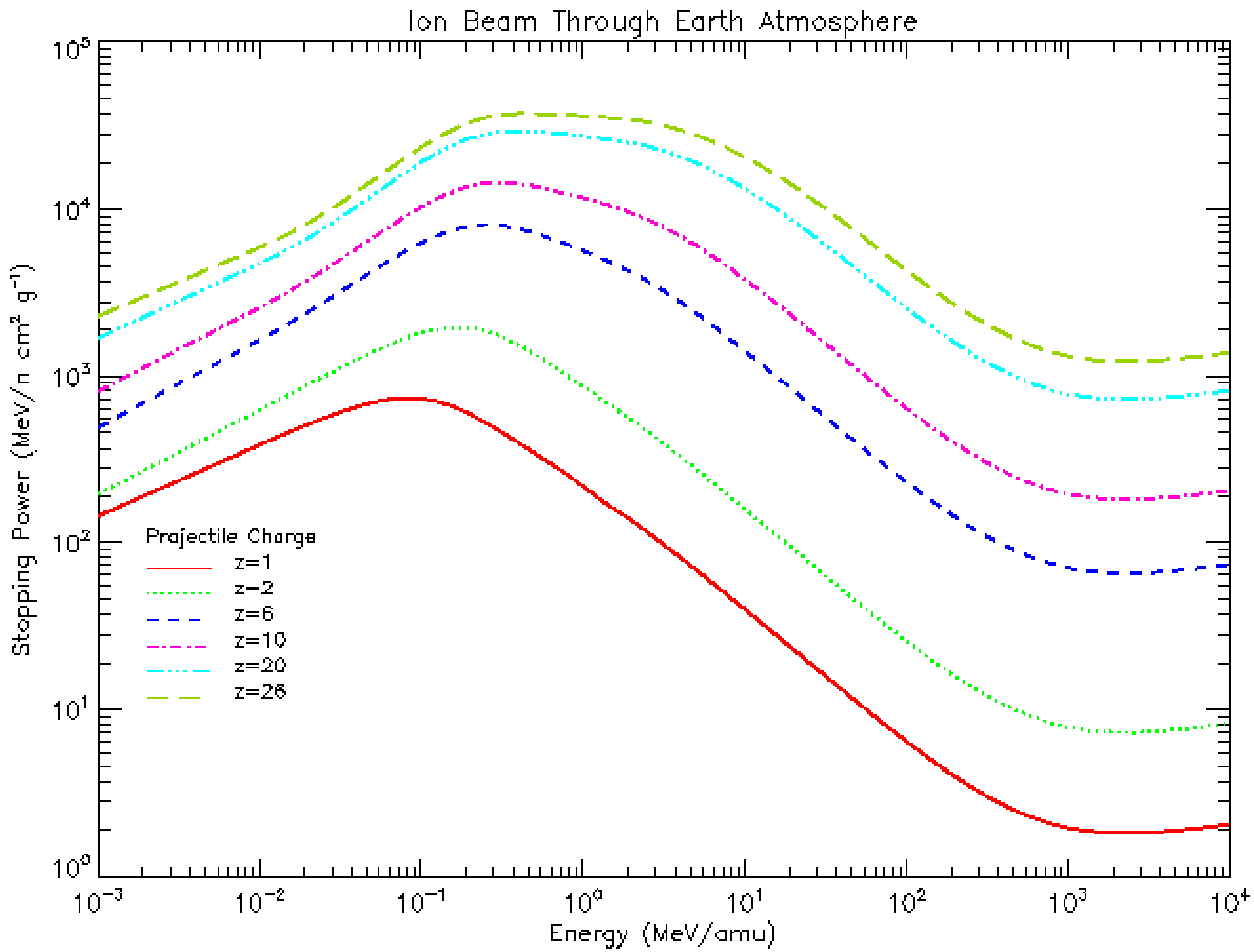

Ion Beam Through Earth Atmosphere
Stopping Power (MeV/n cm² g⁻¹)
Energy (MeV/amu)
Projectile Charge
z=1
z=2
z=6
z=10
z=20
z=26

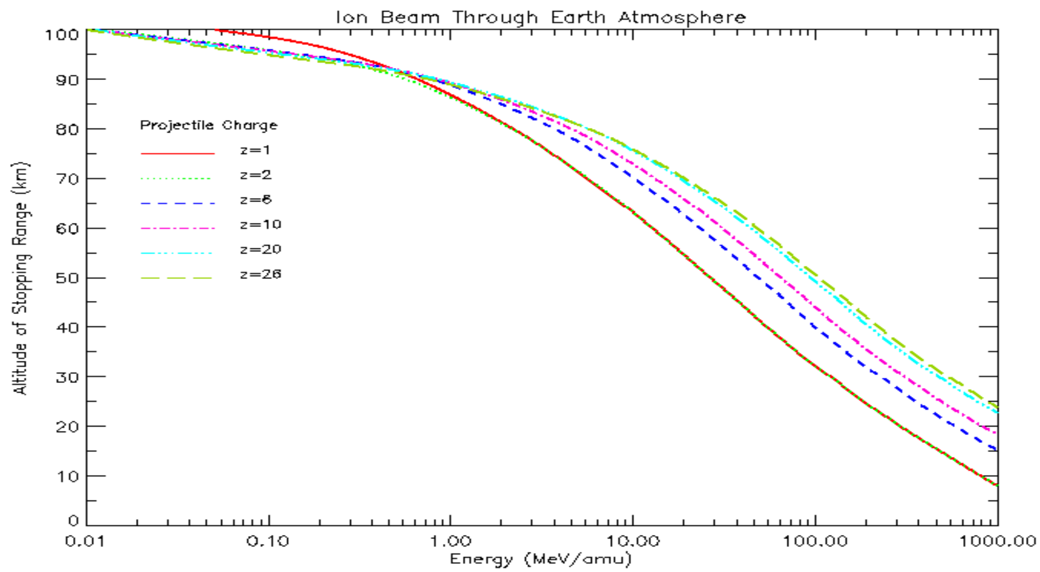
Ion Beam Through Earth Atmosphere
Altitude of Stopping Range (km)
Energy (MeV/amu)
Projectile Charge
z=1
z=2
z=6
z=10
z=20
z=26
0.01
0.10
1.00
10.00
100.00
1000.00
0
10
20
30
40
50
60
70
80
90
100

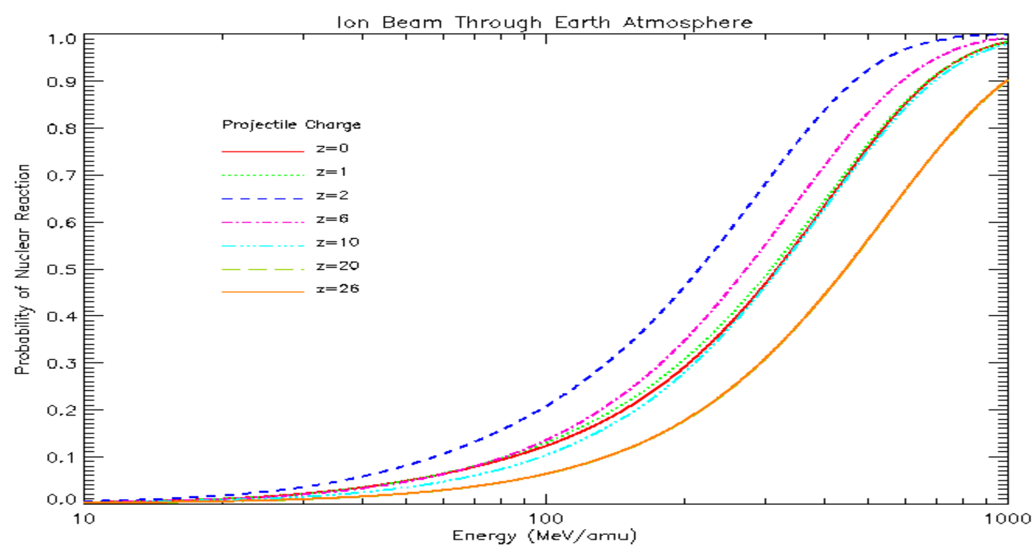
Ion Beam Through Earth Atmosphere
Probability of Nuclear Reaction
Energy (MeV/amu)
Projectile Charge
z=0
z=1
z=2
z=6
z=10
z=20
z=26
10
100
1000
0.0
0.1
0.2
0.3
0.4
0.5
0.6
0.7
0.8
0.9
1.0

Nowcast of Atmospheric Ionizing Radiation for Aviation Safety (NAIRAS) Model

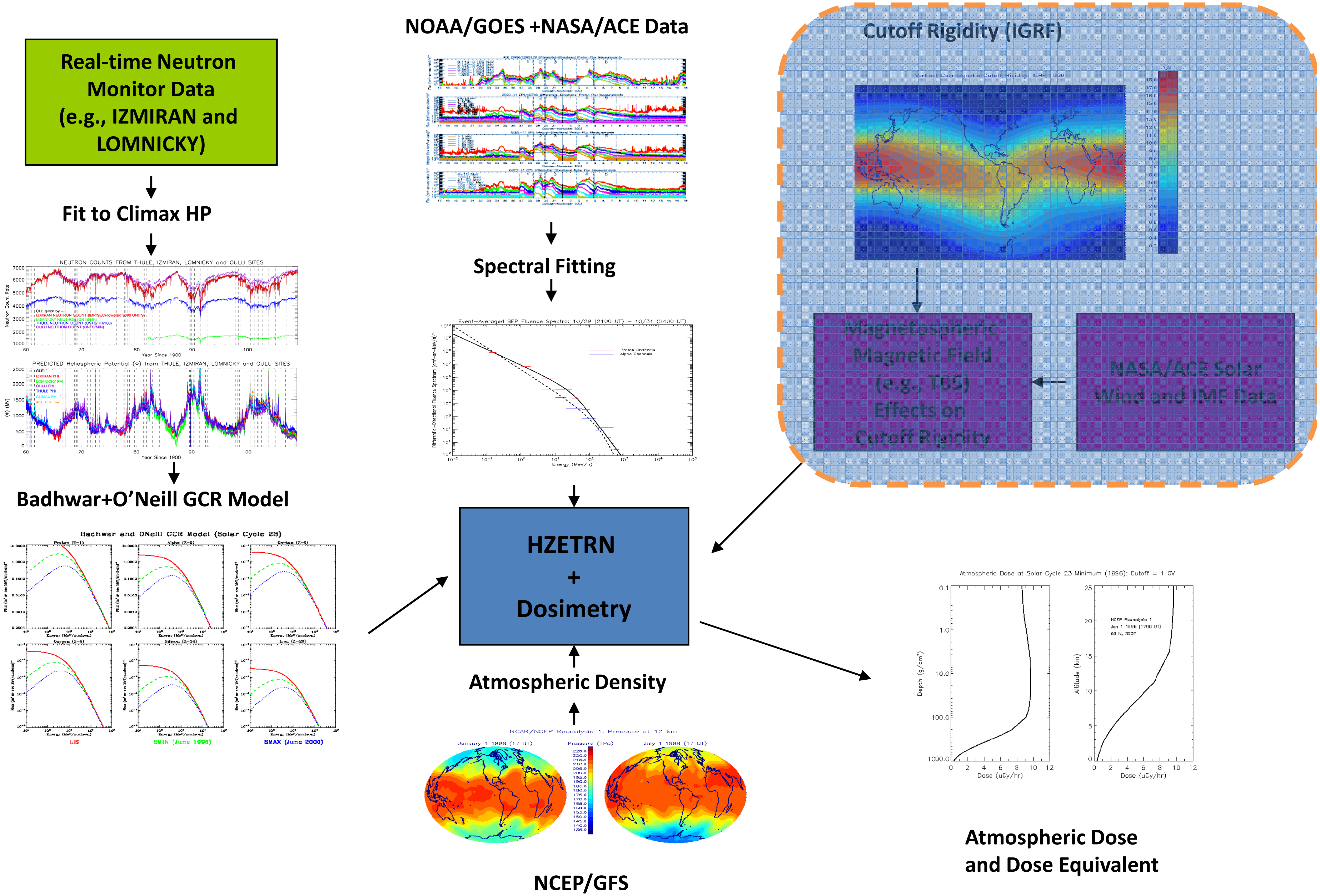

Geomagnetic Shielding

Cutoff Rigidity

$$\frac{d\mathbf{p}}{dt} = \frac{Ze}{c}\,\mathbf{v}\ \mathbf{x}\ \mathbf{B}$$ ⟵ **Lorentz-Force**

$$\frac{R}{B}\frac{d\hat{\mathbf{v}}}{ds} = \hat{\mathbf{v}}\ \mathbf{x}\ \hat{\mathbf{B}}$$ ⟵ **For given B-field, particles with same rigidity follow identical trajectories**

$$R \equiv \frac{pc}{Ze}$$ ⟵ **Rigidity**

Minimum Access Energy

$$E = \left[\sqrt{R_c^{\,2}\left(Z/A \cdot \mathrm{amu} \cdot c^2\right)^2 + 1} - 1\right] \cdot \mathrm{amu} \cdot c^2$$

Space Radiation Environment
Geomagnetic Cutoff Rigidity
Stormer Theory

$$L = -m_o c^2 \sqrt{1-(v/c)^2} + \frac{Ze}{c}\mathbf{v} \bullet \mathbf{A} - Ze\Phi$$ **Lagrangian in EM-field**

$$\mathbf{A}(\mathbf{r}) = M\,\frac{(-\hat{\mathbf{z}}\ \mathbf{x}\ \hat{\mathbf{r}})}{r^2}$$ **Vector Potential for Dipole**

$$\frac{\partial L}{\partial \phi} = 0 \quad \xrightarrow{\text{Lagrange's EOM}} \quad \Pi_\phi = \frac{\partial L}{\partial \dot{\phi}} = \text{constant}$$

Eventually … $R = 14.9\cos^4 \lambda_m$ **Vertical Cutoff Rigidity**

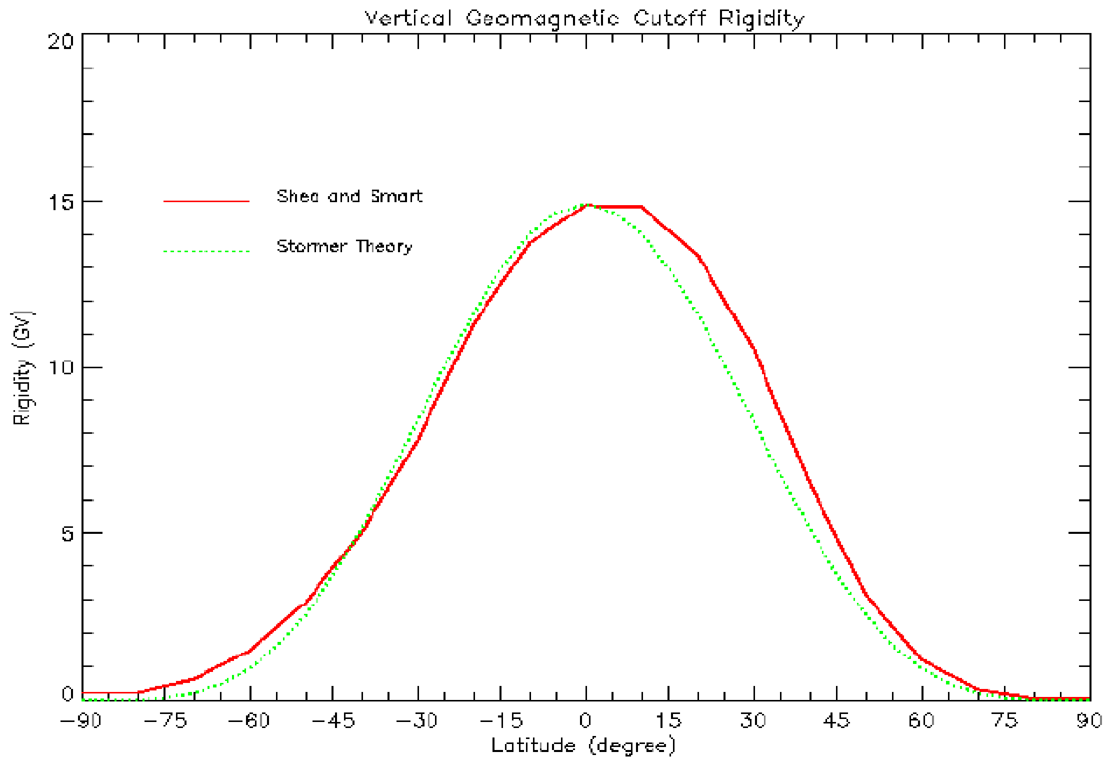

$$R = 14.9 \cos^4 \lambda_m$$

Space Radiation Environment

Geomagnetic Cutoff Rigidity

IGRF-Model

$$V = a\sum_{l=0}^{\infty}\sum_{m=0}^{l}\left(\frac{a}{r}\right)^{l+1}\left[g_l^m \cos m\phi + h_l^m \sin m\phi\right]P_l^m(\theta)$$

$$B_r = \frac{\partial V}{\partial r},\ B_\theta = \frac{1}{r}\frac{\partial V}{\partial \theta},\ B_\phi = \frac{1}{r\sin\theta}\frac{\partial V}{\partial \phi}$$

$$g_l^m(t) = g_l^m(T_0) + (t - T_0)\dot{g}_l^m$$

$$h_l^m(t) = h_l^m(T_0) + (t - T_0)\dot{h}_l^m$$

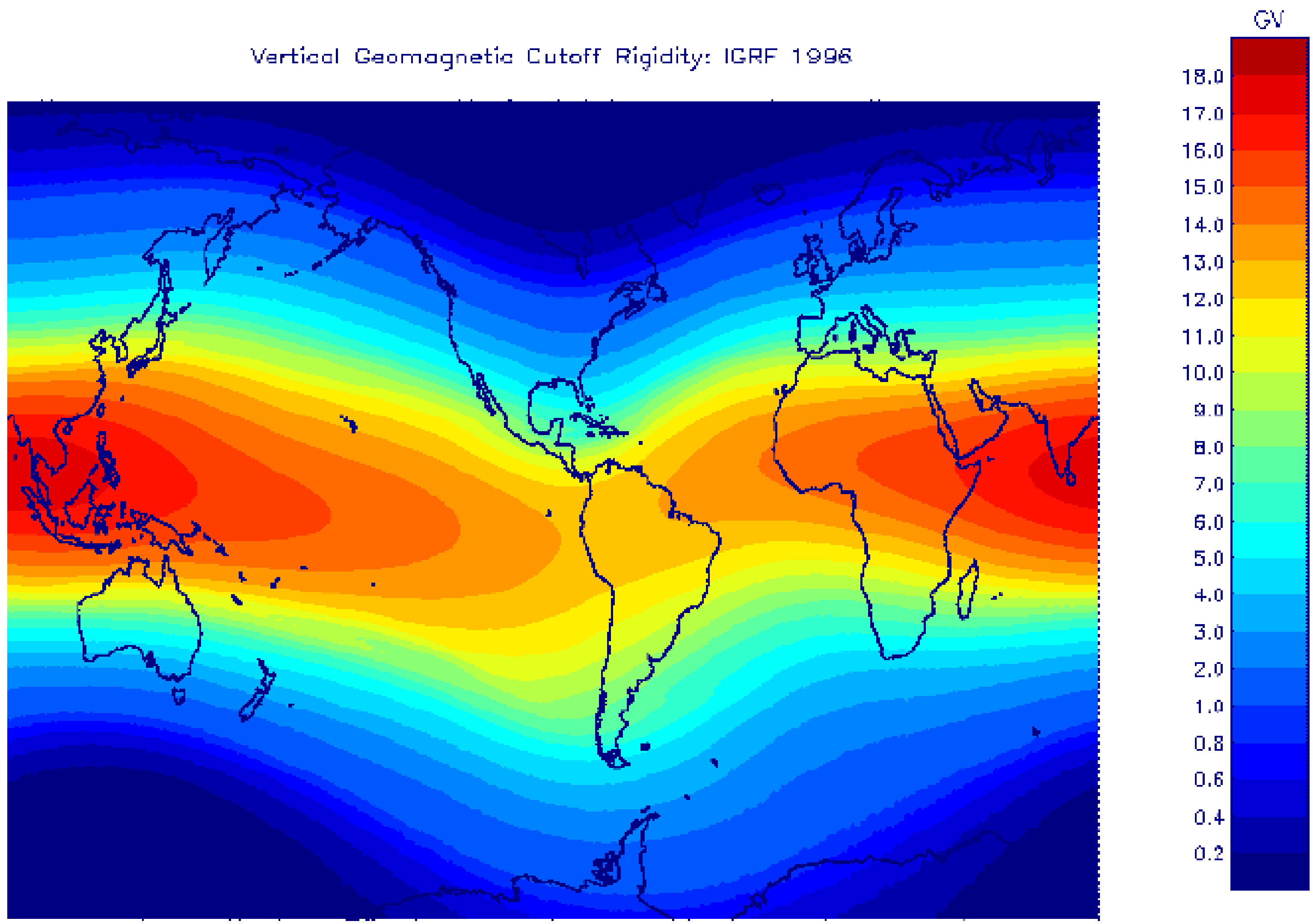

Global grid of quiescent vertical geomagnetic cutoff rigidities (GV) calculated from charged particle trajectory simulations using the IGRF model for the 1996 epoch (solar cycle 23 minimum).

The Magnetosphere

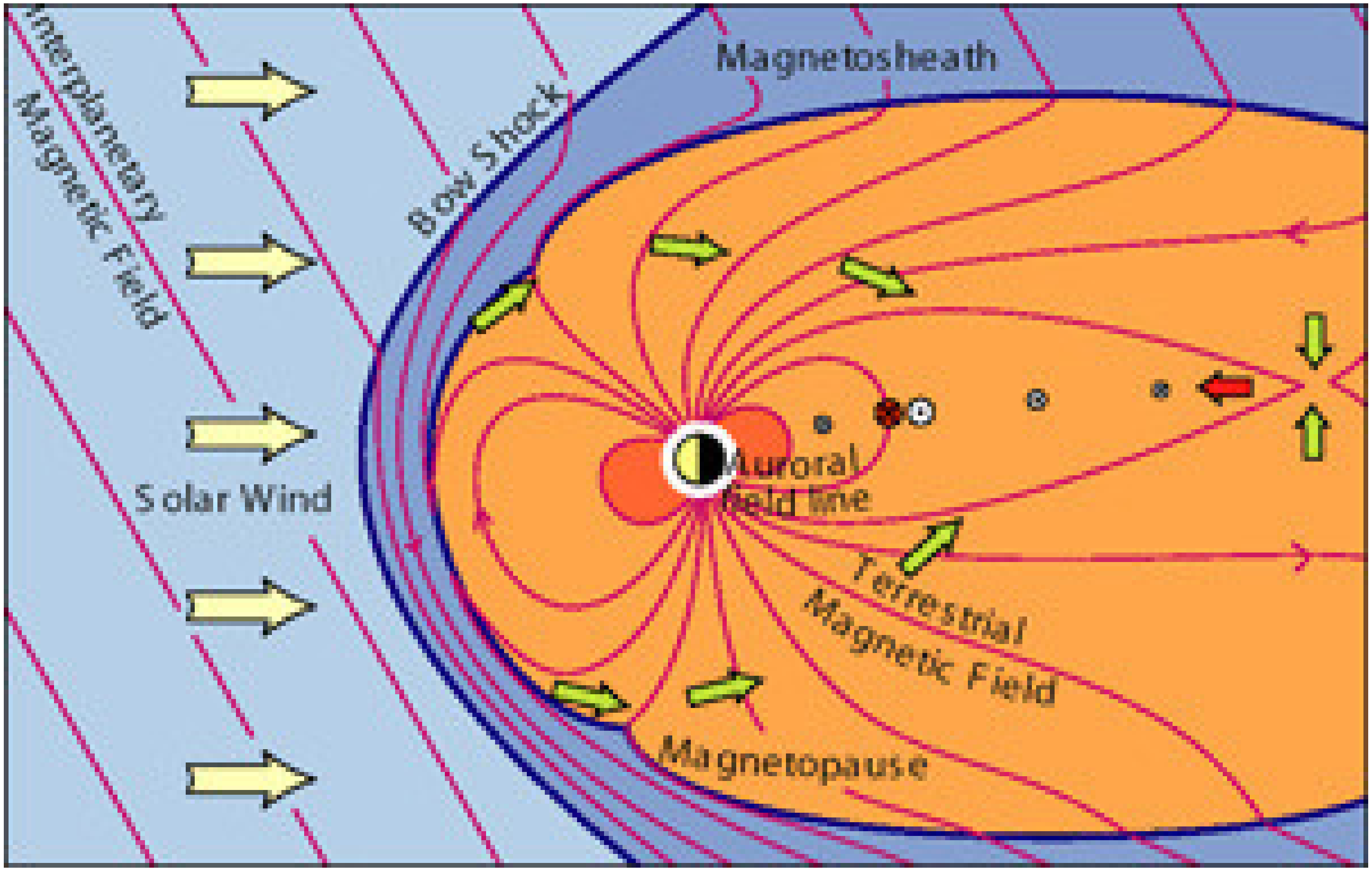

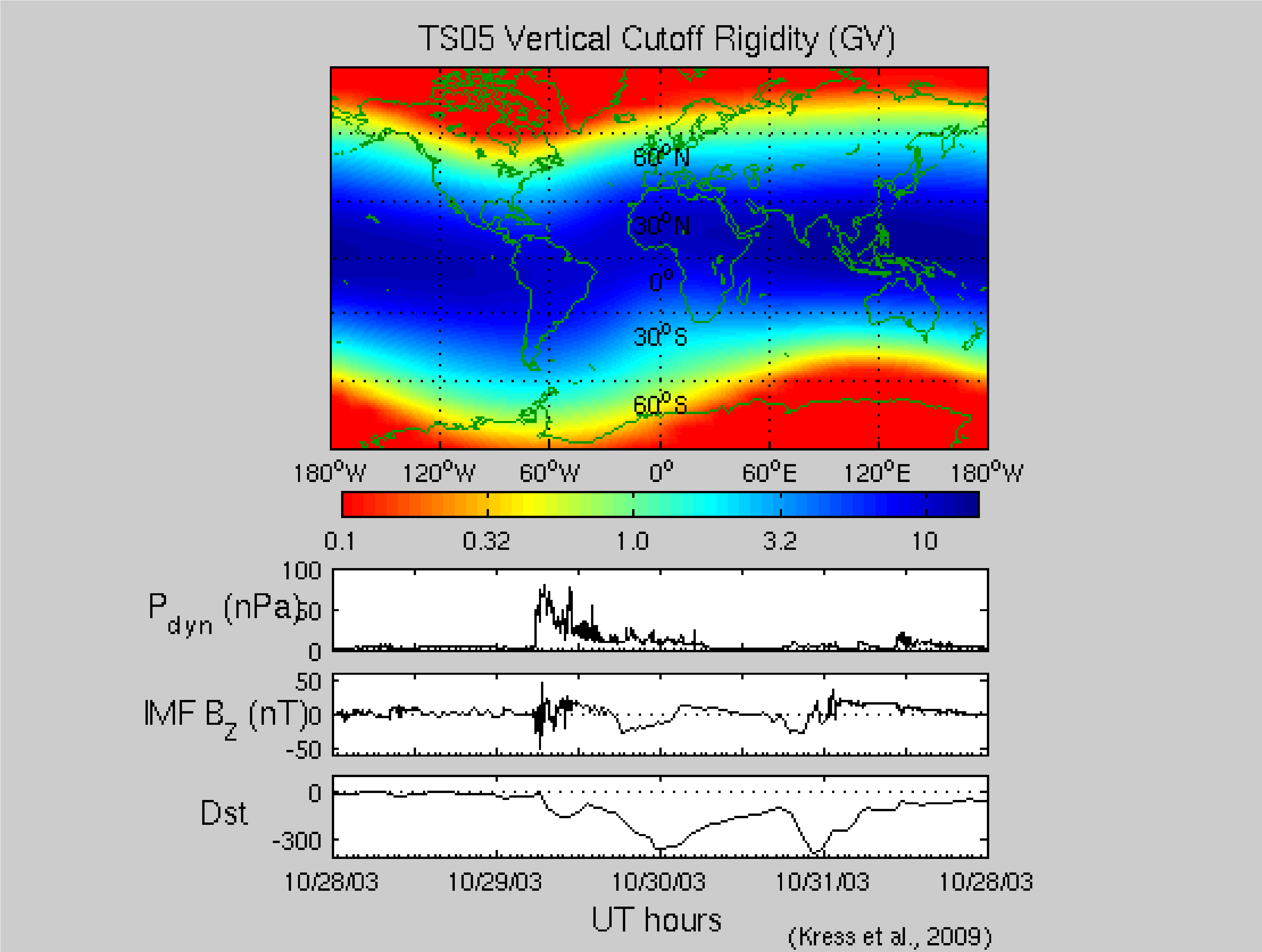
TS05 Vertical Cutoff Rigidity (GV)
60°N
30°N
0°
30°S
60°S
180°W
120°W
60°W
0°
60°E
120°E
180°W
0.1
0.32
1.0
3.2
10
P dyn (nPa)
100
50
0
IMF Bz (nT)
50
0
-50
Dst
0
-300
10/28/03
10/29/03
10/30/03
10/31/03
10/28/03
UT hours
(Kress et al., 2009)

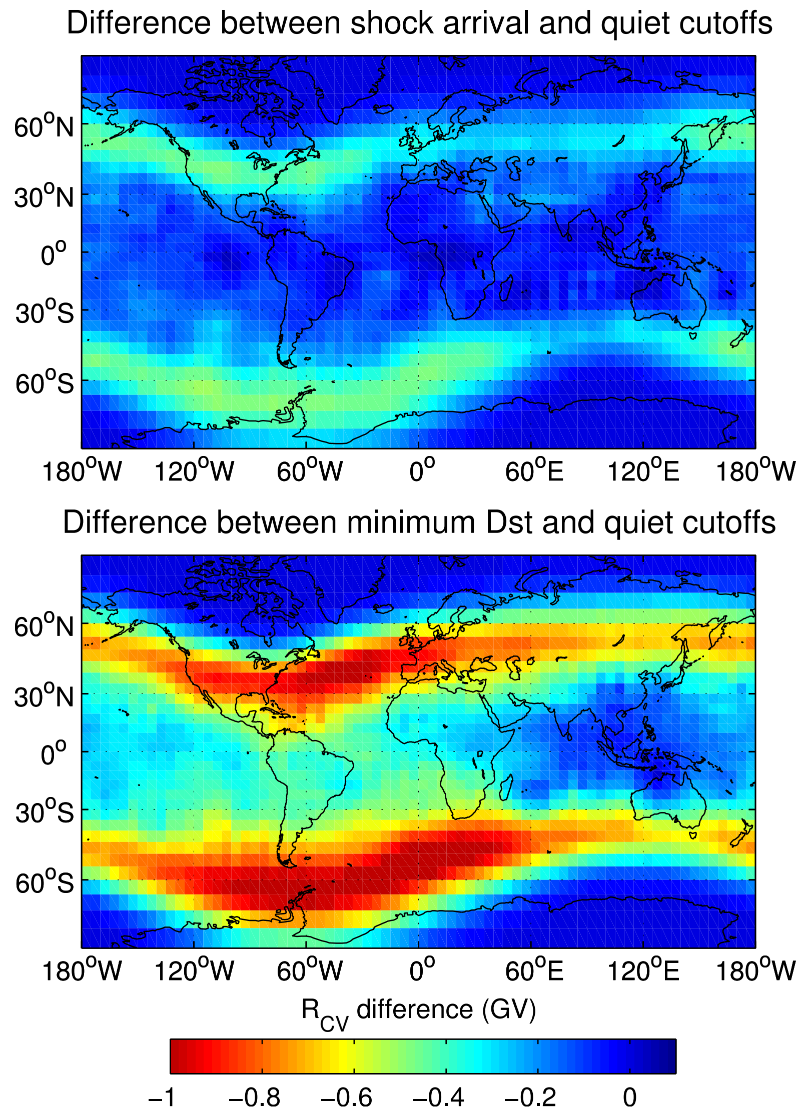

Difference between shock arrival and quiet cutoffs
60°N
30°N
0°
30°S
60°S
180°W
120°W
60°W
0°
60°E
120°E
180°W
Difference between minimum Dst and quiet cutoffs
60°N
30°N
0°
30°S
60°S
180°W
120°W
60°W
0°
60°E
120°E
180°W
R_CV difference (GV)
−1
−0.8
−0.6
−0.4
−0.2
0

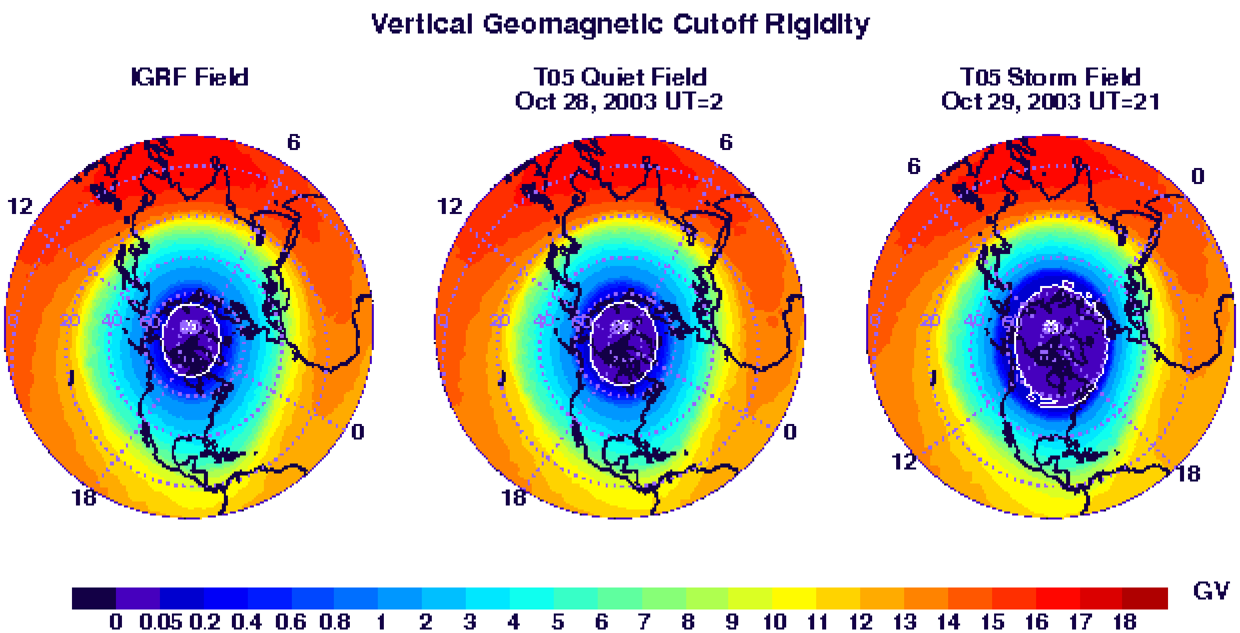

Vertical Geomagnetic Cutoff Rigidity
IGRF Field
T05 Quiet Field
Oct 28, 2003 UT=2
T05 Storm Field
Oct 29, 2003 UT=21
12
6
0
18
12
6
0
18
6
0
12
18
GV
0 0.05 0.2 0.4 0.6 0.8 1 2 3 4 5 6 7 8 9 10 11 12 13 14 15 16 17 18

500 MV Cutoff

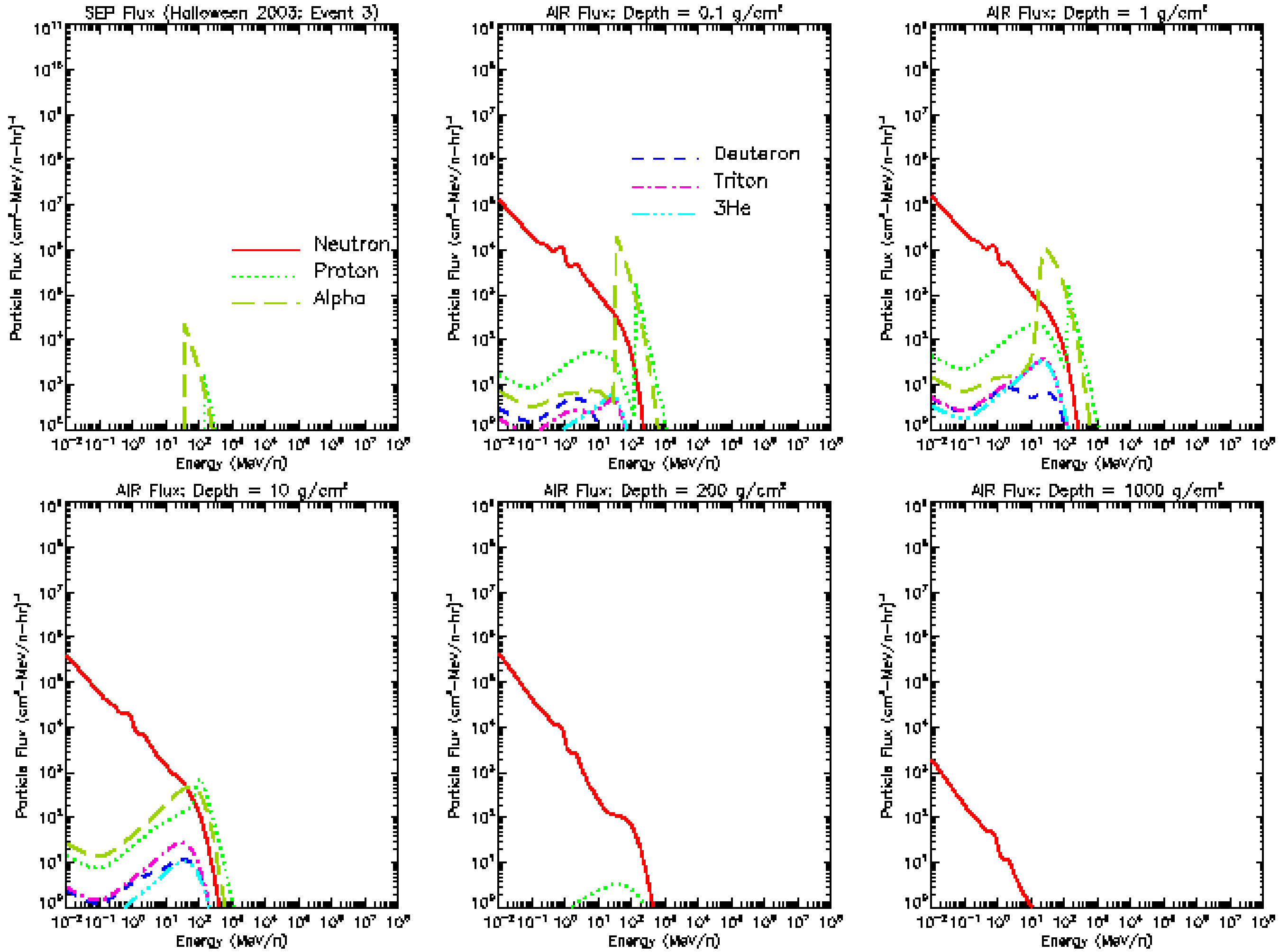

Nowcast of Atmospheric Ionizing Radiation for Aviation Safety (NAIRAS) Model

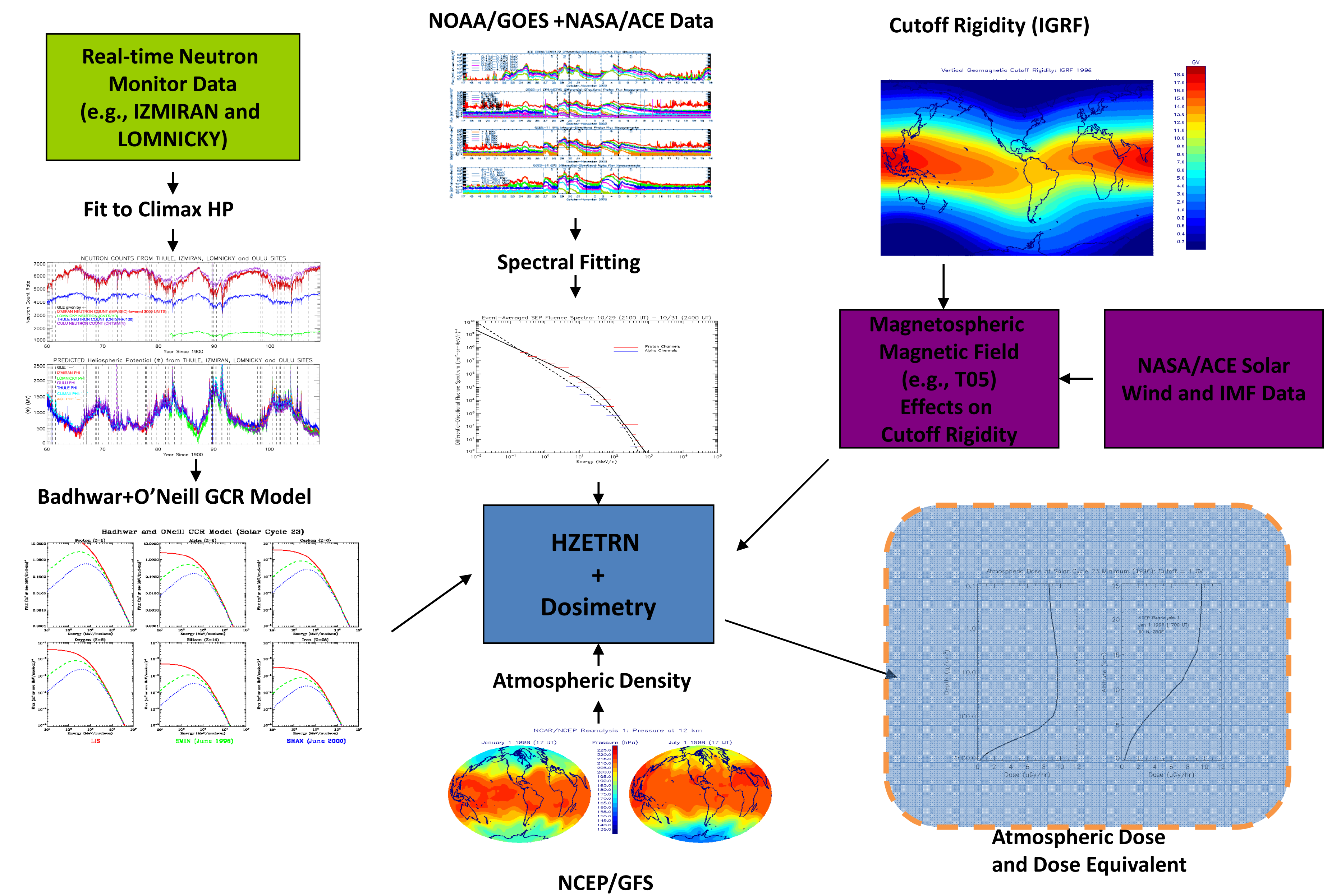

Analysis of Halloween 2003 SEP Event

- Complexity of simultaneous processes
  - Largest geomagnetic storms of solar cycle 23
  - Forbush decreases
  - Ground Level Events (GLE)
  - Anisotropic SEP distribution
- Initial analysis
  - Case study to assess geomagnetic storm influences on radiation exposure
  - Compute SEP event-averaged flux and let geomagnetic effects vary in time
- Current (on-going) analysis
  - Full time-dependent GCR+SEP radiation exposure
  - GCR component (assessing Forbush decrease)
  - Comparisons with in-flight dosimetric measurements

SEP Fluence Spectra

- GOES and ACE observes proton/alpha fluxes and which we need do derive the fluence rates and spectral characteristics
- For the Halloween storms a single power-law did not work
  - Used a double power law spectrum as suggested by *Mewaldt, 2003*
    - Includes a corona and flare seed population
    - Require the power-law functions and first derivatives to be continuous at merge energy

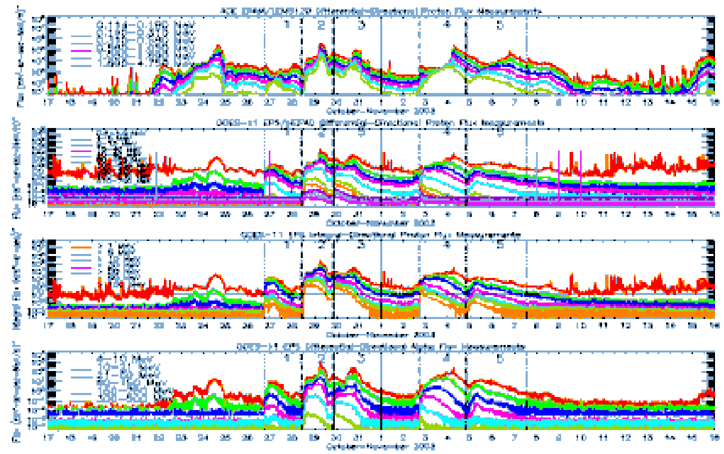

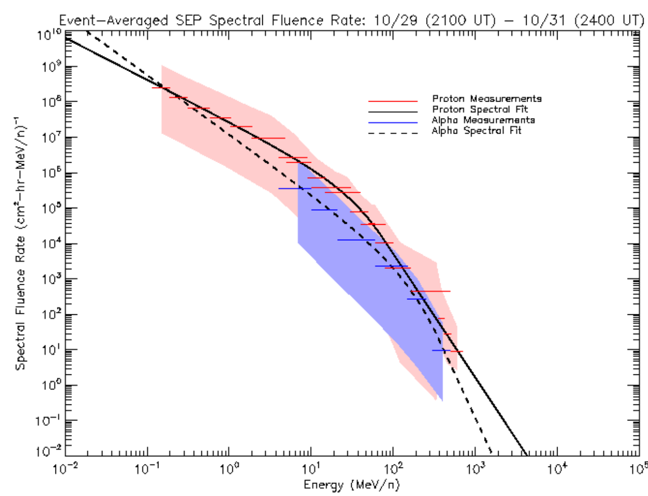

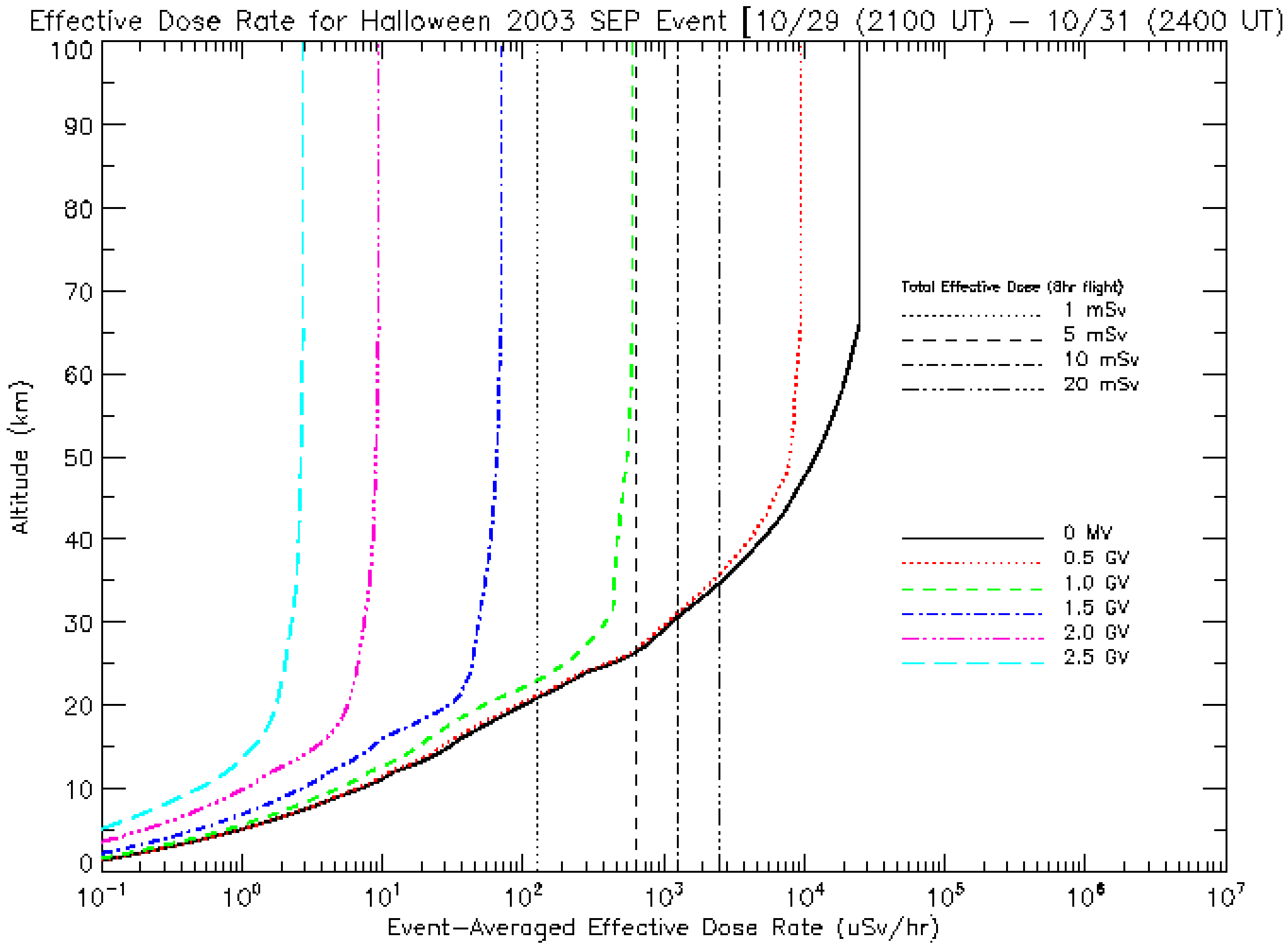

Effective Dose Rate for Halloween 2003 SEP Event [10/29 (2100 UT) – 10/31 (2400 UT)]
Altitude (km)
Event–Averaged Effective Dose Rate (uSv/hr)
Total Effective Dose (8hr flight)
1 mSv
5 mSv
10 mSv
20 mSv
0 MV
0.5 GV
1.0 GV
1.5 GV
2.0 GV
2.5 GV

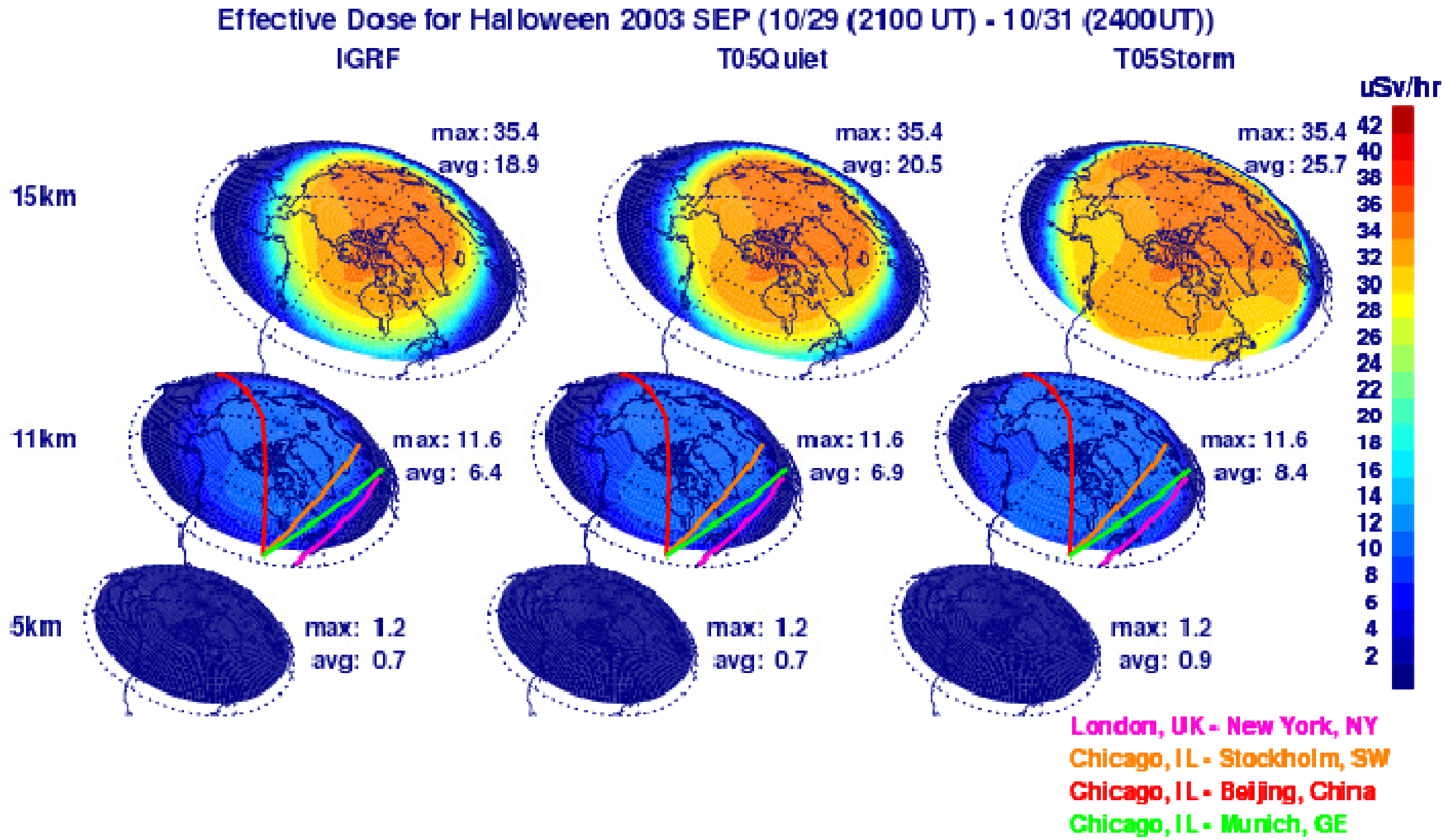

Effective Dose for Halloween 2003 SEP (10/29 (2100 UT) - 10/31 (2400UT))
IGRF
T05Quiet
T05Storm
uSv/hr
42
40
38
36
34
32
30
28
26
24
22
20
18
16
14
12
10
8
6
4
2
15km
max: 35.4
avg: 18.9
max: 35.4
avg: 20.5
max: 35.4
avg: 25.7
11km
max: 11.6
avg: 6.4
max: 11.6
avg: 6.9
max: 11.6
avg: 8.4
5km
max: 1.2
avg: 0.7
max: 1.2
avg: 0.7
max: 1.2
avg: 0.9
London, UK - New York, NY
Chicago, IL - Stockholm, SW
Chicago, IL - Beijing, China
Chicago, IL - Munich, GE

Effective Dose for Halloween Storm

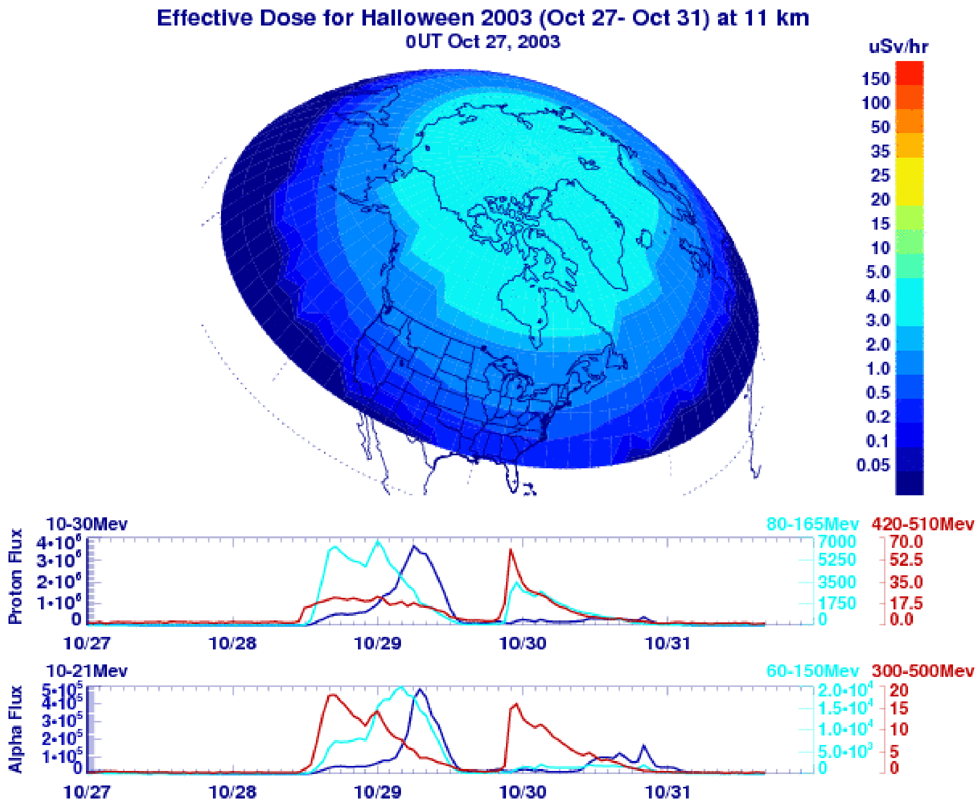

- Using all aspects of the SEP portion of NAIRAS we are able to calculate the effective dose at various altitudes and then include typical flight paths
  - We are also able to consider the role of the magnetic field model by varying which method is used to calculate the cutoff rigidity

Flight Path Comparison
Geomagnetic Effects

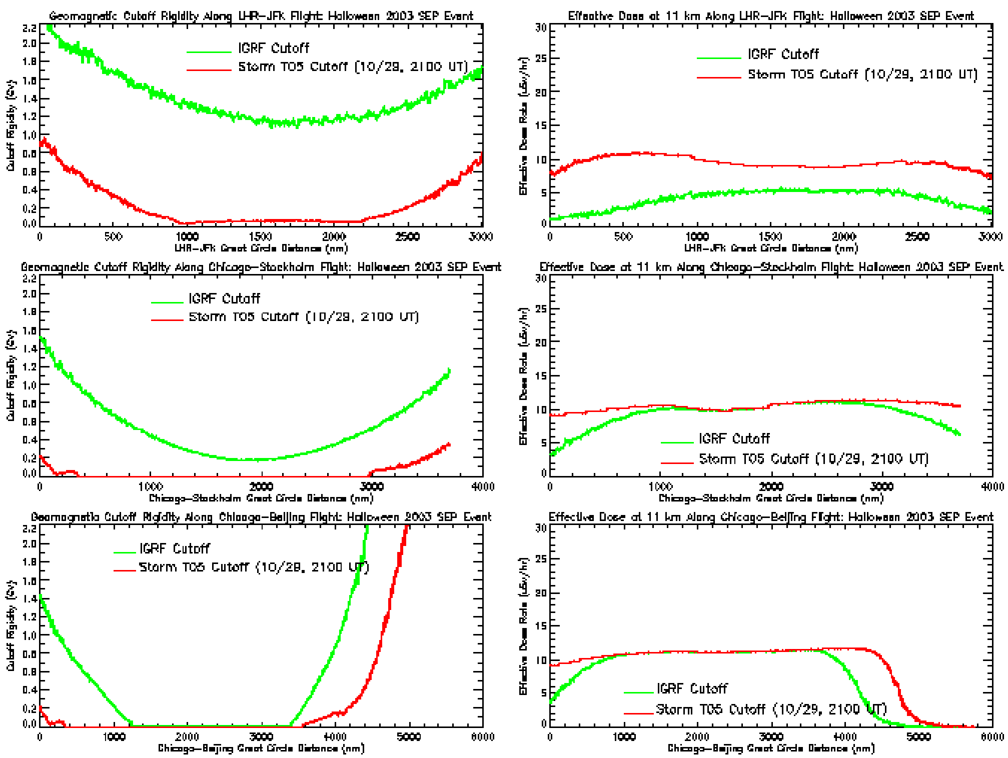

- **LHR-JFK flight path**
  - Significant differences because flight nears or crosses the open/closed field line boundary
- **ORD-PEK flight path**
  - Limited differences since both models include passage into polar cap
  - Significant dosage is seen in both cases

Summary of Total Effective Dose and Influence of Geomagnetic Effects

Neglect geomag effects underestimates dose by ~ factor 2

Flight Path	Dose Eq. T05S (mSv)	Dose Eq. T05Q (mSv)	Dose Eq. IGRF (mSv)	Dose Ratio T05S/IGRF	Dose Ratio T05S/T05Q	Dose Ratio T05Q/IGRF
JFK-LHR	0.054	0.030	0.024	2.25	1.18	1.25
ORD-ARN	0.088	0.084	0.078	1.13	1.05	1.08
ORD-PEK	0.122	0.166	0.102	1.20	1.05	1.14

T05S: Tsyganenko (T05) Storm Field
T05Q: Tsyganenko (T05) Quiet Field

IGRF underestimates geomag quiet condition by ~ 10-20%

Nowcast of Atmospheric Ionizing Radiation for Aviation Safety (NAIRAS) Model

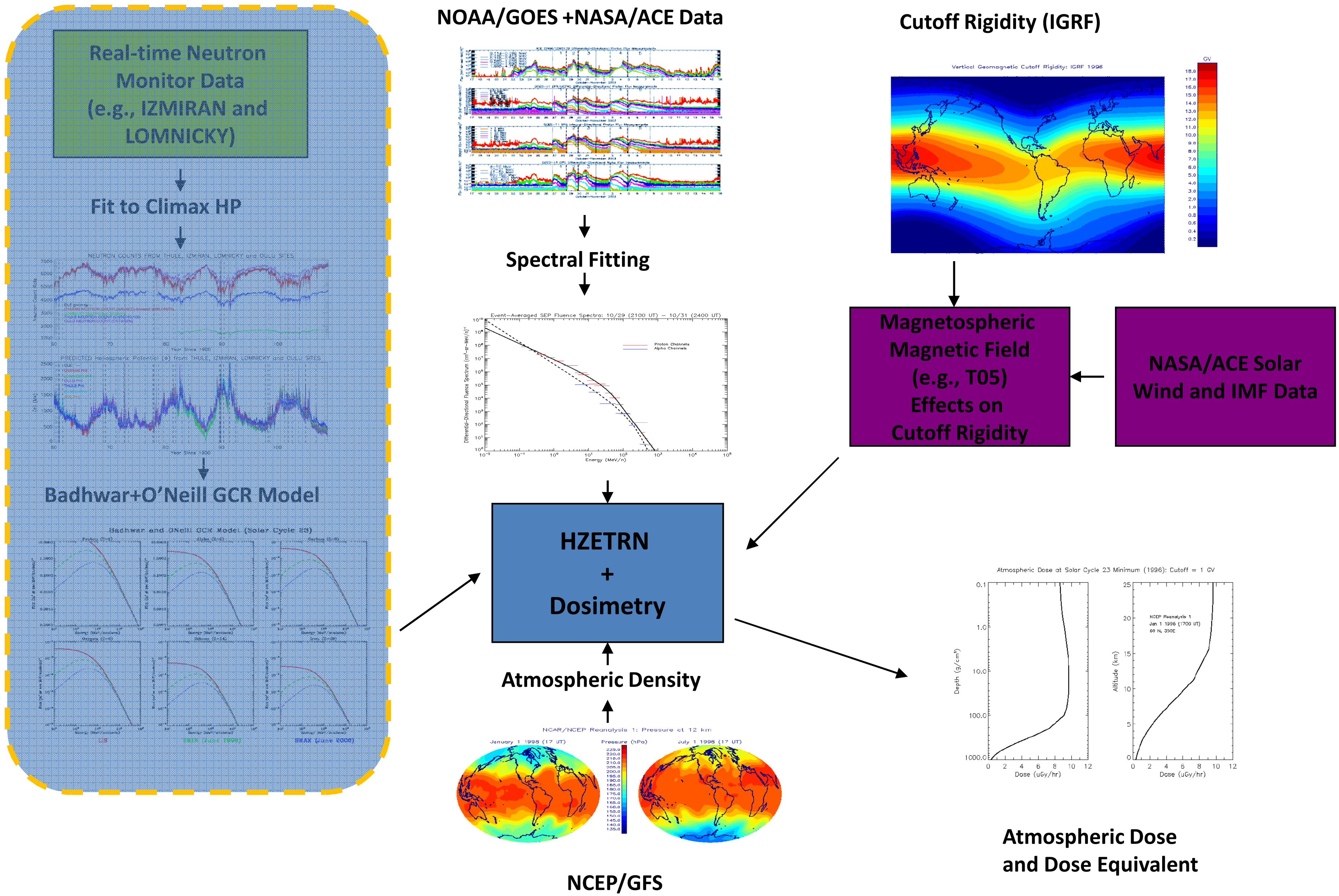

GCR Fluence Spectra
Badhwar and O'Neill GCR Model

$$j_{LIS}(E) = j_o \beta^{\delta} (E + E_o)^{-\gamma}$$

$$k(r,t) = (k_o / V_{SW}) \beta R \left[1 + (r/r_o)^2 \right] / \Phi(t)$$

- **Solution of steady-state Fokker-Planck equation**
- **Proton, Alpha spectra fit to IMP-8 data**
- **Lithium-Nickel (Z=3-28) fit to NASA/ACE/CRIS (50-500 MeV/n)**
- **High-Energy spectra (1-35 GeV) fit to NASA/HEAO-2 data**
- **Reference modulation parameter fit to ACE/CRIS oxygen spectra**
- **Subsequent modulation parameter fit to neutron monitor data**

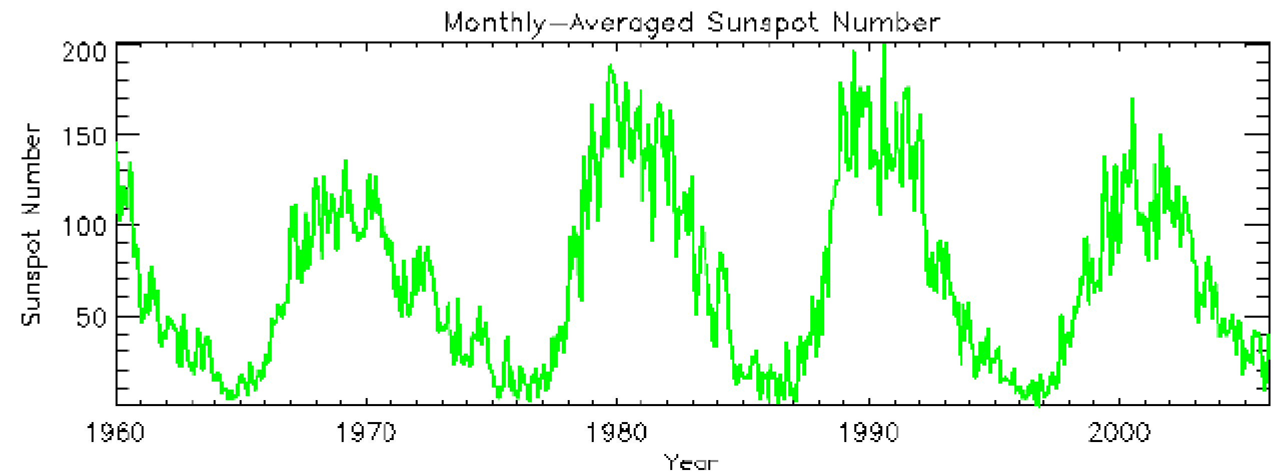
Monthly–Averaged Sunspot Number
Sunspot Number
200
150
100
50
1960
1970
1980
1990
2000
Year

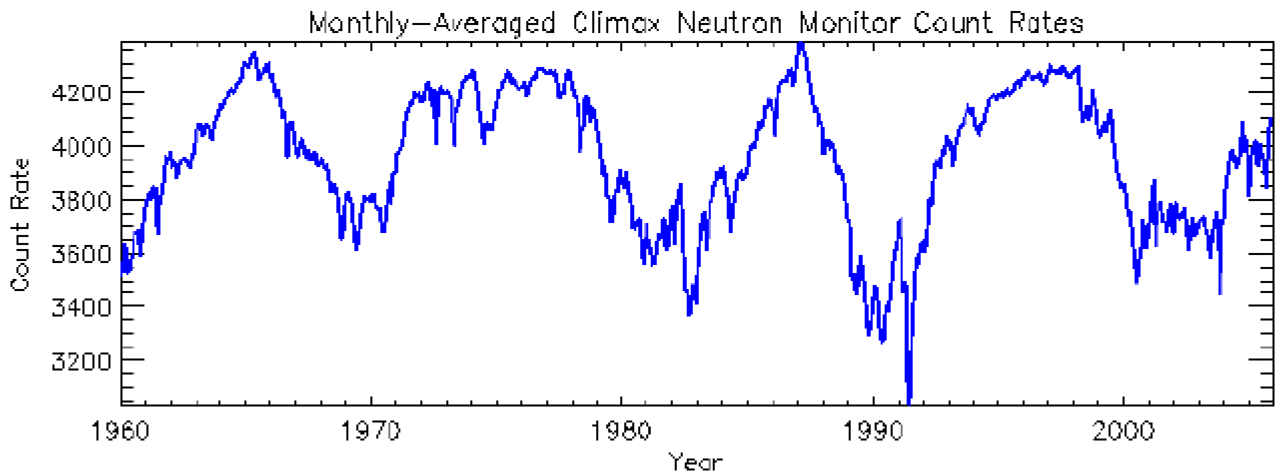
Monthly–Averaged Climax Neutron Monitor Count Rates
Count Rate
4200
4000
3800
3600
3400
3200
1960
1970
1980
1990
2000
Year

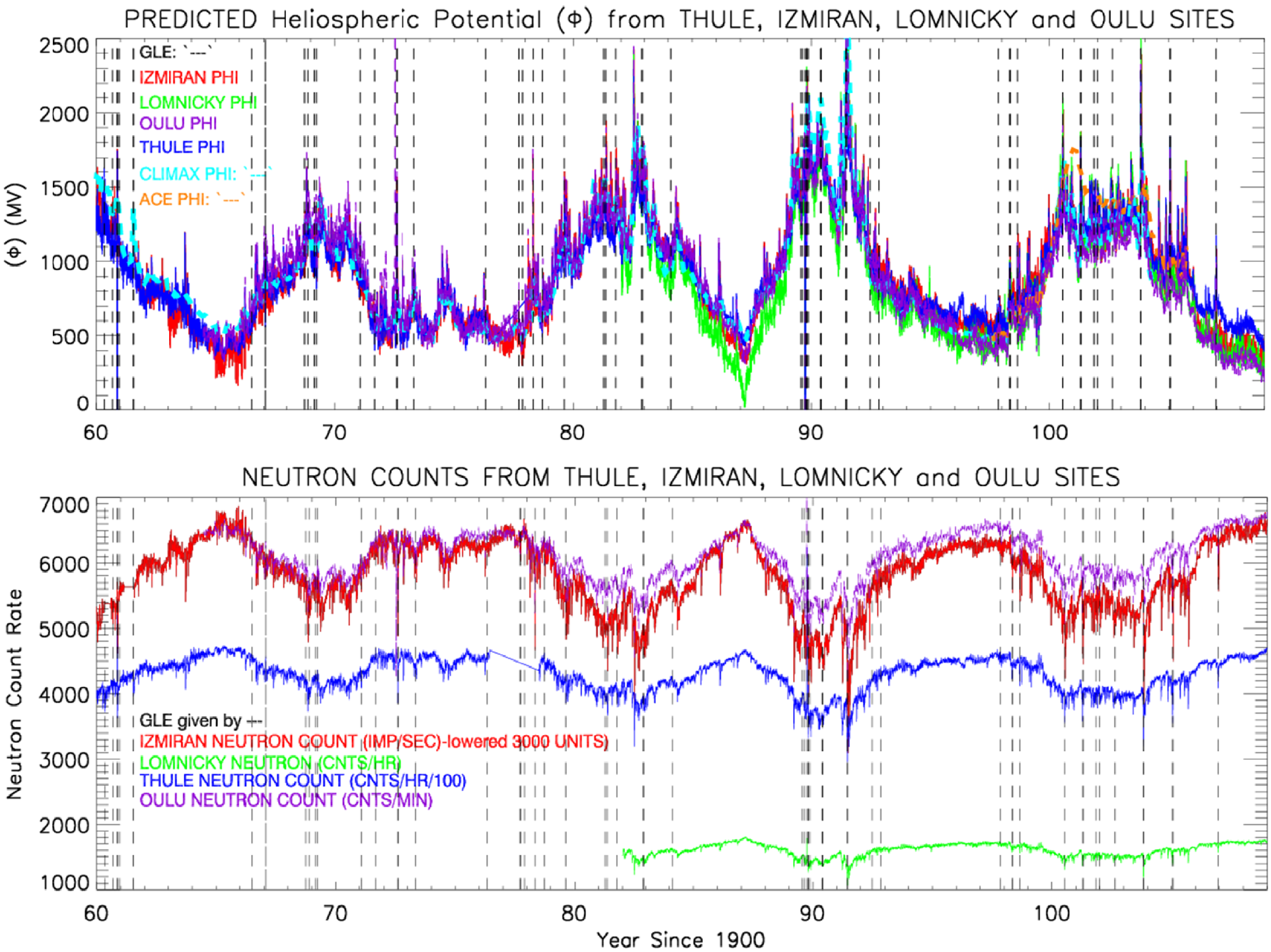

PREDICTED Heliospheric Potential (Φ) from THULE, IZMIRAN, LOMNICKY and OULU SITES
GLE: `---`
IZMIRAN PHI
LOMNICKY PHI
OULU PHI
THULE PHI
CLIMAX PHI: `---`
ACE PHI: `---`
(Φ) (MV)
NEUTRON COUNTS FROM THULE, IZMIRAN, LOMNICKY and OULU SITES
GLE given by ---
IZMIRAN NEUTRON COUNT (IMP/SEC)-lowered 3000 UNITS)
LOMNICKY NEUTRON (CNTS/HR)
THULE NEUTRON COUNT (CNTS/HR/100)
OULU NEUTRON COUNT (CNTS/MIN)
Neutron Count Rate
Year Since 1900

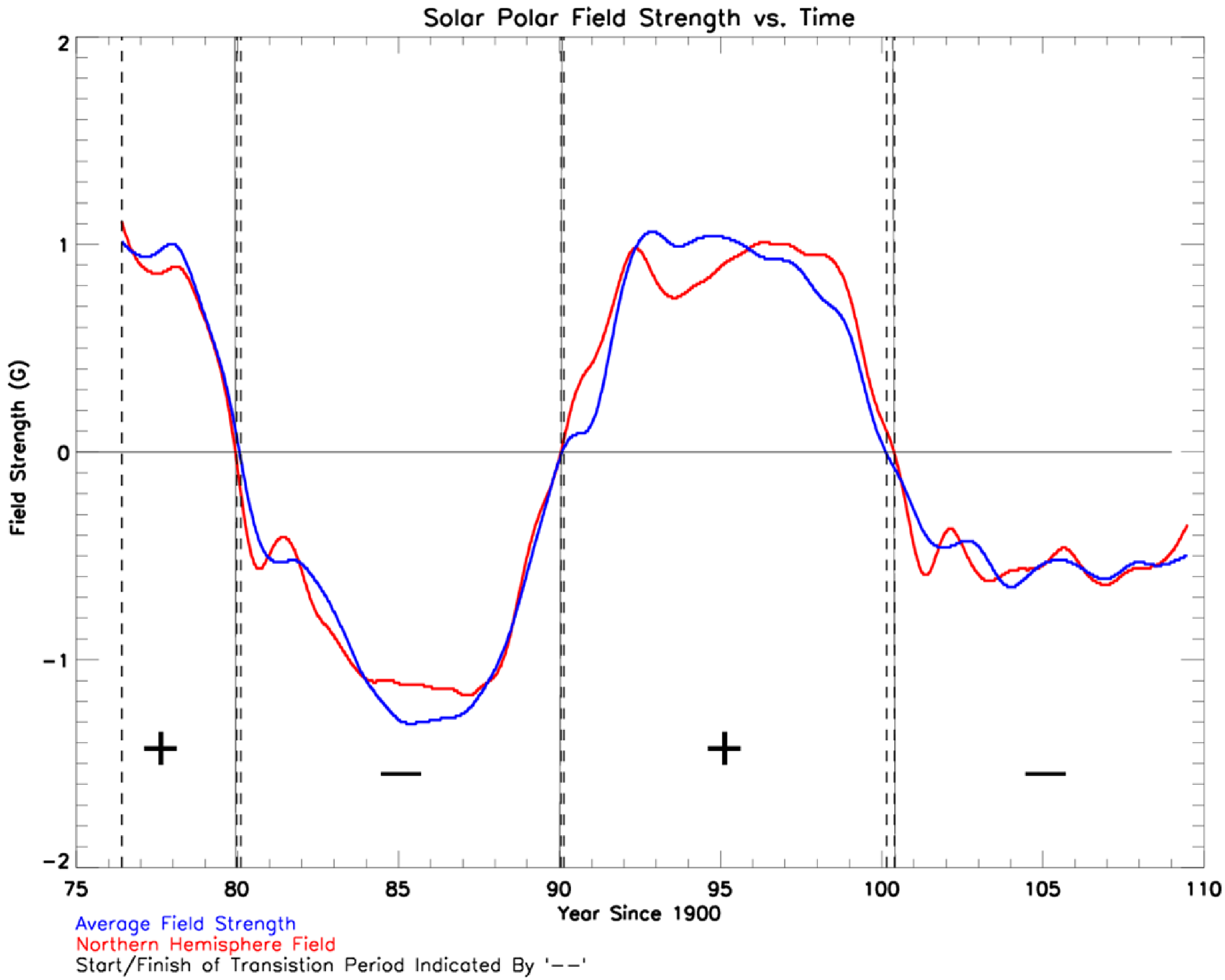
Solar Polar Field Strength vs. Time
Field Strength (G)
2
1
0
-1
-2
75
80
85
90
95
100
105
110
Year Since 1900
+
—
+
—
Average Field Strength
Northern Hemisphere Field
Start/Finish of Transistion Period Indicated By '--'

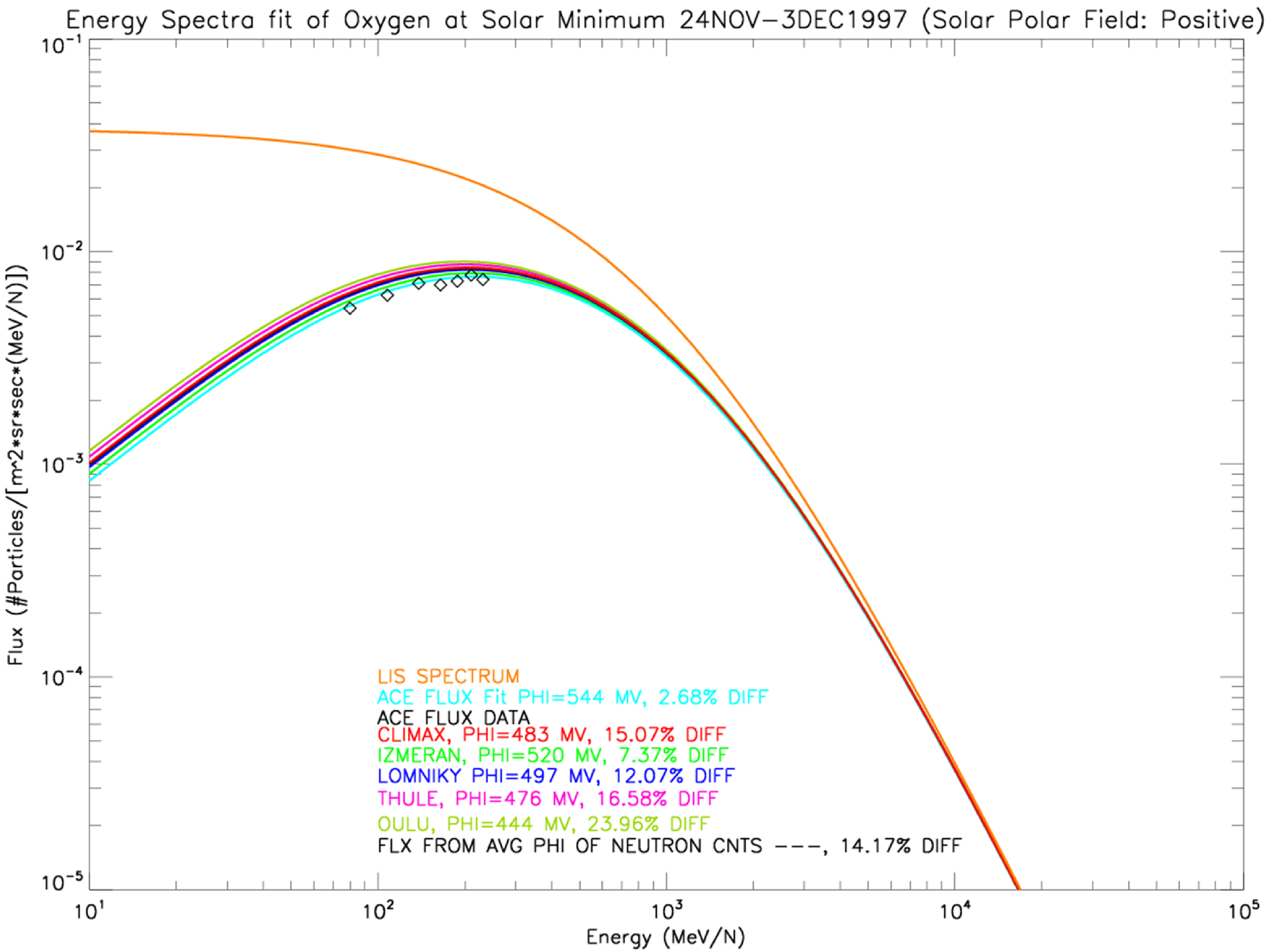

Energy Spectra fit of Oxygen at Solar Minimum 24NOV–3DEC1997 (Solar Polar Field: Positive)
Flux (#Particles/[m^2*sr*sec*(MeV/N)])
Energy (MeV/N)
LIS SPECTRUM
ACE FLUX Fit PHI=544 MV, 2.68% DIFF
ACE FLUX DATA
CLIMAX, PHI=483 MV, 15.07% DIFF
IZMERAN, PHI=520 MV, 7.37% DIFF
LOMNIKY PHI=497 MV, 12.07% DIFF
THULE, PHI=476 MV, 16.58% DIFF
OULU, PHI=444 MV, 23.96% DIFF
FLX FROM AVG PHI OF NEUTRON CNTS ---, 14.17% DIFF

Badhwar and ONeill GCR Model

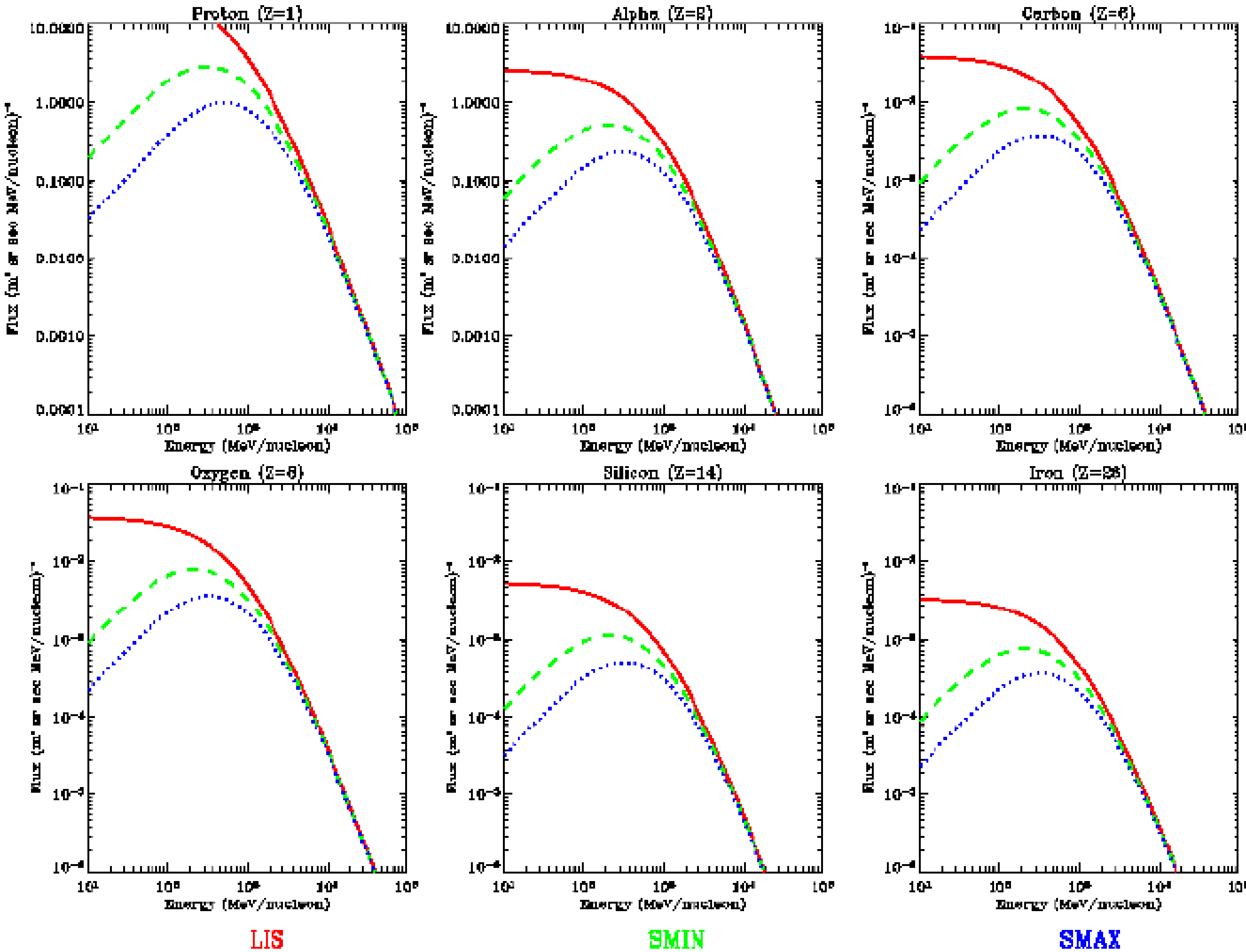

GCR Fluence Spectra

- Ground-based neutron monitor count rates related to incident GCR flux
- Use high-latitude, real-time neutron monitor count rates to derive heliospheric potential (HP)
- Fit real-time neutron count rates to Badhwar & O'Neill GCR HP
  - Steady-state Fokker-Planck transport to 1 AU
  - HP embedded in diffusion coefficient
  - Validated by NASA/ACE

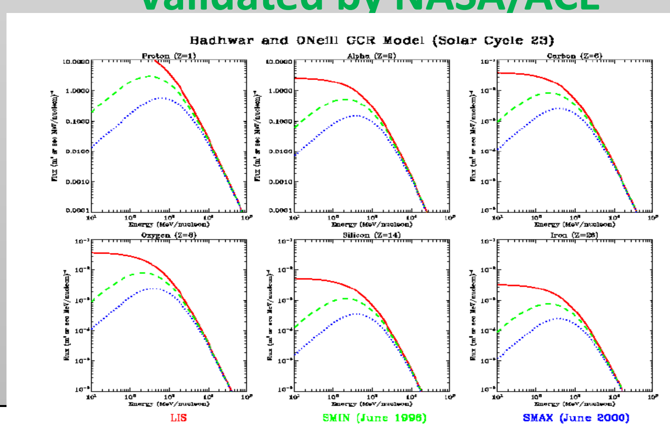

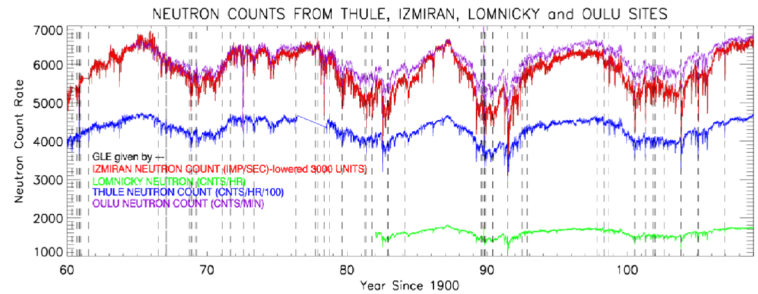

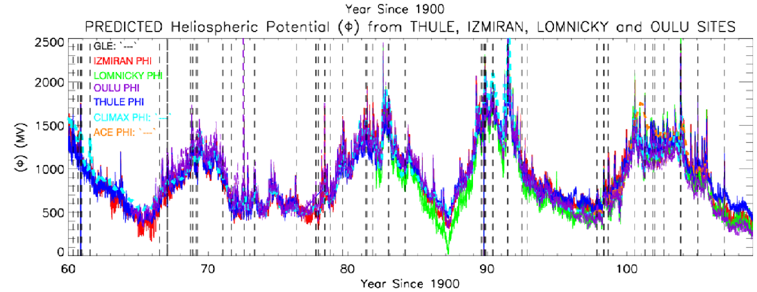

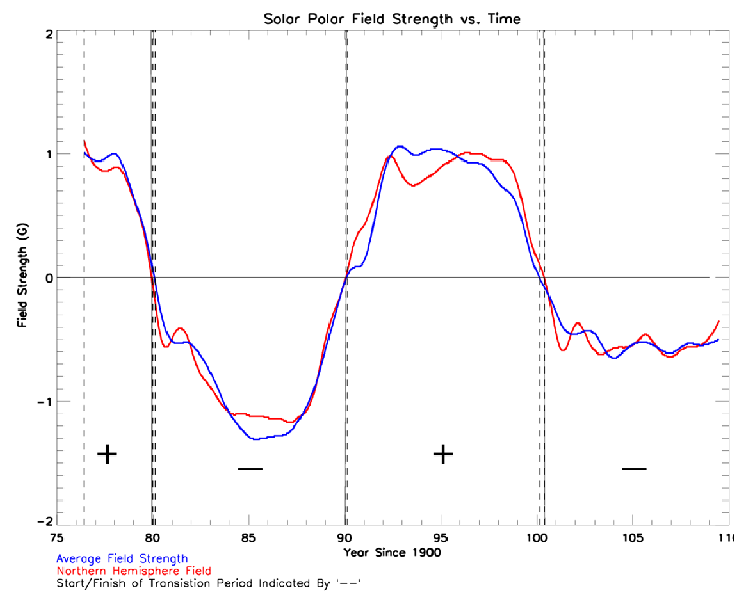

Zero Cutoff

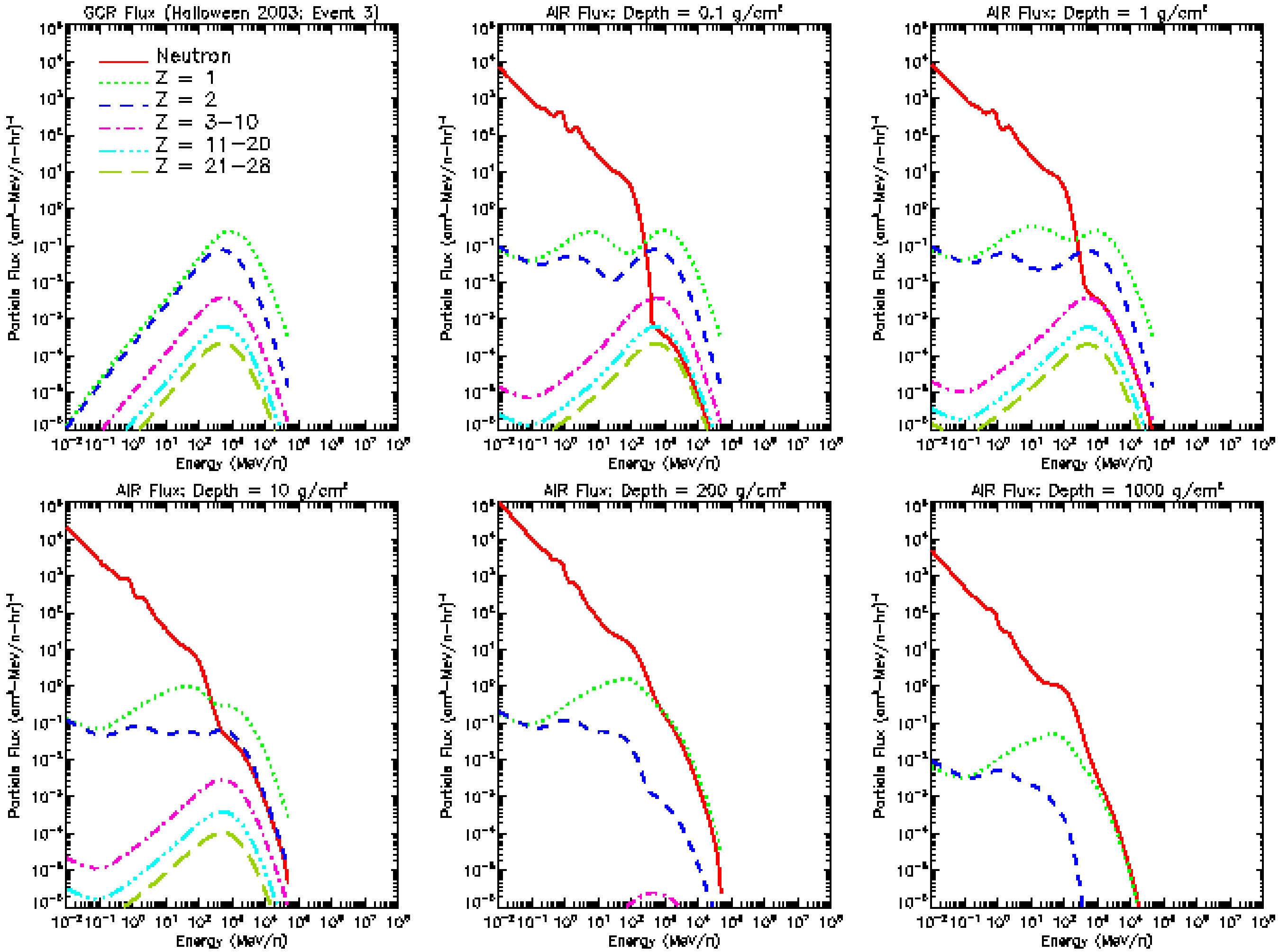
GCR Flux (Halloween 2003; Event 3)
Neutron
Z = 1
Z = 2
Z = 3−10
Z = 11−20
Z = 21−28
AIR Flux; Depth = 0.1 g/cm²
AIR Flux; Depth = 1 g/cm²
AIR Flux; Depth = 10 g/cm²
AIR Flux; Depth = 200 g/cm²
AIR Flux; Depth = 1000 g/cm²
Particle Flux (cm²-MeV/n-hr)⁻¹
Energy (MeV/n)

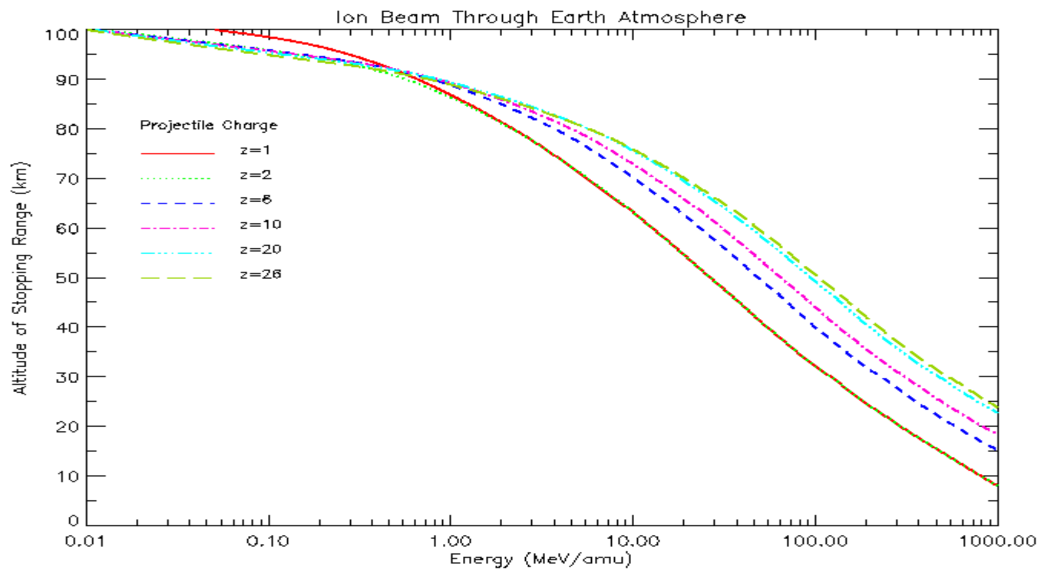
Ion Beam Through Earth Atmosphere
Altitude of Stopping Range (km)
Energy (MeV/amu)
Projectile Charge
z=1
z=2
z=6
z=10
z=20
z=26

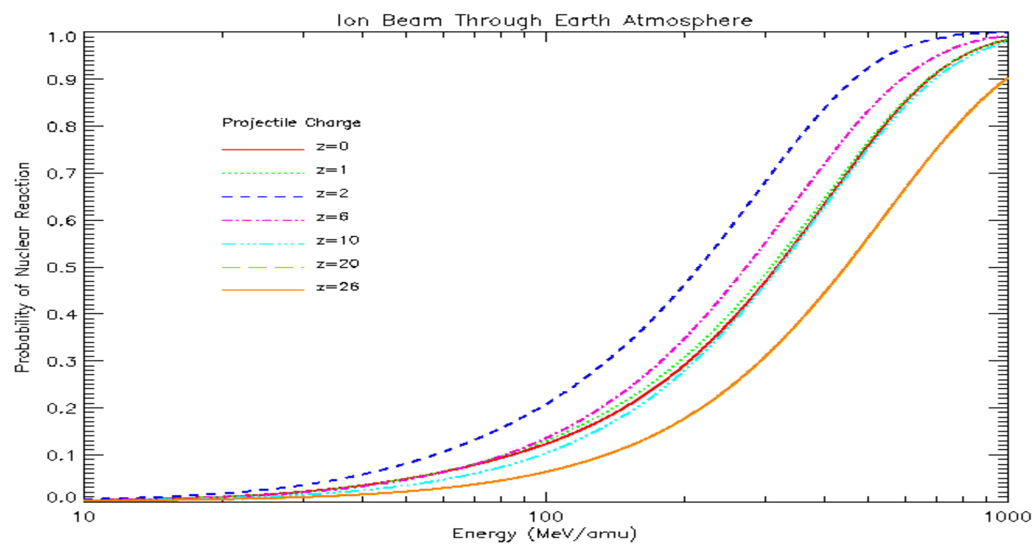
Ion Beam Through Earth Atmosphere
Probability of Nuclear Reaction
Energy (MeV/amu)
Projectile Charge
z=0
z=1
z=2
z=6
z=10
z=20
z=26

1 GV Cutoff

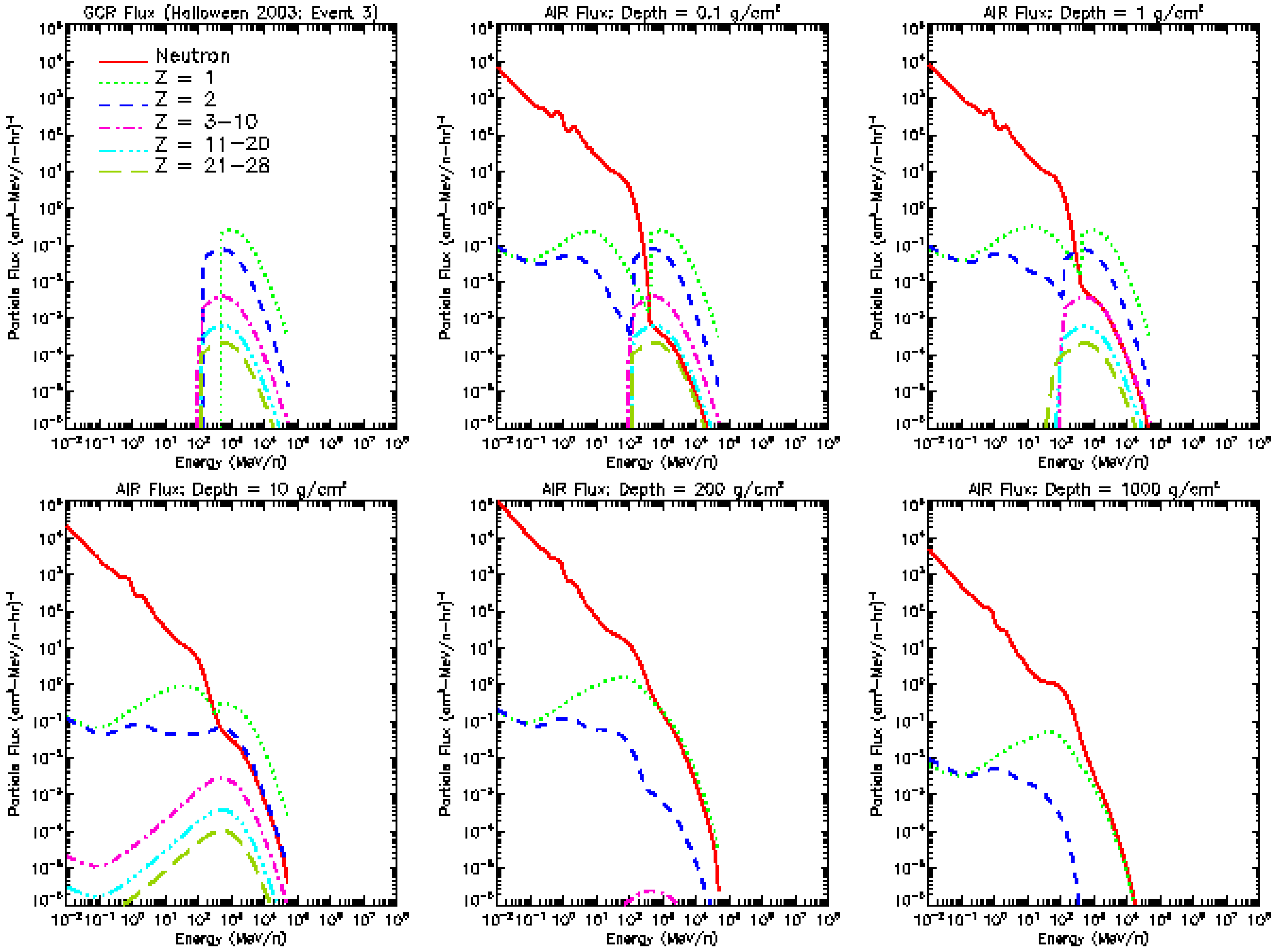

GCR Flux (Halloween 2003; Event 3)
Neutron
Z = 1
Z = 2
Z = 3–10
Z = 11–20
Z = 21–28
AIR Flux; Depth = 0.1 g/cm²
AIR Flux; Depth = 1 g/cm²
AIR Flux; Depth = 10 g/cm²
AIR Flux; Depth = 200 g/cm²
AIR Flux; Depth = 1000 g/cm²
Particle Flux (cm²–MeV/n–hr)⁻¹
Energy (MeV/n)

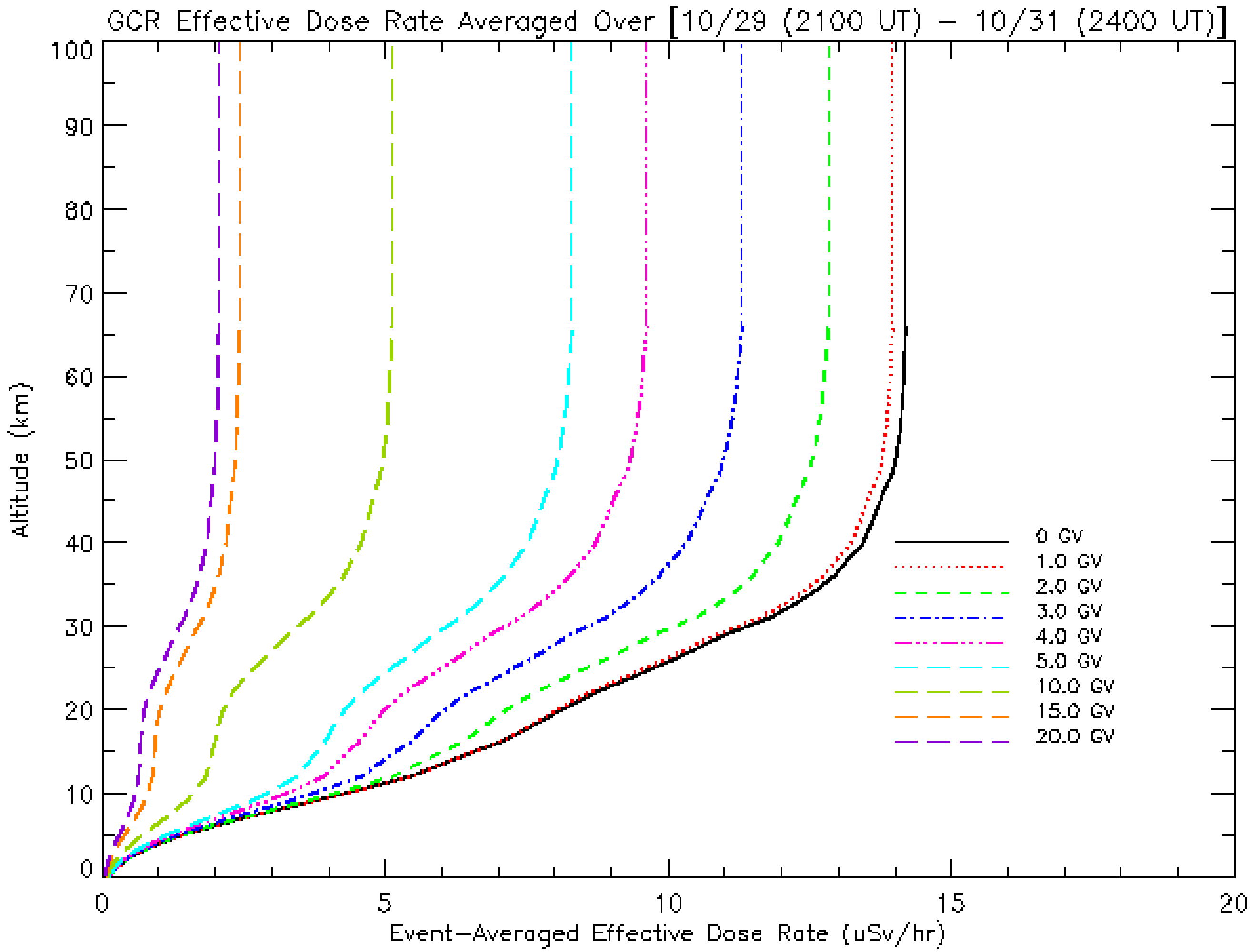
GCR Effective Dose Rate Averaged Over [10/29 (2100 UT) – 10/31 (2400 UT)]
Altitude (km)
Event–Averaged Effective Dose Rate (uSv/hr)
0 GV
1.0 GV
2.0 GV
3.0 GV
4.0 GV
5.0 GV
10.0 GV
15.0 GV
20.0 GV

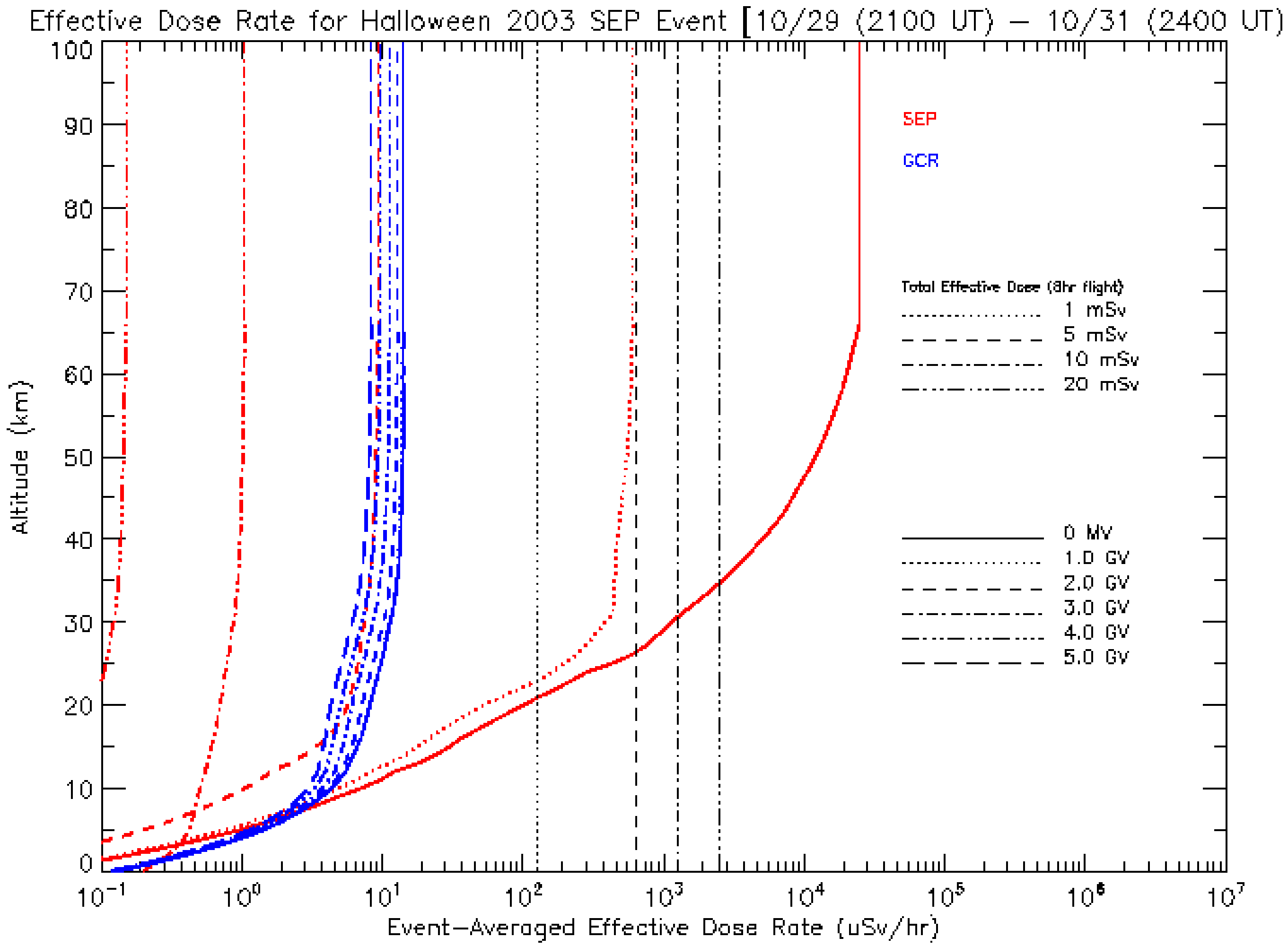
Effective Dose Rate for Halloween 2003 SEP Event [10/29 (2100 UT) – 10/31 (2400 UT)]
Altitude (km)
Event–Averaged Effective Dose Rate (uSv/hr)
SEP
GCR
Total Effective Dose (8hr flight)
1 mSv
5 mSv
10 mSv
20 mSv
0 MV
1.0 GV
2.0 GV
3.0 GV
4.0 GV
5.0 GV

Effective Dose for Halloween 2003 SEP [10/29 (2100 UT) – 10/31 (2400 UT)]
T05 Storm Field: October 29, 2003 (2100 UT)

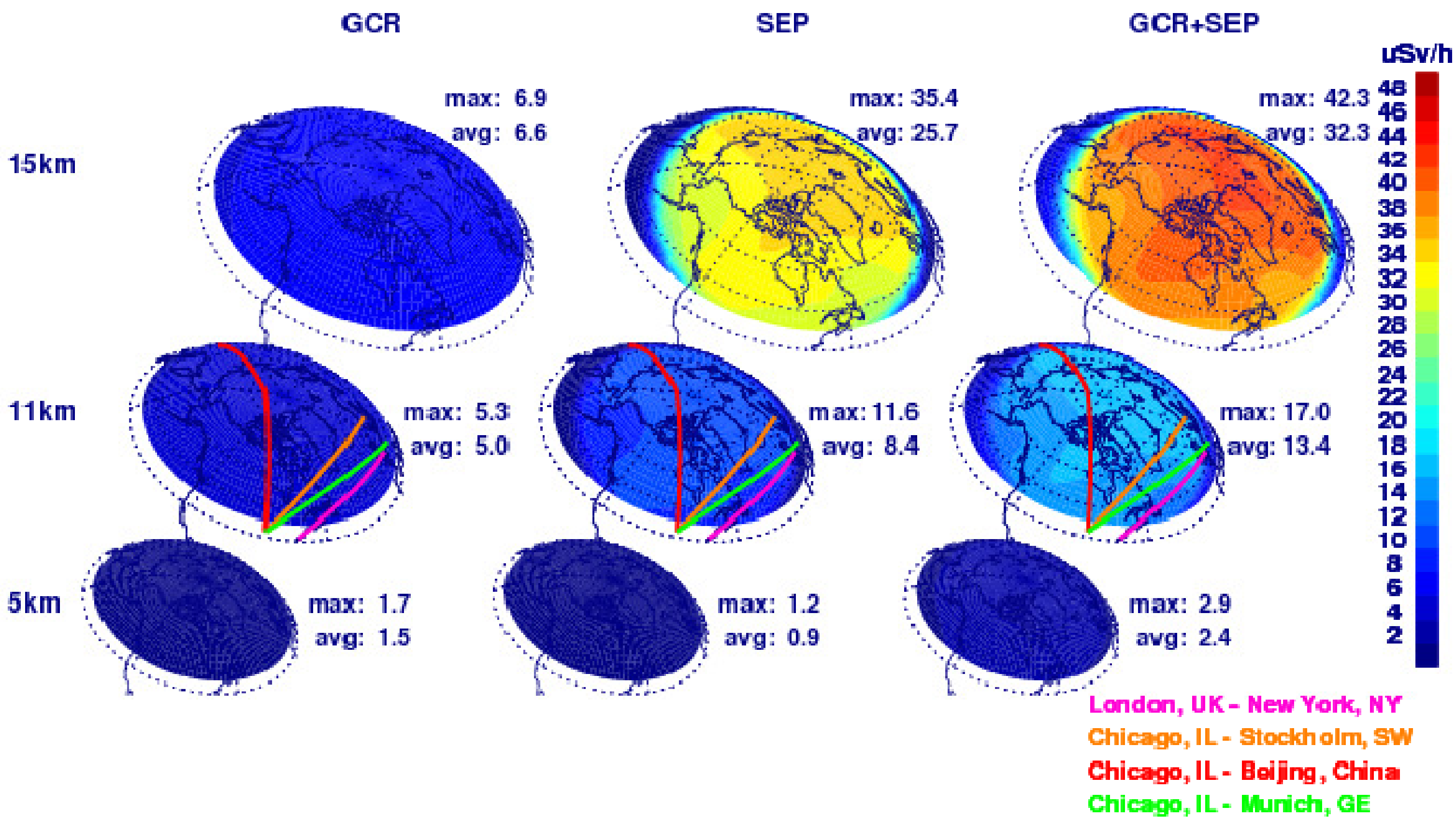

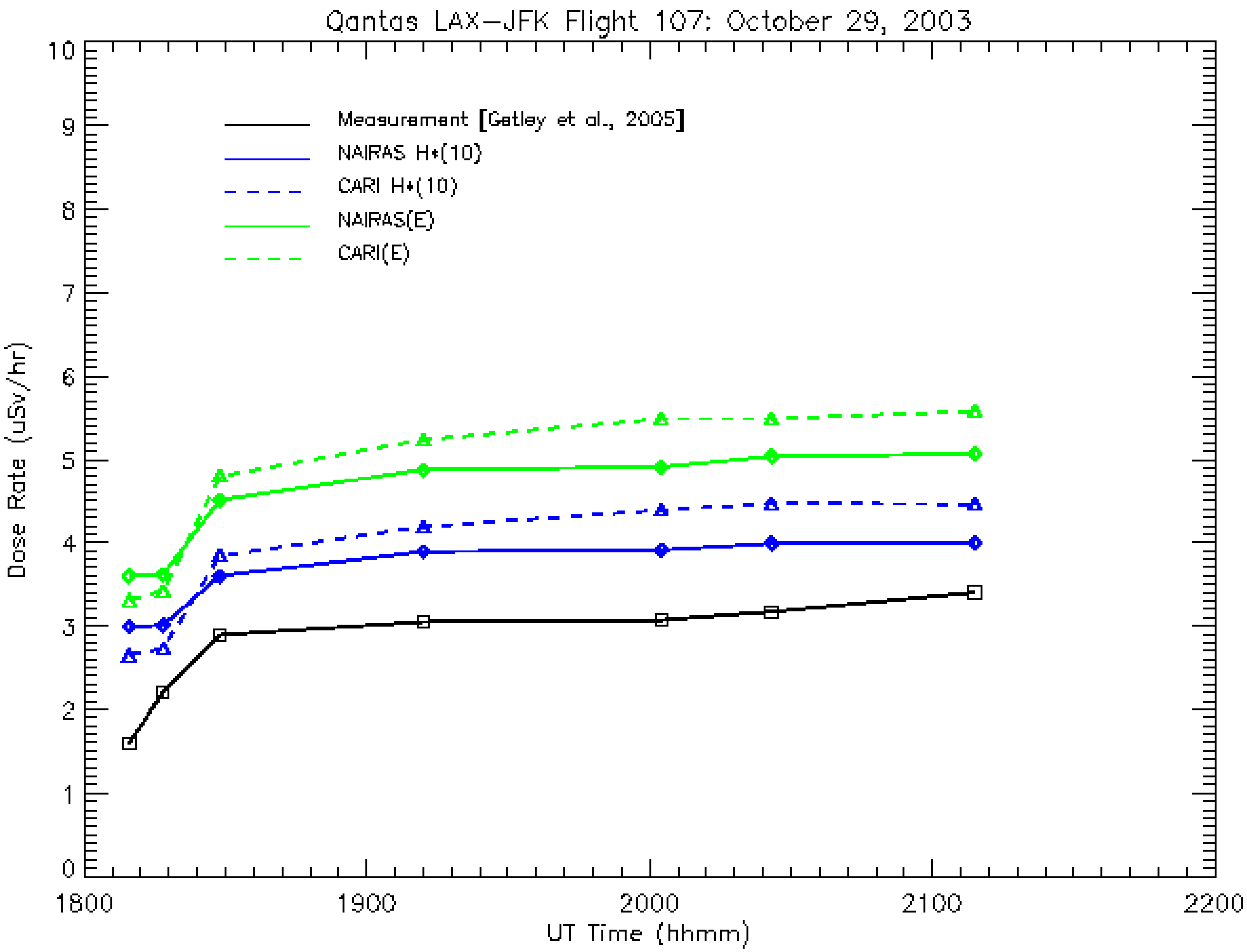

Qantas LAX–JFK Flight 107: October 29, 2003
Measurement [Getley et al., 2005]
NAIRAS H*(10)
CARI H*(10)
NAIRAS(E)
CARI(E)
Dose Rate (uSv/hr)
UT Time (hhmm)
0
1
2
3
4
5
6
7
8
9
10
1800
1900
2000
2100
2200

Conclusions

- Programmatic
  - NAIRAS has adopted the terrestrial weather prediction paradigm to the space weather generated high-LET radiation field
  - Prototype model completion expected in 2011
- Halloween 2003 SEP Case Study
  - Atmospheric radiation exposure during event 3 may have exceed 12% of ICRP recommend prenatal limit for a typically polar route
  - Neglecting time-dependent geomagnetic storm influences on cutoff rigidity may underestimate exposure by <u>more than a factor of two</u>
  - IGRF field can produce an underestimation of ~10-20% in effective dose even without storm effects
- Halloween 2003 GCR Forbush Decrease
  - Initial results are encouraging
- Transition to Operations Issues
  - Instability in NCEP/GFS meteorological data availability. Complex format.
  - NASA/ACE solar wind data drop outs during intense solar storms
    - Effects cutoff rigidity
  - Instability in funding and availability of real-time neutron monitor data
    - Effects incident GCR spectra, high-energy tail of SEP spectra, SEP anisotropy
  - Uncertainty in funding and availability of institutional computer resources needed to couple to the NAIRAS distributed network system